

REVIEW

Quantum simulations and many-body physics with light

To cite this article: Changsuk Noh and Dimitris G Angelakis 2017 *Rep. Prog. Phys.* **80** 016401

View the [article online](#) for updates and enhancements.

Related content

- [Quantum simulation with interacting photons](#)
Michael J Hartmann
- [Keldysh field theory for driven open quantum systems](#)
L M Sieberer, M Buchhold and S Diehl
- [Non-standard Hubbard models in optical lattices: a review](#)
Omjyoti Dutta, Mariusz Gajda, Philipp Hauke et al.

Recent citations

- [Microwave photonics with superconducting quantum circuits](#)
Xiu Gu *et al*
- [Rydberg excitation of cold atoms inside a hollow-core fiber](#)
Maria Langbecker *et al*
- [Nonlinear polariton localization in strongly coupled driven-dissipative microcavities](#)
Said Rahimzadeh Kalaleh Rodriguez *et al*

Review

Quantum simulations and many-body physics with light

Changsup Noh^{1,2} and Dimitris G Angelakis^{1,3}¹ Centre for Quantum Technologies, National University of Singapore, 3 Science Drive 2, 117543, Singapore² Korea Institute for Advanced Study, 85 Hoegiro, Seoul 02455, Korea³ School of Electrical and Computer Engineering, Technical University of Crete, Chania, Crete, 73100, GreeceE-mail: dimitris.angelakis@gmail.com

Received 19 April 2016, revised 24 August 2016

Accepted for publication 13 September 2016

Published 4 November 2016



CrossMark

Abstract

In this review we discuss the works in the area of quantum simulation and many-body physics with light, from the early proposals on equilibrium models to the more recent works in driven dissipative platforms. We start by describing the founding works on Jaynes–Cummings–Hubbard model and the corresponding photon-blockade induced Mott transitions and continue by discussing the proposals to simulate effective spin models and fractional quantum Hall states in coupled resonator arrays (CRAs). We also analyse the recent efforts to study out-of-equilibrium many-body effects using driven CRAs, including the predictions for photon fermionisation and crystallisation in driven rings of CRAs as well as other dynamical and transient phenomena. We try to summarise some of the relatively recent results predicting exotic phases such as super-solidity and Majorana like modes and then shift our attention to developments involving 1D nonlinear slow light setups. There the simulation of strongly correlated phases characterising Tonks–Girardeau gases, Luttinger liquids, and interacting relativistic fermionic models is described. We review the major theory results and also briefly outline recent developments in ongoing experimental efforts involving different platforms in circuit QED, photonic crystals and nanophotonic fibres interfaced with cold atoms.

Keywords: quantum simulations, quantum optics, quantum many body physics, quantum optical implementations of quantum information processing, cavity QED

(Some figures may appear in colour only in the online journal)

1. Introduction

Quantum simulators offer a promising alternative when analytical and numerical methods fail in analysing models with strong correlations. Strong correlations characterise effects in many different fields of physical science. To date, a collection of such effects in different areas ranging from condensed matter physics to relativistic quantum theories and nanotechnology have been simulated [1, 2], using different platforms such as trapped ions [3] and cold atoms in optical lattices [4].

In parallel with the progress in laser cooling that led to ultracold atoms and ion traps, the field of quantum nonlinear optics and cavity QED has seen great advances in the last two decades. This has motivated proposals to study many-body physics using strongly correlated photons (SCPs). Initially, coupled resonator arrays (CRAs) were considered where photons trapped in resonators were assumed to be interacting with real or artificial atoms. Pioneering works suggested the simulation of Mott transitions in CRAs assuming either (i) two-level dopants leading to what is now known as the Jaynes–Cummings–Hubbard (JCH) model [5] or (ii) four-level atoms

with configurations used in electromagnetically induced transparency, giving rise to strongly interacting polaritons [6], and calculated the phase diagram of the JCH model using mean field theory [7]. These were followed soon after by a number of works investigating: beyond-mean-field effects using numerical methods [8], strongly correlated polaritons in photonic crystals [9], quantum state transfer [10–12], propagation of photonic or atomic excitations [13], quantum phase transition in the Tavis–Cummings lattice model [14], simulation of spin models [15–17], and the fractional quantum Hall effect [18]. We would like to mention here that there also exists a line of works which bring the exotic physics of single particle relativistic effects into the laboratory. These have also been categorised as quantum or optical simulations and range from numerous theoretical works involving the Dirac equation and associated phenomena including *Zitterbewegung* and Klein-tunneling [19–26] to experimental implementations of them in various platforms like the ones mentioned above [27, 28] and linear optics [29, 30]. In this review however, we will focus on simulations of strongly correlated phenomena with strongly interacting atom-photon systems (see also a review by Hartmann [31] with a similar emphasis).

These early proposals, and the numerous ones that followed studying the JCH system from different perspectives, marked the beginning of a novel direction in doing many-body physics and quantum simulations using light-matter systems. To mention a few of the works without trying to be exhaustive, we refer the reader to: proposals for entanglement generation [17, 32, 33, 34], polaritonic phase diagram studies using numerical and approximate analytic techniques [35–39], works on different connecting geometries [40, 41], two component models and the emergent solitonic behaviour [42, 43], the strong coupling theory for JCH [44], and applications in quantum information processing [45]. Implementations-wise, the coupled QED resonators found its ideal realisation in circuit QED platforms [46], enjoying widely-tunable coupling strengths and low decoherence rates. Other technologies such as photonic crystal structures and open cavities configurations have also been explored [47, 48]. There have also been proposals to couple superconducting circuits with nitrogen-vacancy centres for the purpose of quantum simulations [49–51].

The next major development in the field was proposals for simulations of 1D continuous interacting models with photons and polaritons in quantum nonlinear optical setups. Here, light pulses trapped in hollow-core fibres interacting with cold atoms were shown to behave as a Tonks–Girardeau gas [52]. This was soon extended to Luttinger liquids exhibiting spin charge separation [53]. More recently, a simulation of 1D interacting relativistic theories as described by the Thirring model was proposed, using polarised photons acting as effective fermions [54]. The ability to efficiently measure correlation functions of photonic states, the integrability of the proposed structures with other optical components on a chip, and the ability to operate at higher and even room temperatures, made quantum simulations with SCPs a quickly evolving field with many theoretical and experimental groups actively pursuing research.

We note here that the idea of using exciton polaritons (excitons coupled to photons in semiconductor materials) to realise quantum fluids has been developed in parallel, motivated by progress in controlling light-matter interactions in semiconductor structures [55]. The interaction strength is typically weak in exciton-polariton systems but ways to enhance polariton-polariton interaction strength have been proposed (see for example [56]). Experimentally, the observation of Bose–Einstein condensation by Kasprzak *et al* in 2006 [57] has stirred enormous interest in this system. For example, a BEC of exciton-polaritons in a flat band system has been reported recently [58], paving the way for the investigation of the interplay of frustration and interaction in nonequilibrium systems. The relationship between the paraxial propagation of a light beam in bulk-nonlinear media and the many-body quantum nonlinear Schrödinger equation has been pioneered by Lai and Haus [59, 60] and the possibility to use the latter type of system for quantum simulation has been recently addressed in [61]. Exciting developments in these fields have been extensively reviewed in [55], to which we refer the interested reader.

The aim of the current report is to review the evolution of SCPs as they have emerged from the early cavity QED approaches. The first part of this manuscript briefly reviews the early proposals on the simulations of Mott transition, the use of Mott state in quantum computing, quantum Heisenberg spin models, and the fractional quantum Hall effect in CRAs. The second part presents more recent results in the direction of out-of-equilibrium properties of lossy driven CRAs. We discuss similarities and differences between the JCH and the Bose–Hubbard systems and review various phenomena arising in either or both of these systems. Fermionisation and crystallisation of photons are first reviewed, which is followed by the works on dynamical signatures of the superfluid–Mott transition and the so-called localisation–delocalisation transition. We then review more exotic effects such as photonic supersolid-like phases and Majorana-like modes and finish off with a survey of studies on smaller arrays and possible experimental implementations. The final part of this review is devoted to reviewing the recent progress in simulating strongly correlated 1D systems using slow light in a hollow-core or tapered fibre coupled to an ensemble of cold atoms. In this part, we first review the proposal for realising a photonic Tonks–Girardeau gas, and then proceed to follow up works on simulating spin-charge separation and a photonic Luttinger liquid, the so-called pinning transition, BCS–BEC crossover, and interacting relativistic theories with photons. Although the focus in this part is on the main theoretical proposals, we also refer to the most recent developments in ongoing experimental efforts in nonlinear fibre systems.

2. Equilibrium many-body effects with coupled resonator arrays

The early proposals on simulations of quantum many-body effects with coupled resonator arrays were partially motivated by: (1) advances in realising coupled resonator optical waveguides (CROWs) and (2) breakthroughs in achieving strong

coupling between quantum emitters and single photons in various light-matter interfaces. CROWs were initially envisioned in photonic crystals structures [62] and were used mainly for classical microwave optics applications. These works were followed by studies in the optical frequencies for applications such as efficient guiding of light [63] and building Mach Zehnder interferometers [64, 65]. The latter were extended, among others, to 2D CROW structures in 2D photonic crystals for tunable optical delay components and nonlinear optics [66]. Strong coupling between single emitters and single photons was also implemented soon after both in semiconductor [67] and circuit QED platforms [68]. Motivated by these progress, and the race for coming up with efficient QIP implementations, the use of cavity QED physics in CROWs doped with quantum emitters was proposed for implementing photonic phase gates [69].

Next, the use of CRAs for quantum many-body simulations was proposed in an array of coupled QED resonators interacting strongly with *single* two level systems. Such a setup was envisioned as a photonic analogue of an optical lattice in atomic systems, that could allow both the trapping of photonic excitations and strong interactions between them. Taking advantage of the photon blockade effectó naturally arising when the atom is strongly coupled to the localised resonator photon [70, 71]ó it was shown that an insulator phase of the total (atomic + photonic or simply *polaritonic*) excitations was possible in an array of atom-resonator systems [5]. In the same work, it was shown that, in parallel with optical lattices, one could mimic a quantum phase transition from the photonic insulator to the superfluid phase by varying the strength of the effective nonlinearity through the tuning of the atom-resonator detuning. Soon after, the complete phase diagram has been reproduced, first in 2D using mean field theory [7] and then in 1D using numerical methods based on DMRG techniques [8].

The Jaynes Cummings Hubbard (JCH) Hamiltonian as it came to be known, involves a combination of bosonic (photons) and spin excitations (the atoms). In general, the insulator-to-superfluid transition in this system is also accompanied by a transition in the nature of the excitations from polaritonic to photonic. Another important difference is that here quasi-particles are formed from *hybrid light-matter excitations*, rather than real physical particles such as atoms, and the former's internal structure makes the phase diagram extremely rich as we will discuss in detail later. In addition to the phase transition, the possibility to simulate the dynamics of XY spin chains with individual-spin manipulation was proposed in the same work [5], using a mechanism different from that of optical lattices [72]. In parallel with the above, the possibility to use 4-level atoms and external fields to simulate strongly interacting dynamics was proposed by Hartmann *et al* [6]. In this case, a time-dependent approach was employed, where the hopping/interaction ratio is varied in time such that the system initially starts deep in the Mott regime and ends up in the superfluid regime. A good agreement between the actual system and the BH model is found upon comparing the dynamics of the number fluctuations. This and subsequent works on simulating spin models using the four-level system approach have been reviewed in [73].

2.1. Photon-blockade induced Mott transitions and the Jaynes–Cummings–Hubbard model

In the following we describe in detail the initial proposal by Angelakis *et al* [5] (first appeared in June 2006 and published in 2007), to implement the JCH model using two-level-system-doped CRAs in order to observe the Mott-superfluid transition of photons.

Consider a series of optical resonators coupled through direct photon hopping. The hopping could be generated through an overlap in the photonic modes as we assumed here or using mediating elements such as fibres [48]. The system is described by the Hamiltonian

$$H = \sum_{k=1}^N \omega_d a_k a_k - \sum_{k=1}^N J (a_k a_{k+1} + \text{H.c.}) \quad (1)$$

which corresponds to a series of coupled quantum harmonic oscillators. The photon frequency and hopping rate is ω_d and J respectively and no nonlinearity is present yet. In order to simulate strongly correlated effects, interaction is necessary and the most natural way to induce it is to dope each resonator with a two level system. The latter could be an atom or a quantum dot or a superconducting qubit. Let us denote $|g\rangle_k$ and $|e\rangle_k$ as its ground and excited states at site k , respectively. The Hamiltonian describing the total system can be divided into three terms: H_{free} the Hamiltonian for the free resonators and dopants, H_{int} the Hamiltonian describing the local coupling of the photon and the dopant, and H_{hop} for the photon hopping between cavities. Explicitly, these read

$$H_{\text{free}} = \omega_d \sum_{k=1}^N a_k a_k + \omega_0 \sum_k |e\rangle_k \langle e|_k, \quad (2)$$

$$H_{\text{int}} = g \sum_{k=1}^N (a_k |g\rangle_k \langle e|_k + \text{H.c.}), \quad (3)$$

$$H_{\text{hop}} = -J \sum_{k=1}^N (a_k a_{k+1} + \text{H.c.}), \quad (4)$$

where g is the atom-photon coupling strength. The local part of the Hamiltonian $H_{\text{free}} + H_{\text{int}}$ can be diagonalised in a basis of mixed photonic and atomic excitations. These excitations, known as dressed states or polaritons in quantum optics and condensed-matter communities respectively, involve a mixture of photonic and atomic excitations and are defined by annihilation operators $P_k^{(\pm, n)} = |g, 0\rangle_k \langle n \pm |_k$. The polaritonic states of the k th atom-resonator system are given by $|n+\rangle_k = (\sin \theta_n |g, n\rangle_k + \cos \theta_n |e, n-1\rangle_k) / \sqrt{2}$ and $|n-\rangle_k = (\cos \theta_n |g, n\rangle_k - \sin \theta_n |e, n-1\rangle_k) / \sqrt{2}$, where $|n\rangle_k$ denotes the n -photon Fock state in the k th resonator, $\tan 2\theta_n = 2g\sqrt{n}/\Delta$, and $\Delta = \omega_0 - \omega_d$ is the atom-light detuning. These polaritons have the energies $E_n^\pm = n\omega_d + \Delta/2 \pm \sqrt{ng^2 + (\Delta/2)^2}$ and are also eigenstates of the sum of the photonic and atomic excitation operators $\mathcal{N}_k = a_k a_k + |e\rangle_k \langle e|_k$ with the eigenvalue n (figure 1).

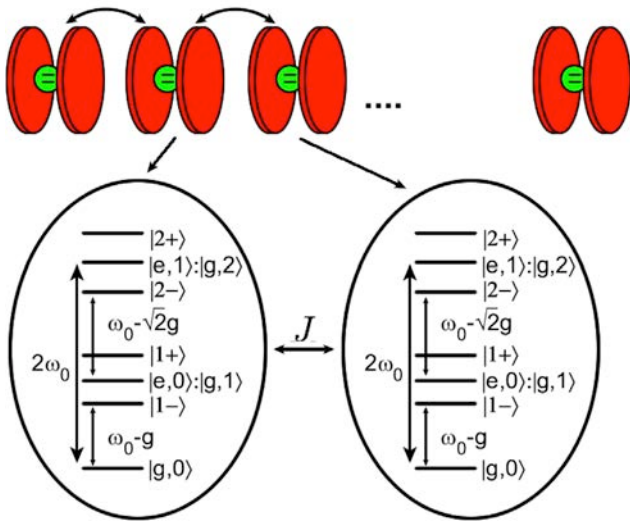


Figure 1. (Top) Schematic representation of a series of cavities coupled through photon hopping. (bottom) The local energy structure in each atom-resonator system where the system's bare states are denoted as $\{|e, n-1\rangle_k, |g, n\rangle_k\}$ and $|n \pm\rangle_k$ denotes the local eigenstates also known as dressed states. Reprinted with permission from Angelakis *et al* [5]. Copyright 2007 by the American Physical Society.

Studying the energy eigenstates of the system consistent with a given number of net excitations per site (or filling factor), it was shown that the ground state of the system reaches a Mott state of the polaritons for integer values of the filling factor. In contrast to the optical lattice systems where the lattice depth is tuned, here the detuning $\Delta = \omega_0 - \omega_d$ is varied. The latter results in further shifts of the dressed states from the bare resonances, providing an effective control over effective nonlinearity. The hopping strength J is usually fixed by the fabrication process and is harder to change experimentally. To see how the Mott state arises, it is convenient to rewrite the Hamiltonian in terms of the polaritonic operators (assuming $\Delta = 0$):

$$\begin{aligned}
 H = & \sum_{k=1}^N \sum_{n=1}^{\infty} \left[n(\omega_d - g) P_k^{(-,n)} P_k^{(-,n)} \right. \\
 & + n(\omega_d + g) P_k^{(+,n)} P_k^{(+,n)} + g(n - \sqrt{n}) P_k^{(-,n)} P_k^{(-,n)} \\
 & \left. + g(\sqrt{n} - n) P_k^{(+,n)} P_k^{(+,n)} \right] \\
 & - J \sum_{k=1}^N (a_k a_{k+1} + \text{H.c.}). \quad (5)
 \end{aligned}$$

Remember that the lower of the two energy eigenstates of the local system with a given number of excitations η is the $-i$ dressed state $|\eta-\rangle$. Therefore, assuming the regime $Jn \ll g\sqrt{n} \ll \omega_d$, one needs only consider the first, third and last terms of the above Hamiltonian for determining the low-lying energy eigenstates of the whole system. The first line corresponds to a linear spectrum, equivalent to that of a harmonic oscillator of frequency $\omega_d - g$. If only that part were present in the Hamiltonian, then it would not cost any extra energy to add an excitation (of frequency $\omega_d - g$) to a site

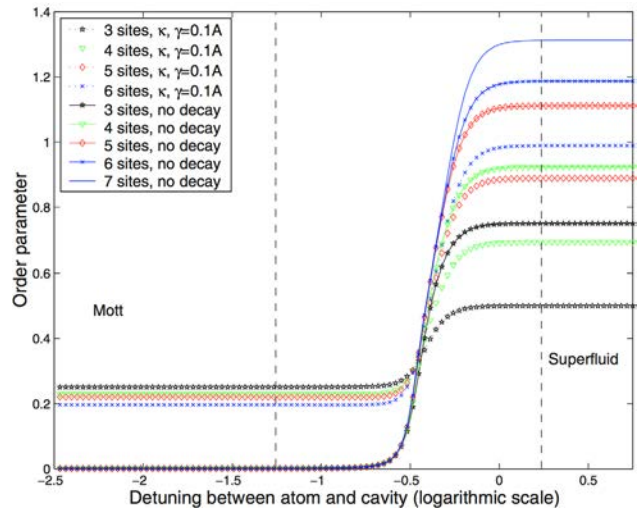


Figure 2. The order parameter ($\text{var}(\mathcal{N}_k)$) as a function of the detuning Δ for 3–7 sites, with and without atomic dissipation and resonator leakage. Close to the atom-photon resonance ($0 \leq \Delta/g \leq 10^{-1}$), where the effective on-site repulsion is maximum (and much larger than the hopping rate $A(=J)$), the system is forced into a polaritonic Fock state with the same number of excitations per site, i.e. the Mott insulator state. Increasing the detuning by applying external fields and inducing Stark shifts ($\Delta \geq g$) weakens the repulsion, leading to the appearance of different coherent superpositions of excitations per site, i.e. a photonic superfluid state. The increase in the system size leads to a sharper transition as expected. Reprinted with permission from Angelakis *et al* [5]. Copyright 2007 by the American Physical Society.

already filled with one or more excitations, as opposed to an empty site.

The third term, on the contrary, provides an effective on-site *photonic repulsion*, leading to the formation of the Mott state of polaritons as the ground state of the system for a commensurate filling. Reducing the strength of the effective nonlinearity (or the photonic repulsion) through detuning, one can then drive the system to the superfluid (SF) regime. This could be done, for example, by Stark shifting the atomic transitions from the resonator by an external field. The shift being inversely proportional to the detuning, the new detuned polaritons are not as well separated as before, and in the case of large detuning, it costs little extra energy to add excitations (excite transitions to higher polaritons) in a single site. As a result, the system moves towards the SF regime with increasing detuning. Note here that the mixed nature of the polaritons could in principle allow for excitations that are mostly photonic, resulting in a photonic Mott state [74].

2.2. Mott and superfluid phases of light in the Jaynes–Cummings–Hubbard model

Beyond the qualitative description reproduced above, an exact numerical simulation was performed in [5], for a different number of sites (from three to seven) using the Hamiltonian $H = H_{\text{free}} + H_{\text{int}} + H_{\text{hop}}$. Note that such finite-size calculations are often employed to study the physics of the transition between Mott and superfluid phases [75] because mean-field theories in low dimensions are not guaranteed to

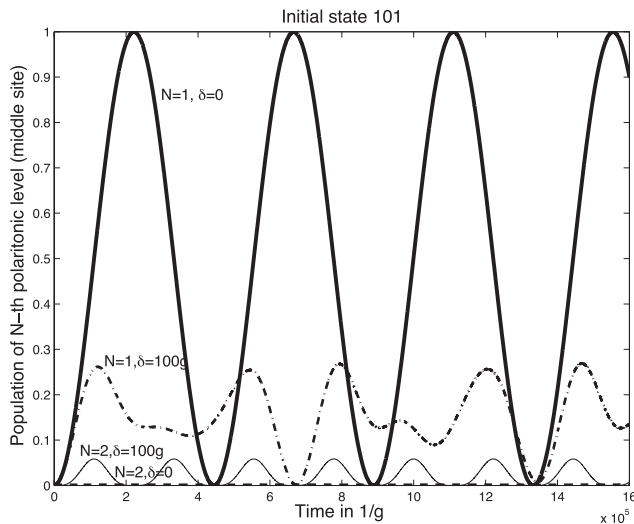


Figure 3. The probability of exciting the polaritons corresponding to one (thick solid line) or two (thick dashed line) excitations for the middle resonator which is taken initially to be empty (in the resonant regime). In this case, as we have started with fewer polaritons than the number of cavities, oscillations occur for the single polariton excitation. The double excitation manifold, however, is never occupied due to the blockade effect (thick dashed line). For the detuned case, hopping of more than one polaritons is allowed (SF regime) which is evident as the higher polaritonic manifolds are being populated now (dot-dashed line and thin solid line). Reprinted with permission from Angelakis *et al* [5]. Copyright 2007 by the American Physical Society.

work. We also note here that numerical simulations of the JCH Hamiltonian are more computationally costly than the ones for the BH Hamiltonian due to the existence of both bosonic (photon) and atomic operators in every site.

As discussed in [5], an appropriate order parameter in the JCH lattice is the variance of the polariton number per site, as the usual order parameter employed in other cases⁶ like the expectation value of the annihilation operator in the BH model⁶ is identically zero in a closed system. The variance $\text{var}(\mathcal{N}_k)$ is plotted in figure 2 as a function of $\log_{10}(\Delta/g)$ for a filling factor of one net excitation per site. For this plot, we have taken the parameter ratio $g/J = 10^2$ ($g/J = 10^1$ gives quantitatively similar results), with Δ varying from $\sim 10^{-3}g$ to $\sim g$ and $\omega_d, \omega_0 \sim 10^4g$. The order parameter for dissipationless atoms and cavities is displayed as solid curves and corresponding curves in the presence of a resonator dissipation and atomic spontaneous emission of $\sim 0.01g$ are depicted with dotted lines.

In figure 3 the quantum dynamics characterising the excitation probability of the middle site in a chain of three cavities for different regimes are calculated assuming the middle resonator is initially empty. We observe the blockade of higher than one excitation in the limit of resonant interaction (where the Mott phase is expected) as discussed in figure 2.

The phase diagram of the JCH model has first been studied in 2D using mean field theory [7] and in 1D using a numerical method based on DMRG techniques [8]. Figure 4(top) shows slices of the superfluid order parameter $\psi = \langle a_i \rangle$ as a function of the photon hopping and the chemical potential for different values of atom-photon detuning. A triangular lattice was assumed and the usual decoupling approximation

$a_i a_j = \langle a_i \rangle a_j + a_i \langle a_j \rangle + \langle a_i \rangle \langle a_j \rangle$ was used [7]. The bottom panels of figure 4 show the numerically-calculated phase diagram (top row) and the compressibility ($\kappa = \partial \rho / \partial \mu$, $\rho =$ filling factor) (bottom row) as functions of the hopping strength for a 1D chain.

In both figures the corresponding Mott and SF phases are explored by changing the hopping strength and the effective photonic chemical potential (the free energy term in the JCH Hamiltonian), following the standard treatment of quantum phase transitions. We note that in CRA experiments the hopping strength is in general not tunable but fixed by the fabrication process. In these systems, it is easier to control the effective repulsion (the photon blockade), as discussed in the previous section. Nevertheless, the phase diagrams are useful in showing the existence of Mott lobes in this photonic system and how they depend on system parameters. These works have been supplemented using the variational cluster approach, where on top of the phase diagram, single-particle spectra and finite temperature effects have been investigated [35]. Quantum Monte-Carlo method has also been employed to find various properties of the JCH-type systems [36, 76–78].

An application of the Mott regime for implementing quantum information processing (QIP): The typical implementation of cluster state quantum computing requires initialising all qubits in a 2D lattice in the $|+\rangle = (|0\rangle + |1\rangle)/\sqrt{2}$ state and then performing controlled-phase gates (CP) between all nearest-neighbours [79]. In the resonator array system the first proposal to create cluster states utilised the Mott state and the resulting XY dynamics [16]. The ground state $|g, 0\rangle$ and the first excited state $|1-\rangle$ of the combined atom-photon (polaritonic) system in each site was used as a qubit as depicted in figure 5.

The need to disable the evolution was realised by combining the system's natural dynamics with a protocol where some of the available physical qubits are used as gate mediators and the rest as the logical qubits. The mediators can be turned on and off on demand by tuning the atoms in the corresponding sites on and off resonance from their cavities. This is done by Stark shifting them through the application of an external field (gates A, B, C D in figure 5), effectively shifting the site frequencies and inhibiting photon hopping, thereby isolating each logical qubit. Soon after there have also been other approaches focusing on the generation of the Ising interaction [80] and also towards the simulation of a family of effective spin models in CRAs [15, 41, 81–84]. These will be analysed in the next section.

2.3. Effective spin models

Quantum spin models have played a crucial role as basic models accounting for magnetic and thermodynamic properties of many-body systems. In implementations involving arrays of Josephson junctions [85] or quantum dots [86], the spin-chain Hamiltonian naturally emerges from the spin-like coupling between qubits, albeit with limited control over the coupling constants. In optical lattice simulators, perturbative dynamics with respect to the Mott-insulator state allows for an effective spin-chain Hamiltonian [72, 87]. This direction has the

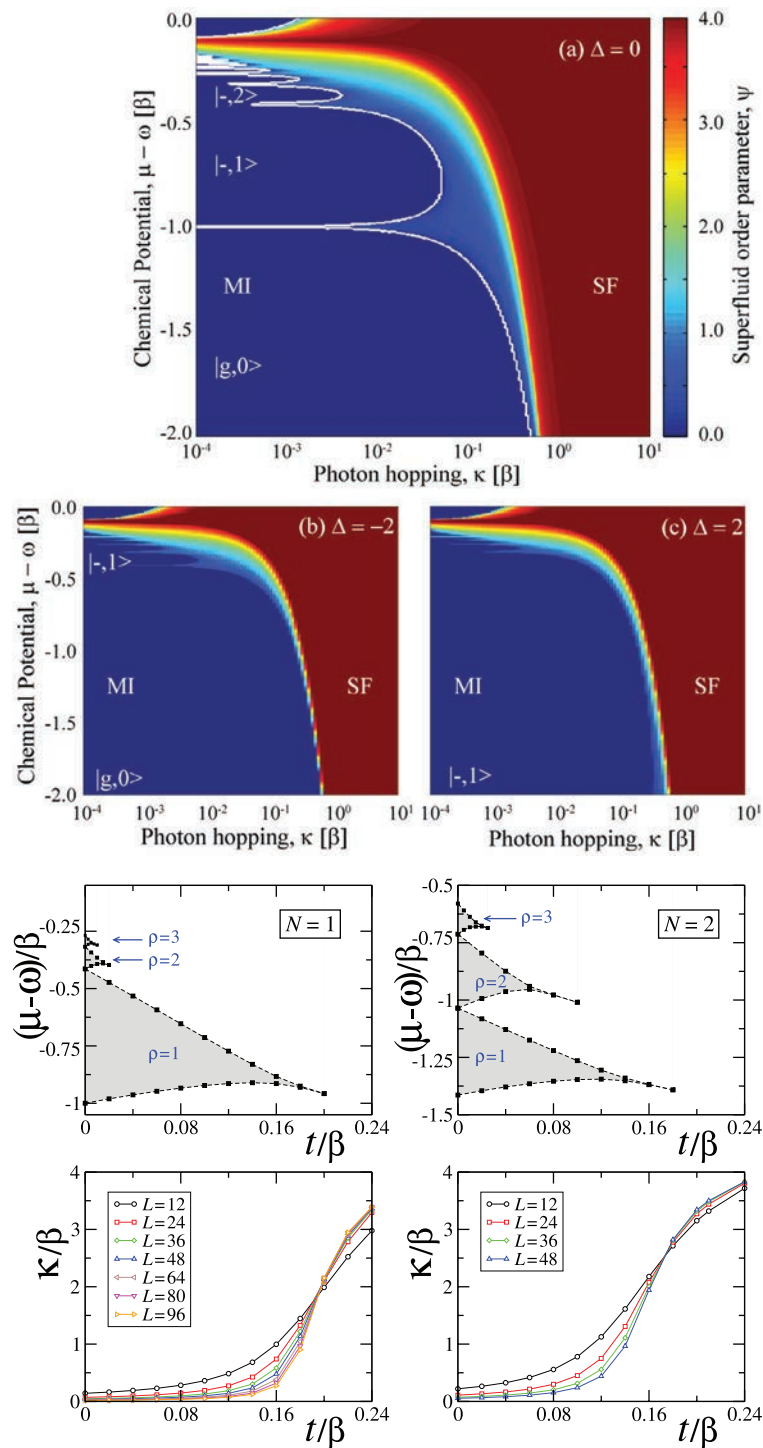


Figure 4. (Top) The phases diagram of a 2D JCH system calculated using mean field theory for three different values of atom-photon detuning $\Delta = 0$ (a), $-2g$ (b), and $2g$ (c). μ is the chemical potential introduced separately to the Hamiltonian, κ is the hopping strength ($=J$), β is the atom-photon coupling strength ($=g$), and ω is the bare resonator frequency ($=\omega_d$) [7]. Reprinted with permission from Greentree *et al*, Macmillan Publishers Ltd: [7]. Copyright 2006. (Bottom, top row) The phase diagram of a 1D JCH array, calculated using DMRG simulations. μ is the chemical potential, β is the atom-photon coupling strength ($=g$), t is the hopping strength ($=J$), and ρ is the filling factor in the Mott phase. (Bottom, bottom row) The compressibility κ as a function of hopping strength, for different system sizes L . $N = 1$ (left column) and $N = 2$ (right column) denotes the number of atoms inside each resonator [8]. Reprinted with permission from Rossini and Fazio [8]. Copyright 2007 by the American Physical Society.

advantage that the spin-coupling constants can be optically controlled to a great extent. In CRAs, a spin is represented by either polariton states or hyperfine ground levels of the embedded emitter and the system was shown to generate an effective Heisenberg model with optically tunable interactions

$$H_{\text{eff}} = - \sum_{\langle j,k \rangle} \lambda_z \sigma_j^z \sigma_k^z + \lambda_x \sigma_j^x \sigma_k^x + \lambda_y \sigma_j^y \sigma_k^y + h \sum_j \sigma_j^z, \quad (6)$$

where the angled brackets denote the sum over nearest neighbours. We will use the same notation throughout this review.

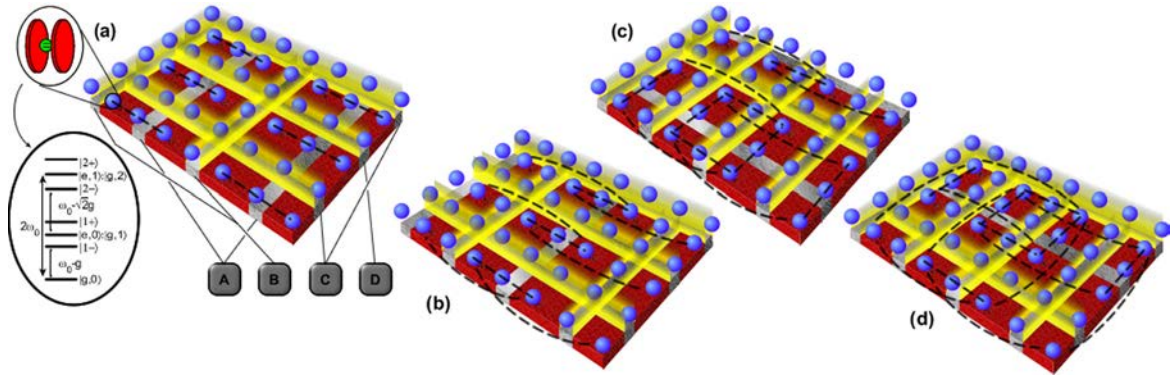


Figure 5. A 2D array of atom-resonator systems in the Mott state can be used to implement cluster state quantum computing, utilising the natural evolution, which in this case is of an XY spin type, and applying external global gates to switch on and off the dynamics, by properly applying local external fields, utilising the fact that the cavities can be well separated. Reprinted with permission from Angelakis and Kay [16]. Copyright 2008 IOP Publishing and Deutsche Physikalische Gesellschaft.

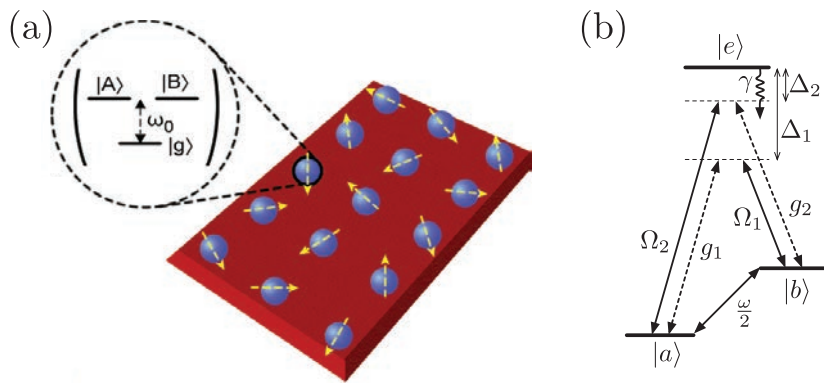


Figure 6. (a) 2D CRA for simulating Heisenberg spin models. Each resonator is doped with a V-type atom which is coupled to two orthogonal modes [81]. Reprinted with permission from Kay and Angelakis [81]. Copyright 2008 Europhysics Letters Association. (b) The atomic level structure and optical transitions involved in order to simulate higher-spin Heisenberg models [88]. Reprinted with permission from Cho *et al* [88]. Copyright 2008 by the American Physical Society.

In the work [81], an array of cavities was assumed on the vertices of a 2D lattice (note that any array is in principle possible) as depicted in figure 6(a). Each resonator is doped with a single system (which we refer to as an atom), whose energy level structure comprises of a ground state $|g\rangle$ and two degenerate excited states $|A\rangle$ and $|B\rangle$. Within each lattice site, the Hamiltonian takes the form

$$H_0 = \omega_0 (a_i a_i + b_i b_i + |A\rangle\langle A|_i + |B\rangle\langle B|_i) + g (|A\rangle\langle g|_i \otimes a_i + |g\rangle\langle A|_i \otimes a_i) + g (|B\rangle\langle g|_i \otimes b_i + |g\rangle\langle B|_i \otimes b_i),$$

where a_i and b_i create photons of orthogonal polarisations at site i and the atomic levels and the resonator modes are assumed to be on resonance. The strength of the coupling between the resonator and the atom is denoted by g . Coupling between nearest-neighbour resonators is described by the Hamiltonian

$$H_{\text{hop}} = \sum_{\langle i,j \rangle} J_a (a_i a_j + \text{H.c.}) + J_b (b_i b_j + \text{H.c.}). \quad (7)$$

Assuming strong atom-photon interaction regime, $g \gg J_{a,b}$, and restricting to the unit filling fraction, such that

one excitation per site is expected, one obtains an effective Hamiltonian (6) with

$$h = \frac{5}{8g} (J_a^2 - J_b^2), \quad \lambda_z = \frac{9}{32g} (J_a^2 + J_b^2), \\ \lambda_x = \lambda_y = \frac{9J_a J_b}{16g}.$$

Note that we have ignored the constant term $\kappa = \frac{31}{32g} (J_a^2 + J_b^2)$. The local magnetic fields can be manipulated by applying local Stark fields, thereby leaving an XXZ Hamiltonian where the coefficients λ_z and λ_x are independently tunable (at device-manufacture stage). This approach allows a stronger spin spin coupling than an alternative one in [15], but lacks the optical control of the coupling. The latter exhibits greater optical controllability, but relies on rapid switching of optical pulses and the consequent Trotter expansion, which unavoidably introduces additional errors and makes the implementation more difficult.

The question of simulating chains of higher spins, which may have a completely different phase diagram, was dealt with in [88]. In this proposal, a fixed number of atoms are confined in each resonator with collectively applied constant laser fields, and is in a regime where both atomic and resonator excitations

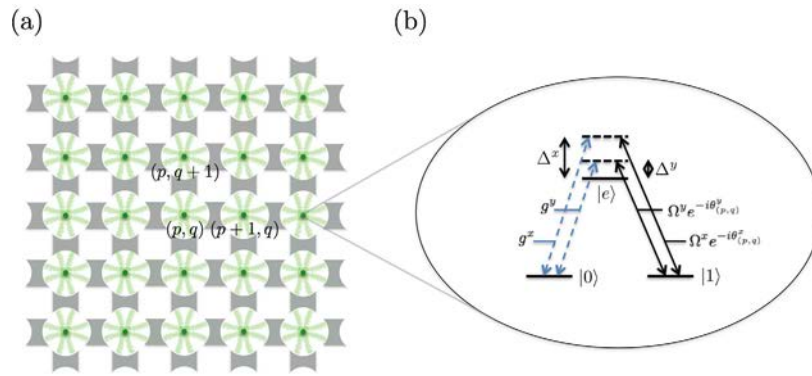


Figure 7. (a) Schematic representation of a 2D coupled resonator array. Each site supports two orthogonal non-degenerate resonator modes that are coupled with a single atom. (b) Involved atomic levels and transitions. The resonator mode x (y) is coupled to the atomic transition $|e\rangle\langle 0|$ with coupling strengths g^x (g^y) and detuning Δ^x (Δ^y). The transition $|e\rangle\langle 1|$ is driven by site-dependent laser fields with Rabi frequencies $\Omega^x e^{-i\theta^x(p,q)}$ and $\Omega^y e^{-i\theta^y(p,q)}$. The subscripts denote the positions of the lattice sites.

are suppressed (figure 6(b)). It was thus shown that as well as optically controlling the effective spin-chain Hamiltonian, it is also possible to engineer the magnitude of the spin.

2.4. Fractional quantum Hall states of photons

Since its first discovery in a semiconductor heterostructure in the early 1980s [89], systems exhibiting FQHE has now become routinely available in laboratories. In a different context, the achievement of trapping ultracold atomic gases in a strongly correlated regime has prompted an interest in mimicking various condensed matter systems with trapped atoms, thereby allowing one to tackle such complex systems in unprecedented ways [90]. The great advantage of this approach is that such a tailored system is highly controllable at the microscopic level and is close to idealised quantum models used in condensed matter systems. In the context of FQHE, a 2D atomic gas can be either trapped in a harmonic potential [91, 92] or in an optical lattice [93, 94]. Since the atoms in consideration have no real charge, the magnetic field is simulated artificially. For instance, it can be done by rapidly rotating the harmonic trap [91], by exploiting electromagnetically induced transparency [92], or by modulating the optical lattice potential [93, 94].

The first proposal to realise the fractional quantum Hall system with strongly correlated photons was based on an optical manipulation of atomic internal states and inter-resonator hopping of virtually excited photons in a 2D array of coupled cavities [18]. It was shown that the local addressability of coupled resonator systems allows one to simulate any system of hard-core bosons on a lattice in the presence of an arbitrary Abelian vector potential. The proposal is based on the realisation of the Heisenberg spin model introduced earlier and is depicted in figure 7. To facilitate a spatially varying gauge potential, an asymmetry in the resonator modes is assumed, where two orthogonal resonator modes along the x and y directions have different resonant frequencies (this asymmetry is not an essential requirement as explained in [18]). Realising this geometry would be viable in several promising platforms, such as photonic bandgap microcavities and superconducting microwave cavities. The

frequency difference between the two modes is assumed to be much larger than the atom-resonator coupling rates. In this way, either direction of the spin exchange can be accessed individually.

Similar works with different approaches and platforms within CRA have appeared since. Ways to introduce synthetic gauge fields allowing one to break the time-reversal symmetry which is crucial in quantum Hall physics have been devised in circuit QED [95, 96] and solid state cavities [97]. A photonic version of the quantum spin Hall system, which does not break the time-reversal symmetry, has also been proposed [98] and experimentally demonstrated [99]. Interacting versions realising fractional quantum Hall-type physics of photons were proposed in Kerr-nonlinear cavities [100] and the JCH cavities [101] and signatures of fractional quantum Hall physics in a nonequilibrium driven-dissipative scenario have been investigated [102]. Experimentally, a building block consisting of three superconducting qubits has been demonstrated recently, where both the signatures of a synthetic magnetic field and strong interaction have been observed [103]. Synthetic Landau levels were demonstrated for photons in a single twisted optical cavity also, opening up a new route towards photonic fractional quantum Hall physics [104].

Here we will take a closer look at the first proposal. But first, to set the stage, let us very briefly describe the model Hamiltonian and its ground state wave function that captures the physics of FQHE in its fermionic counterpart. A system of bosonic particles confined in a 2D square lattice in the presence of an artificial perpendicular magnetic field B is described by the Hamiltonian

$$H_0 = -t \sum_{p,q} \left(c_{p+1,q} c_{p,q} e^{-i2\pi\alpha q} + c_{p,q+1} c_{p,q} + \text{H.c.} \right), \quad (8)$$

where the positions of lattice sites are represented by $a(px + qy)$ with p and q being integers and α is the spacing of the lattice. Here, $\alpha \equiv Ba^2/\Phi_0$, the number of magnetic flux quanta through a lattice cell, plays a crucial role in characterising the energy spectrum, whose self-similar structure is known as the Hofstadter butterfly. In the hardcore (maximum one boson per site) and continuum limit ($\alpha \ll 1$) the ground state is accurately described by the Laughlin state

$$\Psi_m(\{z_j\}) = e^{-\frac{1}{4} \sum_j |z_j|^2} \prod_{j < k} (z_j - z_k)^m, \quad (9)$$

where $z_j = x_j + iy_j$ and the filling factor $\nu = 1/m$, with m even, corresponds to the ratio of the number of bosons to the number of magnetic flux quanta.

Assume now a 2D array of coupled cavities, each confining a single atom with two ground levels as in figure 7(b). Each resonator has two modes along the x and y directions, whose annihilation operators will be denoted by a^x and a^y . The atom interacts with these resonator modes with coupling rates g^x and g^y , and with detunings Δ^x and Δ^y , respectively. Furthermore, to induce site-dependent hopping, two classical fields with (complex) Rabi frequencies $\Omega^x e^{-i\theta_{p,q}^x}$ and $\Omega^y e^{-i\theta_{p,q}^y}$ are applied. In the rotating frame, the Hamiltonian for the system reads

$$\begin{aligned} H = & \sum_{\substack{j=x,y \\ j=(p,q)}} [g e^{-i\Delta} a_j (|e\rangle\langle 0|)_j \\ & + \Omega e^{-i\theta_j} e^{-i\Delta} (|e\rangle\langle 1|)_j + \text{H.c.}] \\ & - \sum_{p,q} (J^x a_{p+1,q}^x a_{p,q}^x + J^y a_{p,q+1}^y a_{p,q}^y + \text{H.c.}), \end{aligned} \quad (10)$$

where J^x (J^y) denotes the inter-resonator hopping rate of the photon along the x (y) direction. We assume $\Delta^x - \Delta^y \gg g^x, g^y$, as mentioned above, and furthermore that $\Delta \gg g \gg \Omega, J$.

In this strong coupling regime, the atomic excitation is suppressed and one can perform adiabatic elimination to obtain an effective Hamiltonian

$$\begin{aligned} H = & \sum_{\substack{j=x,y \\ j=(p,q)}} [\delta a_j a_j (|0\rangle\langle 0|)_j + \omega (e^{i\theta_j} a_j \sigma_j^+ + \text{H.c.})] \\ & - \sum_{p,q} (J^x a_{p+1,q}^x a_{p,q}^x + J^y a_{p,q+1}^y a_{p,q}^y + \text{H.c.}), \end{aligned} \quad (11)$$

where $\delta = (g^y)^2/\Delta$, $\omega = g^y \Omega/\Delta$, and $\sigma^+ = |1\rangle\langle 0|$. Here, we have ignored the ac Stark shift induced by the classical fields, which is negligible in the assumed regime (it may also be compensated by other lasers). We further assume $\delta \gg J \gg \omega$, which can be satisfied, along with the above conditions, when

$$g/\Delta \gg J/g \gg \Omega/\Delta. \quad (12)$$

Now the resonator photon is suppressed and an adiabatic elimination can be applied once more. Keeping the terms up to the third order and taking only the sub-manifold with no photons, the effective Hamiltonian further simplifies to

$$\begin{aligned} H = & -t \sum_{p,q} [\sigma_{p+1,q}^+ \sigma_{p,q}^- e^{i(\theta_{p+1,q}^x - \theta_{p,q}^x)} \\ & + \sigma_{p,q+1}^+ \sigma_{p,q}^- e^{i(\theta_{p,q+1}^y - \theta_{p,q}^y)} + \text{H.c.}], \end{aligned} \quad (13)$$

where δ , ϵ , ω , and J are chosen to yield

$$t = J^x \left(\frac{\omega^x}{\delta^x} \right)^2 = J^y \left(\frac{\omega^y}{\delta^y} \right)^2. \quad (14)$$

It is easy to see that this Hamiltonian reduces to the Hamiltonian H_0 in (8) in the hardcore bosonic limit, if we adjust the phases of the classical fields such that $\theta_{p,q}^x = -pq \cdot 2\pi\alpha$ and $\theta_{p,q}^y = 0$.

The ground state of the Hamiltonian (13) is thus expected to be described faithfully by the Laughlin wavefunction (9), modulo changes due to the difference in gauge and boundary conditions, which can be calculated analytically [105]. For a 4 by 4 lattice with $\alpha = 1/4$, $m = 2$, the fidelity between the numerically calculated ground state of the ideal Hamiltonian and this modified Laughlin state (with $m = 2$) was shown to be excellent indeed (≈ 0.989) [18]. Actually this number is a bit misleading because $\alpha = 1/4$ is quite a large value for which the continuum limit is not guaranteed to be a good approximation. Indeed, for 4 bosons, the bosonic Laughlin state ceases to be a good variational ground state for $\alpha > 0.2$ [106]. In such a case, one can compute topological invariants such as the Chern number [106], or look at the edge properties [99], in order to verify the topological nature of the ground state.

The numerical ground state of the effective Hamiltonian (11) for $\delta^y/10 = 10\omega = J$, corresponding to $\Delta/1000 = g/100 = \Omega = J$, has the fidelity of 0.976 [18]. The ground state can be prepared adiabatically by exciting two atoms at different sites initially without the laser fields ($t = 0$) and then delocalising these excitations via adiabatically tuning up the effective hopping rate. The quasi-excitations can also be generated via local tuning of the laser fields to mimic an infinitely thin solenoid, around which the excitations form. More details on these issues can be found in [18, 107]. Lastly, it should be mentioned that one needs a higher number of bosons in order to perform braiding with anyonic excitations [108, 109].

3. Out-of-equilibrium physics in CRAs

All the works we have reviewed so far have been on equilibrium physics of CRAs. However, as photonic systems are intrinsically dissipative, they are naturally operated in a nonequilibrium setting where some sort of external pumping is often introduced. The equilibrium physics reviewed in the previous section should therefore be observed within a time period shorter than the dissipation time [5, 6] or by engineering an effective chemical potential for photons [110]. The nonequilibrium nature is evident for example in recent experiments on BECs of exciton-polaritons [57], Dicke quantum phase transition with a superfluid gas of atoms in an optical cavity [111], and BECs of photons in an optical microcavity [112]. In fact, one can go way back and regard lasing as a nonequilibrium BEC phase transition. The nature of Bose-Einstein condensation in such nonequilibrium settings have attracted much interest, because of its intrinsic differences to the equilibrium condensation phenomena [113]. Investigations of many-body effects in CRAs in such experimentally relevant driven-dissipative regime have only recently begun [31, 55, 114, 115]. The open nature of CRAs makes it a particularly interesting platform to study nonequilibrium many-body physics. The external driving here can easily be tuned to be incoherent, coherent, or quantum, opening the road for exploration of novel many-body phases out of equilibrium.

Before discussing the efforts in this area, we would like to mention that investigations on driven dissipative regimes in the context of semiconductor polaritons and cold atoms

and ions systems have also been carried out, employing field-theoretical approaches [116], or more conventional quantum optical approaches [117]. These have mostly focused on problems with specifically engineered baths [118] or (quasi-) exactly solvable spin and fermionic models or dynamical phenomena [119, 120].

In this section, we review the early and more recent works on nonequilibrium physics in dissipative JCH or BH models, with or without driving. While there has been a proposal to implement the attractive BH model directly in a circuit-QED system [121], the majority of experimental realisations of a CRA are of the JCH type where the two-level system could be a real or artificial atom. Therefore, we begin by looking at similarities and differences between the two models in a nonequilibrium setting, which was first investigated by Grujic and coworkers [122].

After setting the stage, we look at fermionisation and crystallisation of photons in driven dissipative settings. We then move on to dynamical (transient) effects, first looking at the dynamical signatures of the superfluid-insulator transition and then at the so-called localisation delocalisation transition of photons due to self-trapping effect. The experimental verification of the latter in a circuit-QED platform is also reviewed. Then comes proposals to implement exotic out-of-equilibrium phases, viz photon supersolid and Majorana-like modes. The next section gives a brief survey of further interesting works that investigate photon correlations and entanglement in small-size lattices or using mean field as well as those that investigate phases in 2D lattices with or without artificial gauge fields. Finally, we close the section with a brief discussion on possible experimental platforms.

3.1. Comparison between JCH and BH models

Let us begin by describing how to model the driven-dissipative systems. Firstly, coherent driving by laser fields can be modelled by introducing a driving term in the Hamiltonian, $H_{\text{drive}} = \sum_i [\Omega_i(t)a_i + \Omega_i^*(t)a_i^\dagger]$, where $\Omega_i(t) = \Omega_i \exp(-i\omega_L t)$ is the time-dependent driving field and a_i is the driven resonator mode. As we have noted earlier, we will encounter two types of model Hamiltonians. One is the Bose Hubbard Hamiltonian which, including the driving term, can be written as

$$H_{\text{BH}} = \sum_i \left[\omega_c a_i a_i + \frac{U}{2} a_i a_i a_i a_i \right] - \sum_{\langle i,j \rangle} J a_i a_j + \sum_i [\Omega_i(t)a_i + \Omega_i^*(t)a_i^\dagger], \quad (15)$$

while the other is the JCH Hamiltonian

$$H_{\text{JCH}} = \sum_i [\omega_c a_i a_i + (\omega_c - \Delta) \sigma_i^+ \sigma_i^- + g(a_i \sigma_i^- + a_i \sigma_i^+)] - \sum_{\langle i,j \rangle} J a_i a_j + \sum_i [\Omega_i(t)a_i + \Omega_i^*(t)a_i^\dagger]. \quad (16)$$

In both models, ω_c is the bare resonator frequency and J is the photon hopping rate between the nearest neighbour resonators denoted by the angled brackets. Δ is the detuning

between the resonator and atom and g is the atom-photon coupling strength. σ_i^+ and σ_i^- are the atomic raising and lowering operators at site i .

Secondly, photon losses are modelled by assuming that the system is (weakly) interacting with a bath of harmonic oscillators. Taking the Born Markov approximation, one obtains a quantum master equation describing the dynamics of the reduced density matrix of the system ρ [123]. In this review, we will mostly deal with master equations of the form

$$\dot{\rho} = -i[H_X, \rho] + \frac{\gamma}{2} \sum_{i=1}^N (2a_i \rho a_i - a_i a_i \rho - \rho a_i a_i) + \frac{\kappa}{2} \sum_{i=1}^N (2\sigma_i^- \rho \sigma_i - \sigma_i \sigma_i \rho - \rho \sigma_i \sigma_i), \quad (17)$$

where X can be JCH or BH (in the latter case, $\kappa = 0$ is assumed); γ and κ are the dissipation rates of photons and atoms, respectively, assumed here to be identical for all sites.

Now we are ready to compare the two models. Let us start from the simplest case: a single-site system. The eigenstates of the Jaynes Cummings Hamiltonian are the dressed states $|n, \pm\rangle$, where n is the total excitation number and \pm labels two polaritonic (hybrid atom-photon) modes with energies $\omega_n^\pm = n\omega_c - \Delta/2 \pm \sqrt{(\Delta/2)^2 + ng^2}$. Because of the dependence on n , the energy of $|2, -\rangle$ is not twice that of $|1, -\rangle$, as illustrated in figure 8(a) for $\Delta = 0$. Comparing with the energy levels of the Kerr-nonlinear model shown in figure 8(b), one thus concludes that if $-$ polaritons are driven and if the driving is sufficiently weak such that only the lowest states are occupied, an effective interaction strength U_{eff} can be defined to formally connect the two models. That is, one can assign an effective BH parameter

$$\frac{U_{\text{eff}}}{g} = \frac{\omega_2^- - 2\omega_1^-}{g} = \frac{\Delta}{2g} + 2\sqrt{\left(\frac{\Delta}{2g}\right)^2 + 1} - \sqrt{\left(\frac{\Delta}{2g}\right)^2 + 2}, \quad (18)$$

to the JCH model.

Deep in the strongly interacting regime, we would thus expect the two models to yield similar qualitative behaviour: the polaritons will delocalise to minimise the kinetic energy, but the double occupation of any site is inhibited at the same time. On the other hand, we also know that the two models should converge in the opposite limit of linear CRAs. These two observations give a heuristic argument as to why we can see the Mott-superfluid transition in a JCH system. However, this does not mean that the two types of systems are similar in all aspects. After all, there are additional atomic degrees of freedom in the JCH systems. To illustrate similarities and differences in the two models, figure 9 plots various expectation values of the nonequilibrium steady state (NESS) for a homogeneously-driven periodic three-site CRA.

Upon comparing the JCH (figure 9(a)) and the BH (figure 9(b)) results, we immediately see that the JCH has a more complex structure. Broadly, the spectrum is divided into two parts. The left (right) wing is mostly composed of the $-$ ($+$) polaritons for the small value of J used here ($U = 20J$). The vertical dash-dotted line indicates the driven single-excitation eigenstate while the dotted lines indicate the

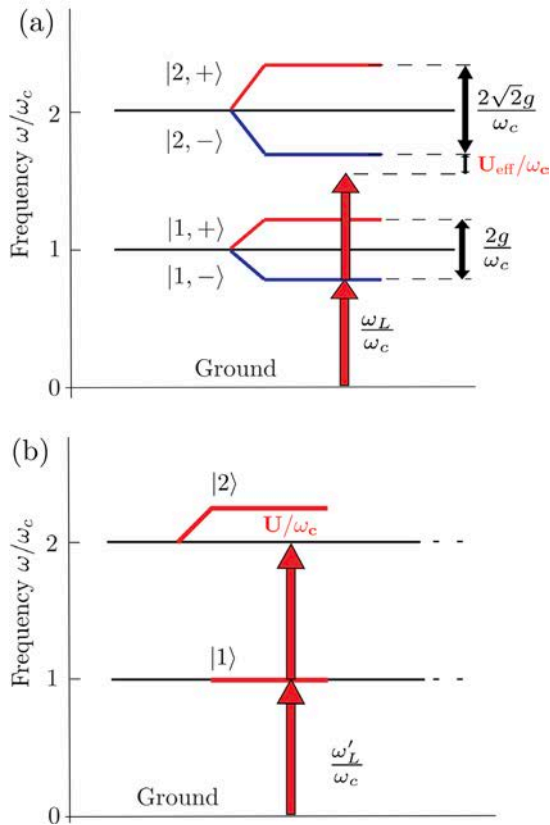


Figure 8. Comparison between the lowest eigenmodes of (a) the Jaynes-Cummings model for $\Delta = 0$ and (b) the Kerr-nonlinear model. Reprinted with permission from Grujić *et al* [122]. Copyright 2012 by the American Physical Society.

eigenstates of a single resonator ($J = 0$ case). A BH system by comparison has a relatively simple spectrum with peaks near (but not exactly at) the single-site n -photon energies indicated by the dotted vertical lines. Note that the spectrum is quite broad as we have assumed $\gamma = J$. Despite these differences, there is a notable similarity when the systems are driven at the single-particle resonance (vertical dash-dotted lines) enhanced steady-state photon number is accompanied by a dip in the same-time intensity-intensity correlation function $g^{(2)} = g^{(2)}(i_1, i_1)$. The latter is defined as

$$g^{(2)}(i_1, i_2) = \langle a_{i_1} a_{i_2} a_{i_2} a_{i_1} \rangle / \langle a_{i_1} a_{i_1} \rangle \langle a_{i_2} a_{i_2} \rangle, \quad (19)$$

where the expectation values are taken with respect to the steady state density operator. The dip in $g^{(2)}$ signifies that two excitations do not want to occupy the same site simultaneously. This quantifies the photon blockade effect mentioned earlier, arising due to the strong effective repulsion between photons.

At this point, the reader might be wondering whether it is possible at all to achieve a good quantitative agreement between the two models. It is indeed possible in the photonic regime, in which the atom-photon detuning is so large that the polaritons are mostly photonic. In this limit, however, the effect of atom-photon interaction is to merely shift the resonance (figure 9(c)). To counteract the reduced nonlinear effect, one needs a very large value of g . In figure 9(d), $\Delta/g = -10$ and $g = 6 \times 10^4 \gamma$ were used. Since these kind

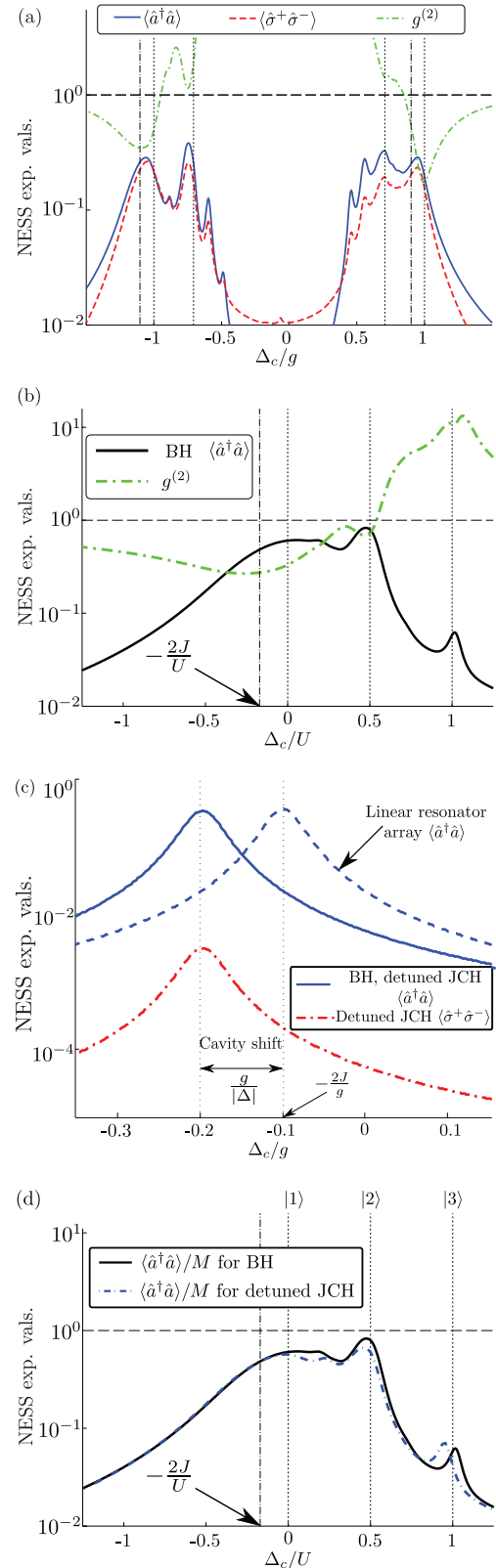


Figure 9. Steady state expectation values for a homogeneously driven, cyclic three-site coupled resonator array. (a) A JCH-type system with $\Delta = 2J = 2$ and (b) a BH-type system with the effective nonlinearity set by $g = 20$. (c) $\Omega = 0.3$, $g = 20$, $\Delta/g = -10$. (d) $g = 1.6 \times 10^4$, $\Omega = 2$ in all figures except (c) and all parameters are in units of γ . Reprinted with permission from Grujić *et al* [122]. Copyright 2012 by the American Physical Society.

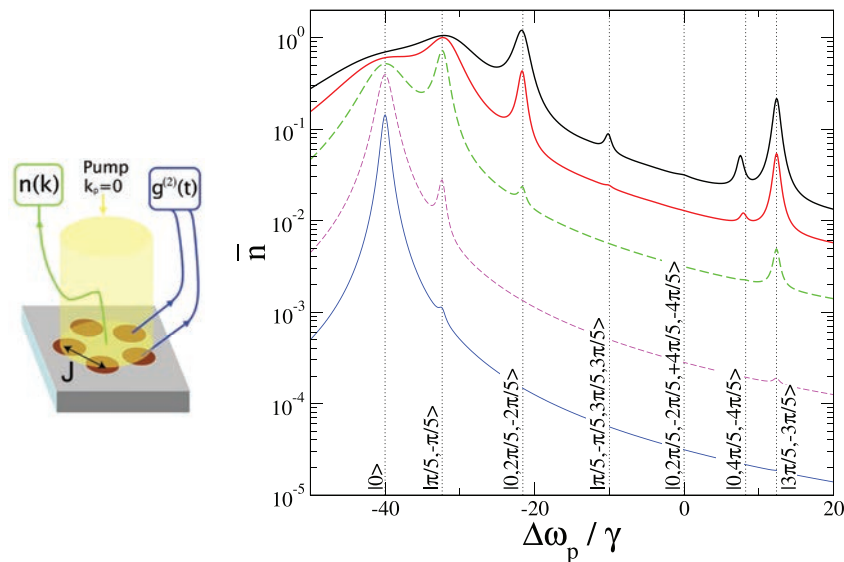


Figure 10. Left: schematic diagram of the system. Right: total transmission spectra as a function of driving frequency for 5 cavities in the impenetrable boson limit, $U/J = \infty$ and $J/\gamma = 20$. Decreasing pump amplitude from top to bottom: $\Omega/\gamma = 3, 2, 1, 0.3, 0.1$. The vertical dotted lines indicate the predictions of the Bose-Fermi mapping where the states corresponding to the spectral peaks are written in the momentum basis. Reprint with permission from Carusotto *et al* [124]. Copyright 2009 by the American Physical Society.

of numbers lie well outside the experimental realm, we conclude that differences between the two types of systems are there in realistic systems and one must be careful in choosing the correct model to describe a given CRA. In particular, one should check whether a phenomenon found in a BH system can also be observed in a JCH system in a reasonable parameter regime. We will come across such examples below.

3.2. Fermionisation and crystallisation of photons and polaritons in BH and JCH models

Initial investigations on many-body physics in driven-dissipative CRAs employed the 1D BH model. Signatures of strong on-site interaction leading to fermionisation and crystallisation of the excitations (much as in Tonks-Girardeau gases) were shown to be visible in the NESS of driven-dissipative CRA systems [124, 125]. JCH versions of these models have been studied by Grujic *et al* [122], confirming that the predicted phenomena also occur in the JCH versions. The effect of geometric frustration on the steady-state has also been studied more recently, where it was shown that in a homogeneously-driven flat-band lattice, the steady state exhibits an incompressible state of photons characterised by a short-ranged crystalline order [126].

3.2.1. Fermionisation of photons. We begin with the work of Carusotto and coworkers [124]. The system is composed of Kerr nonlinear cavities coupled in a cyclic fashion as illustrated in figure 10. The master equation describing the system is given by (17) with $X = \text{BH}$, with homogeneous driving fields such that $\Omega_i = \Omega$. As shown on the right panel of figure 10, the transmission spectrum of the total transmitted intensity $n_T = \sum_i \text{Tr}[\rho a_i a_i] \equiv \langle a_i a_i \rangle$ show the traces of strong interaction between photons. For the case of impenetrable bosons

($U \gg J$), the Bose-Fermi mapping can be employed [127], which translates an interacting Boson model into a free Fermion model to enable calculations of the energy eigenvalues. These eigenvalues with their eigenstates are shown in the figure, showing excellent agreement between the spectra of the driven-dissipative system and the eigenvalues of the closed system.

To further illustrate the fermionisation of photons, figure 11 plots the on-site ($g^{(2)}(i_1 = i_2)$) and nearest-neighbour ($g^{(2)}(i_1 \neq i_2)$) correlations as functions of U/J , when the pump lasers are kept on resonance with the lowest two-photon transition. Clearly, both the JCH and BH systems yield qualitatively similar results when the effective nonlinearity is matched via equation (18). In the weak interaction limit, all the levels are harmonic and the emitted light inherits the Poissonian nature of the pump. In the intermediate regime, $U/J \approx 1$, the (driven) two-photon peak starts to separate from the single-photon peak leading to bunching. Finally, in the large U/J limit, the two photons fermionise, resulting in strong antibunching with enhanced cross-correlations.

A detailed investigation on the fluorescence spectrum and the spectrum of the second-order correlation function under coherent and incoherent driving for a two coupled cavities of JCH type was carried out by Knap *et al* [128]. Similar to the work described above, the resonance peaks of the measured spectra of the dissipative system were matched to the eigenenergies of the closed system.

3.2.2. Crystallisation of polaritons. In an independent work, Hartmann has studied the effects of strong interaction between polaritons in coupled resonators (described by the BH model in which a_j is the polariton annihilation operator) [125]. In that setup, instead of driving the system homogeneously, a flow of polaritons is created via modulation of the phase of

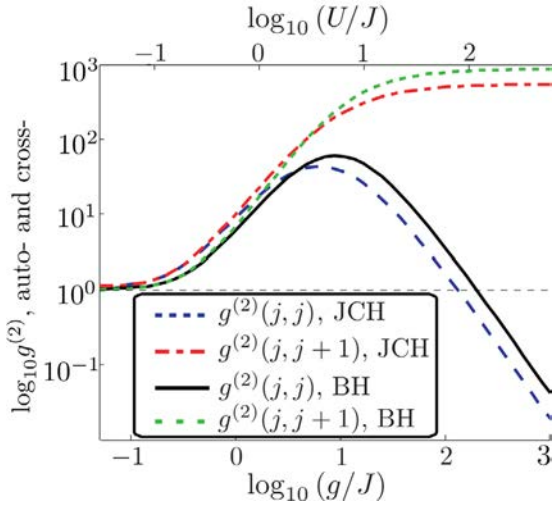


Figure 11. Auto- (black, solid line) and cross- (red, dashed line) correlations as functions of the interaction strength. JCH systems with different couplings g are compared with BH systems with U calculated from (18). $J/\gamma = 20$, $\Omega/\gamma = 0.5$, and $\Delta = 2J$. Reprinted with permission from Grujic *et al* [122]. Copyright 2012 by the American Physical Society.

the driving laser such that $\Omega_j = \Omega e^{-i\phi_j}$, where $\phi_j = j\pi/2$. The interplay between this flow and the nonlinearity then results in polariton crystallisation, where excitations are predominantly found within a specific distance from one another. To describe this phenomenon in detail, we will use the spatial correlation function $g^{(2)}(i, j)$ as well the momentum correlation function defined by

$$g_{\text{BM}}^{(2)}(p, q) = \langle B_p B_q B_q B_p \rangle / \langle B_p B_p \rangle \langle B_q B_q \rangle, \quad (20)$$

where the momentum eigenmode operator is defined as $B_p = 1/\sqrt{N} \sum_j \exp(ipj) a_j$, with N the total number of cavities and $p = 2\pi l/N$ for $l = -N/1 + 1, -N/2 + 2, \dots, N/2$.

There are two interesting regimes determined by the relative strength between the nonlinearity U and the driving strength Ω : (1) Weakly nonlinear regime, $\Omega \gg U$, and (2) Strongly nonlinear regime, $U \gg \Omega$. Let us start with the weakly nonlinear regime. In this strongly-driven regime, a semiclassical treatment is valid, i.e. $B_p = \sqrt{N} \beta \delta_{p, \pi/2} + b_p$, where β is a mean amplitude for the driven mode at $p = \pi/2$ and b_p is an annihilation operator for the quantum of fluctuations. To second order in fluctuations the Hamiltonian, neglecting the driving term for now, can be written as

$$H = \sum_p \left[(\omega_p + 2Un) b_p b_p + \left(\frac{U\beta^2}{2} b_p b_p + \text{H.c.} \right) \right], \quad (21)$$

where $p = \pi p/l$ $|p| = -p$ and $n = |\beta|^2$ is the mean number of polaritons. This Hamiltonian is known to exhibit two-mode squeezing between the modes p and p , arising due to the scattering between p and p modes induced by the nonlinear term. The latter also induces density density correlations between the modes, which can be seen from the intensity correlation function between the Bloch modes evaluated to the leading order in $1/(Nn)$:

$$g_{\text{BM}}^{(2)}(p, q) \approx 1 + \delta_{p \neq \pi/2} (\delta_{p, q} + \delta_{p+q, \pm\pi} \frac{|g|^2}{m^2}) - \delta_{p, \pi/2} \delta_{q, \pi/2} \frac{2m}{Nn}, \quad (22)$$

where $m = 2U^2 n^2 / (12U^2 n^2 + \gamma^2)$ is the contribution to the mean photon number from quantum fluctuations and $g = \langle B_p B_p \rangle = -\beta^2 (4U^2 n + iU\gamma) / (12U^2 n^2 + \gamma^2)$. The term $\delta_{p+q, \pm\pi} \frac{|g|^2}{m^2}$ clearly shows the correlations between the modes p and p for non-driven modes, while the driven mode $p = \pi/2$ exhibits slight antibunching $g_m^{(2)}(\pi/2, \pi/2) \approx 1 - 2m/Nn$.

In the strongly nonlinear regime, the semiclassical description is no longer valid. Instead, the time evolving block decimation (TEBD) algorithm (see [129, 130] for reviews) was used to calculate the steady state for an array of 16 cavities (for other methods to deal with larger systems, see e.g. [131, 132]). Contrary to the weakly nonlinear regime, there is now strong correlations between the same Bloch modes ($g_m^{(2)}(p, p) > 1$), while different modes are strongly anticorrelated ($g_m^{(2)}(p, q) < 1, p \neq q$), as shown in figure 12.

The same figure also shows an evidence of photon crystallisation, by which we mean the following: if a polariton is found in one resonator, a second polariton is most likely to be found in an adjacent resonator and this happens at the reduced probability of finding a polariton at farther sites. This is clearly observed in the polariton correlation function between the cavities, where $g^{(2)}(j, j+1) > 1$ and $g^{(2)}(j, j+k) < 1$ for $k = 1, 2, \dots$. The correlations fall below 1 only when the driving phase is $\neq 0$, indicating that the observed phenomenon emerges due to the interplay between the nonlinearity and the flow of polaritons. For comparison, figure 12 also plots (green lines) the density correlations of a Tonks Girardeau (TG) gas $g_{\text{TG}}^{(2)}(i, j) = 1 - (\sin(\pi n(i-j)) / \pi n(i-j))^2$, where n is the number of polaritons per resonator. While the TG gas shows an oscillation in the density density correlation, no such oscillation is observed in crystallised polaritons. Similar behaviour is observed for the JCH model when the polaritonic mode $|1, -\rangle_{p=\pi/2}$ is driven, as depicted in figure 13. It is interesting to note that the on-site repulsion is strengthened with increasing Δ/g_0 this can be attributed to an increase in the atomic portion of the JC polariton with the detuning.

3.3. Dynamical phenomena

In the previous section we have seen that the steady states of driven-dissipative CRAs are capable of exhibiting signatures of underlying many-body states in the equilibrium system and furthermore that interesting phases can be created due to driving. However, this is not the only nonequilibrium scenario that reveals interesting physics. One well-known example is quenching, in which the system is initially excited in a particular initial state and subsequent dynamics is observed. Here we review two early works taking this approach. We begin with a study of the nonequilibrium signatures of the superfluid-insulator transition by Tomadin *et al* [133] and briefly summarise a similar study on a hybrid system by Hummer

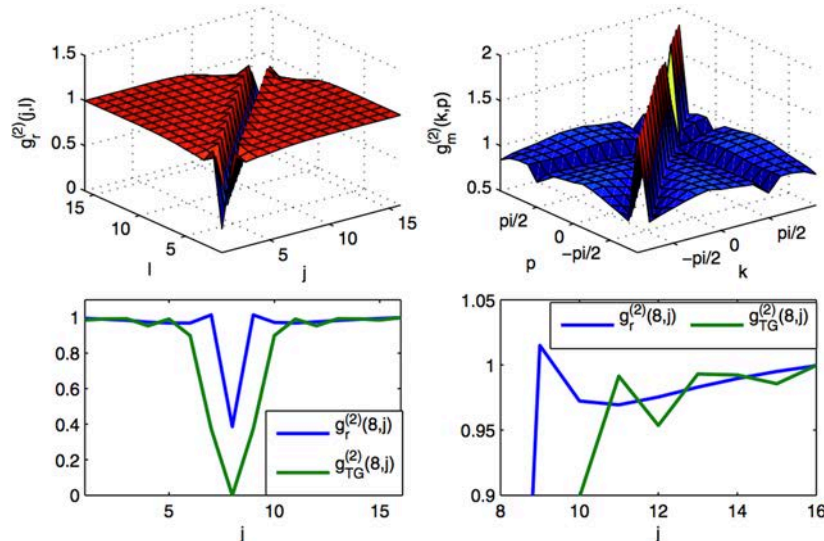


Figure 12. Intensity correlations of the steady state for 16 cavities in the strong interaction regime driven at resonance. $U/\gamma = 10$, $J/\gamma = 2$, $\Omega/\gamma = 2$ and $\Delta_L = 0$, where Δ_L is the polariton-laser detuning. Top row: steady state intensity correlations between spatial modes (left) and Bloch modes (right). Bottom row: comparison with the correlation functions of a Tonks–Girardeau gas. Reprinted with permission from Hartmann [125]. Copyright 2010 by the American Physical Society.

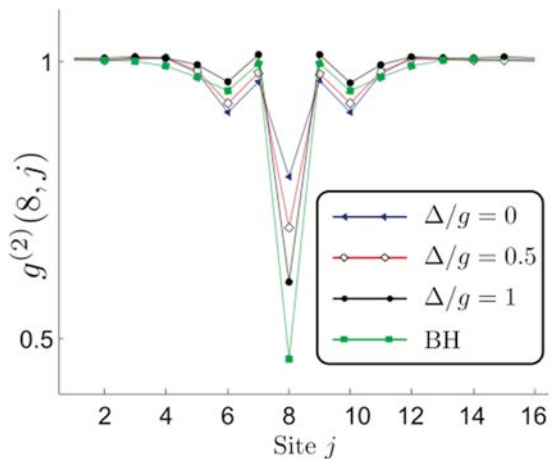


Figure 13. Steady state photon density density correlations for the JCH model for various values of Δ/g as compared with that from the BH model. $g/\gamma = 10$ ($U_{\text{eff}} \approx 6$), $J/\gamma = 2$, and $\Omega = 2$. Reprinted with permission from Grujić *et al* [122]. Copyright 2012 by the American Physical Society.

et al [49]. Then we review the localisation delocalisation transition of photons [134], which has been verified experimentally in a superconducting circuit setup [135].

3.3.1. Superfluid-insulator transition. In [133], Tomadin and coworkers investigated a dissipative BH system in 2 dimensions without any driving field, initially prepared in a Mott-like state. Much as in the quantum quench scenario, subsequent transient evolutions depend sensitively on the underlying equilibrium phase (without dissipation). A self-consistent cluster mean-field approach was employed with up to two sites per cluster, where the evolution within a cluster is exact but the interaction with the rest of the system is treated at the mean-field level.

Let us first consider the dynamics of the initial Mott state. With negligible dissipation, the dynamics obviously depends

sensitively on the value of J/U . For small J/U , the system is expected to stay more or less in the same state, whereas for large J/U , nontrivial dynamics are expected. As in the equilibrium case, a useful observable to distinguish between these distinct cases is the second-order correlation function, since strong antibunching is expected to persist for small J/U . In fact, in the transient scenario, a more useful observable was shown to be the time-averaged second-order correlation function, which we denote $\langle g \rangle_t$. Figure 14 illustrates the usefulness of this quantity, where the averaging is over $2/\gamma < t < 4/\gamma$. The inset shows the time-averaged mean-field order parameter $\langle |\psi| \rangle_t$, displaying similar behaviour as $\langle g \rangle_t$; z is the coordination number denoting the number of nearest neighbours. For small J/U , the average intensity correlation is 0 indicating that the system remains in the initial Mott state. However, for large J/U , the initial state becomes unstable and a crossover towards Poisson statistics ($g^{(2)} = 1$) is observed, the latter occurring over a narrow region of J/U near the critical point indicated by the vertical dashed line.

Experimentally, the initial state is most likely to be prepared by a series of laser pulses. In this case, there will inevitably be some imperfections in preparing the Mott state. Tomadin *et al* have studied the effect of such imperfections by considering non-ideal filling factors in the initial state. Figure 15 shows the results. Clearly, a deviation from the ideal initial state does not destroy the stark difference between the superfluid (triangles) and Mott (circles) regimes as measured by $\langle g^{(2)} \rangle_t$. The same conclusion holds for a general initial condition, with up to 20% depletion of the average filling, for the whole range of initial coherences allowed by the manifold spanned by 0 and 1 Fock states in each resonator.

A similar investigation on nonequilibrium signatures of the phase transition has been carried out by Hummer *et al* [49], in a hybrid system of flux qubits coupled with nitrogen-vacancy centres. The model describing this system is different from the BH system in that (i) each site comprises of qubits coupled to

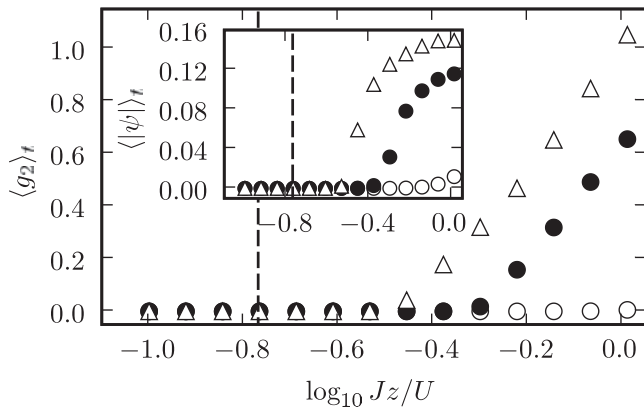


Figure 14. Time averaged intensity correlations averaged in the interval $2/\gamma < t < 4/\gamma^{-1}$. The laser field is resonant to the bare cavity frequency while the dissipation rate takes the values $\gamma/U = 4 \times 10^{-2}$ (empty circles), $\gamma/U = 2 \times 10^{-2}$ (filled circles), and $\gamma/U = 1 \times 10^{-2}$ (empty triangles). The inset shows the mean-field order parameter. The vertical dashed line indicates the critical point where the Mott-superfluid phase transition occurs in the equilibrium case. Reprinted with permission from Tomadin *et al* [133]. Copyright 2010 by the American Physical Society.

collective bosonic modes of NV centres surrounding it, and (ii) the coupling is between the qubits, not bosons. Despite these differences, the time averaged probability to find two excitations in a single site is shown to be a very good indicator of the underlying phase transition in the equilibrium case.

3.3.2. Localisation–delocalisation transition of photons. The transient phenomenon to be reviewed here is not associated with the underlying phases of the equilibrium system, but with the dynamics of the system. The concept was initially introduced by Schmidt *et al* [134] essentially in a closed Jaynes Cummings dimer, but the subsequent experimental demonstration [135] showed that dissipation can play an important role in achieving the transition dynamically. As this experiment provides the state-of-the-art realisation of a CRA, we discuss it in some detail. The essential physics of the localisation delocalisation transition is similar to that of self-trapping: when two nonlinear systems are tunnel-coupled, the oscillation between the systems can be inhibited by the on-site nonlinearity. While previous studies in optical fibres [136], molecules [137], cold atoms [138–140], and polaritons [141] have concentrated on the Kerr nonlinearity, Schmidt *et al* showed that the same phenomenon also occurs in a Jaynes Cummings dimer. The effect has been generalised to more than two sites by Schetakis and coworkers [142].

As first explained in [134], the physics of the localisation delocalisation transition are nicely captured in the semiclassical picture without dissipation. One resonator is assumed to be initially in a coherent state with N photons on average, while the other resonator is assumed to be empty. Then, the semiclassical analysis shows that the photon imbalance $Z(t) = (n_L(t) - n_R(t))/N$ undergoes an oscillation whose frequency decreases with increasing g and furthermore goes to 0 at the critical coupling strength $g_c^{cl} \approx 2.8\sqrt{N}J$. This behaviour survives in the quantum regime as shown in figure 16

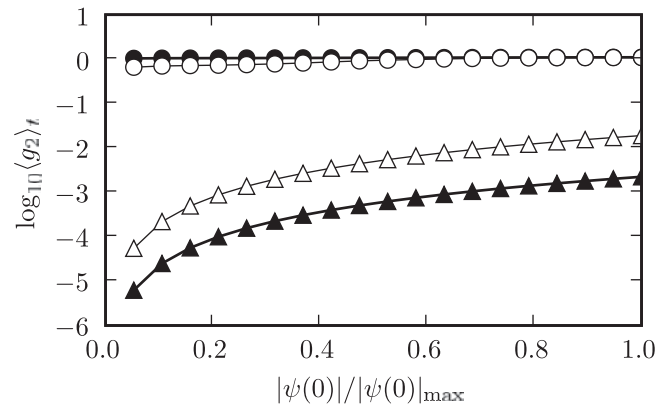


Figure 15. Time-averaged intensity correlations, averaged over the interval $2/\gamma < t < 4/\gamma^{-1}$, for resonant driving and $\gamma = 2 \times 10^{-2}$. The vacuum population of the initial state is $\rho_0 = 0.02$ for the filled symbols and $\rho_0 = 0.2$ for the empty symbols. Results below the critical point ($zJ/U = 0.1$) are denoted by triangles while those above the critical point ($zJ/U = 1.0$) are denoted by circles. Reprinted with permission from Tomadin *et al* [133]. Copyright 2010 by the American Physical Society.

for a lossless dimer with 7 photons initially placed in the left resonator. $Z(t)$ is the time averaged imbalance up until time t . While the initial imbalance is washed out over time below the critical coupling strength, $g = 0.3g_c^{cl}$ (figure 16(a)), the signature of photon localisation is evident above the critical coupling strength, $g = 2.0g_c^{cl}$ (figure 16(b)). The localisation behaviour can be explained as follows. For a symmetric dimer, the two states with opposite imbalance 1 and -1 are approximate eigenstates of the system when $g \gg J$. Using the degenerate perturbation theory the period of oscillation between these states can be calculated as $1/(c_{N_0}J(J/g)^{N_0-1})$ with c_{N_0} a constant that depends on the total photon number N_0 . Clearly, this number diverges rapidly with increasing N_0 when $J/g \ll 1$.

A detailed analysis shows that there are features not captured by the semiclassical treatment such as a beating in the coherent oscillation that is observable in the weakly-nonlinear case, smoothing of the transition, and a shift in the critical coupling strength where $g_c^{qu} < g_c^{cl}$ [134]. The shift in the critical coupling strength has been explained recently using a Fock-state WKB approach, yielding an analytical expression for the classical phase boundary depending on the initial state of the spins [143]. Rather than delving into these features further, let us move on to the experimental realisation of the dissipative localisation delocalisation transition, where dissipation plays a key role in driving the transition dynamically. The latter occurs due to the photon number dependence of the critical coupling strength. For an experimental setup with fixed g , the initial photon number N_0 decides whether the system is in the localised regime ($g > g_c^{qu}(N_0)$) or in the delocalised regime ($g < g_c^{qu}(N_0)$). In a closed system, the system has no choice but to remain in a given regime. However, in a dissipative system, the decrease in the total number of photons can take the system from a delocalised regime to a localised regime (because g_c^{qu} decreases with N).

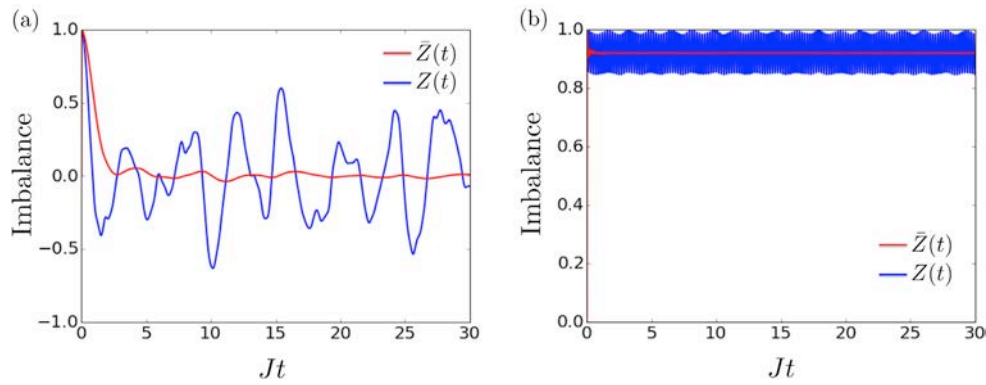


Figure 16. Photon number imbalance (blue curves) and the time-averaged imbalance (red curves) for a lossless dimer containing 7 photons initially localised in the left resonator. (a) Below the critical coupling strength, $g = 0.3g_c^{cl}$, exhibiting delocalised dynamics. (b) Above the critical coupling strength, $g = 2.0g_c^{cl}$, exhibiting localised dynamics.

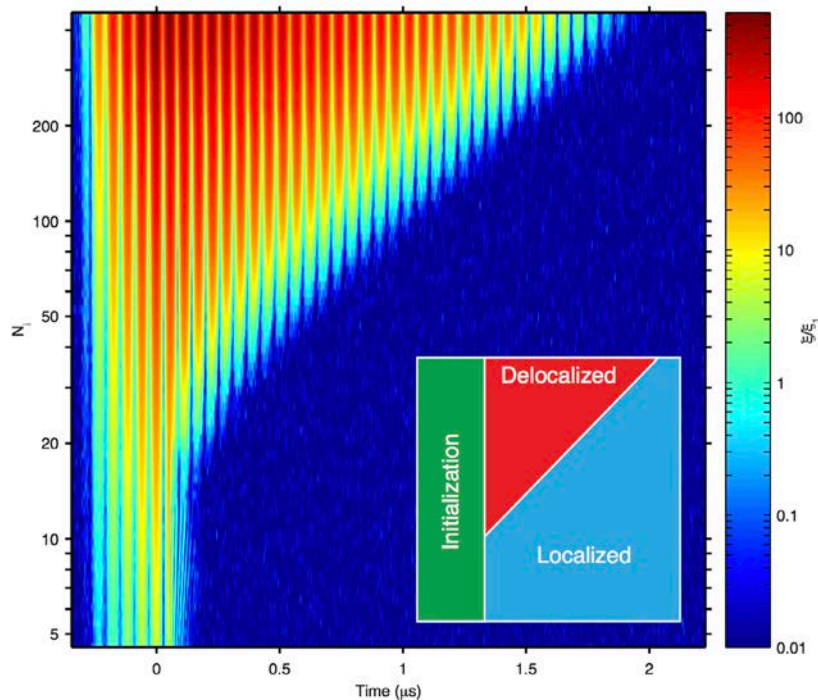


Figure 17. Phase diagram of the dissipation-induced delocalisation-localisation transition for an open Jaynes-Cummings dimer. Homodyne signals from the initially unoccupied resonator as a function of initial photon number N_i and time. For $N_i \gtrsim 20$ the system starts in the delocalised regime because $g < g_c^{qt}(N)$. However, as time progresses the system enters the localised regime as photon losses drive the system into the localised regime characterised by $g \geq g_c^{qt}(N)$. Reprinted with permission from Raftery *et al* [135]. Copyright 2014 by the American Physical Society, [CC BY 3.0](https://creativecommons.org/licenses/by/3.0/)

This effect has been experimentally demonstrated by Raftery and coworkers in a superconducting circuit platform [135]. In the experiment, the initial state was prepared in a coherent state instead of a Fock state, but the described physics remain qualitatively unchanged. Initially, the qubits and the resonators are far-detuned so they are practically uncoupled. Then the system is driven by a coherent pulse and left to evolve a specific period of time, which prepares the system with the imbalance 1. The nonlinearity is then rapidly increased by bringing the qubits into resonance with the resonator mode. The results for various initial photon numbers (N_i) are plotted in figure 17. It shows the homodyne signal in the initially unoccupied resonator as a function of the initial photon number and time. For a small enough N_i , the system

starts off and remains in the localised regime, whereas for a larger N_i the system starts off in the delocalised regime and crosses over to the localised regime after enough photons are lost from the system so that the critical coupling strength is smaller than the experimental coupling strength.

3.4. Exotic phases out of equilibrium

Coupled resonator arrays, especially in the superconducting circuit platform, allow one to engineer different types of interactions that are difficult to achieve in other systems. Here, we look at two proposals utilising this advantage to realise exotic phases in nonequilibrium scenarios. We begin by reviewing a proposal on a photonic supersolid phase in a driven-dissipative

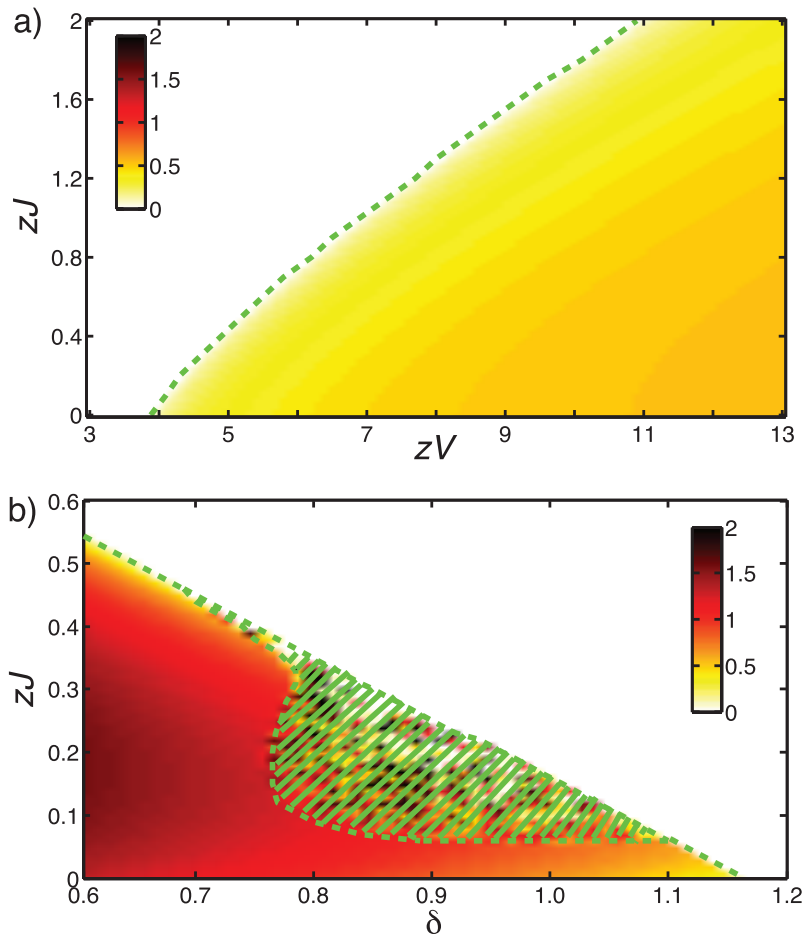


Figure 18. (a) Order parameter as a function of J and V , for $\delta = 0$ and $U = 1$. (b) Order parameter as a function of J and δ , for $zV = 0.6$ and $U = 0$. $\Omega = 0.75$ for both diagrams. For finite values of the detuning (of the driving field), an intermediate regime between staggered and uniform phase appears, which can be seen as a nonequilibrium analogue of supersolid. Green dashed lines are there to provide a guide to the eye. Reprinted with permission from Jin *et al* [144]. Copyright 2013 by the American Physical Society.

setup and then a proposal to achieve Majorana-like modes in a chain of driven cavities.

3.4.1. Photon supersolid phase. Let us start with the proposal by Jin and coworkers, which investigated the consequences of adding a cross-Kerr term between nearest neighbours [144, 145]. Such a term naturally arises in electronic systems due to the Coulomb interaction between electrons, but are necessarily much smaller than the on-site interaction term. However, in CRAs the magnitude of the new term can be made arbitrarily large as compared to the on-site interaction term, giving rise to interesting new phases. The open *extended* Hubbard system studied by the authors is described by the master equation (17) with

$$H_X = H_{\text{BH}} + V \sum_{\langle i,j \rangle} n_i n_j, \quad (23)$$

which, as they show, can be realised using nonlinear coupling elements between the cavities.

Consider a 2D bipartite lattice that divides into two sublattices with homogeneous coherent pumping ($\Omega_i = \Omega$). Due to the presence of the cross-site interaction, a non-zero photon number difference between the sublattices may develop. This broken symmetry phase is characterised

by the order parameter $\Delta n = |\langle n_A \rangle - \langle n_B \rangle|$, where A and B are sublattice indices. Figure 18(a) shows the order parameter as a function of the hopping strength and cross-Kerr nonlinearity for $U = 1$. The coloured region indicates the broken-symmetry (or crystalline) phase, where the photon number distribution exhibits a checkerboard pattern. We see that the interaction term favours the broken symmetry phase, whereas the hopping tends to restore the symmetry. Remarkably though, having $V \neq 0$ is not a prerequisite to obtain the checkerboard phase, unlike in the equilibrium counterpart [144]: it is possible, although much harder, for the nonequilibrium steady-state to have non-zero $\Delta n \neq 0$ even with $V = 0$. The requirements are a non-zero initial imbalance and a finite hopping strength.

In figure 18(b), the effects of driving field detuning, δ , is shown for $U = 0$ and $zV = 0.6$. Here the situation gets more interesting. A new phase appears (shaded green area) where the steady-state never becomes truly stationary in that there is a residual time dependence of $\langle a \rangle$ (on top of a trivial time dependence due to driving). A closer inspection on the reduced density matrix of the sublattice shows that there is a global dynamical phase coherence on top of the checkerboard pattern, which led Jin and coworkers to call this phase a *photon supersolid phase*. Similar phases were also found in the

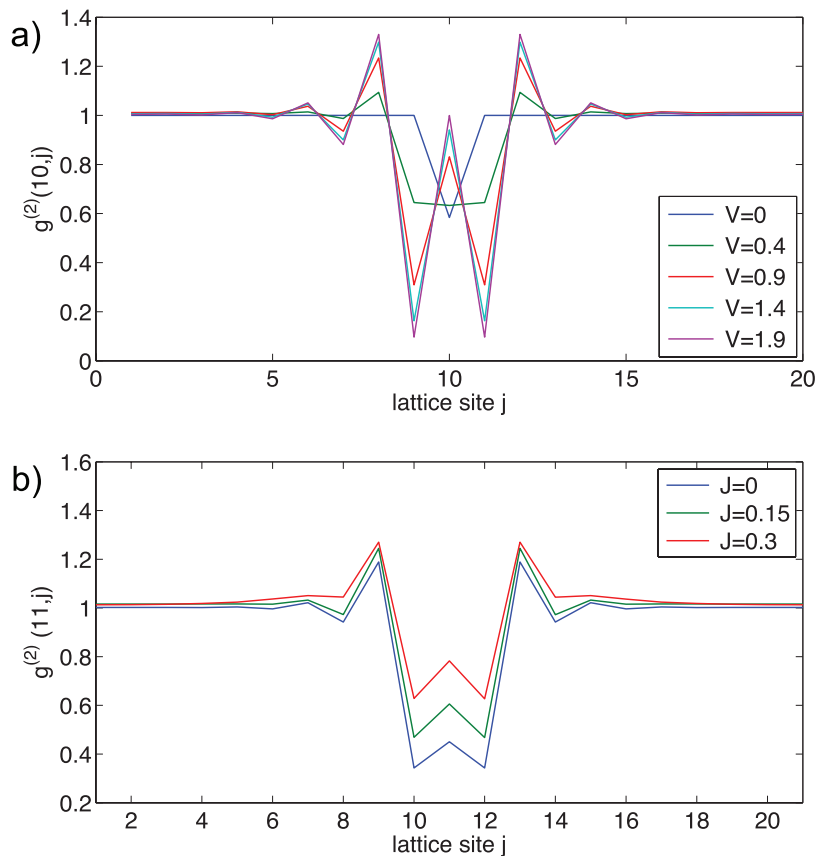


Figure 19. Matrix product operator results for 1D CRA. (a) $g^{(2)}(10,j)$ for $\delta = 0$, $J = 0$, $U = 0.5$, and $\Omega = 0.4$. (b) $g^{(2)}(11,j)$ for $\delta = 0$, $V = 1$, $U = 1$, and $\Omega = 0.4$. Reprinted with permission from Jin *et al* [144]. Copyright 2013 by the American Physical Society.

equilibria setting for an extended JCH model with the nearest neighbour interaction between the qubits [146].

The existence of the crystalline phase was corroborated by performing numerical simulations using the matrix product operator technique in 1D [125]. This approach takes into account quantum fluctuations ignored in the mean-field analysis and is therefore much more reliable. The results are shown in figure 19. The nature of the crystalline phase is displayed in the second-order intensity correlation function $g^{(2)}(i, j)$. Figure 19(a) plots this function for 20 cavities in the absence of hopping ($J = 0$). In this regime, the staggered distribution of photons is manifest, especially for larger values of V . Figure 19(b) plots $g^{(2)}$ for 21 cavities for various values of hopping strengths, displaying the suppression of crystalline phase with increasing hopping strength.

3.4.2. Majorana-like modes. As the last detailed review of this section we look at a proposal by Bardyn and Imamoglu on a photonic realisation of Majorana-like modes (MLMs) in a 1D CRA [147]. The nonequilibrium steady state of the driven-dissipative version of the model has been studied by Joshi and coworkers in a different context [148]. There the model was shown to be equivalent to a transverse field anisotropic XY model, whose NESS was calculated using a matrix product operator representation. Quantum entanglement and correlations near the critical point (of the equilibrium system) were found to reveal interesting similarities and differences to the equilibrium physics. For instance, singular behaviour was

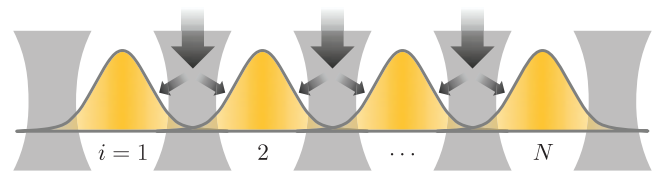


Figure 20. Schematic diagram of a cavity array setup for realising Kitaev's toy model. Cavity modes have strong Kerr-nonlinearity to inhibit occupation of multiple photons, while the parametric pumping of the inter-cavity fields produce the p-wave term. Reprinted with permission from Bardyn and Imamoglu [147]. Copyright 2012 by the American Physical Society.

found in the isotropic limit where the range of entanglement diverges (with vanishing magnitude), which is very distinct from the ground state behaviour. We refer the interested reader to the original article.

The Majorana modes are exotic half-a-fermion zero energy modes that can form, among others, in a 1D topological p-wave superconductor described by Kitaev's toy model [149]. The latter involves the so-called p-wave pairing term, $c_i c_{i+1} + \text{H.c.}$, where c_i is the fermion annihilation operator at site i , and is crucial for the formation of Majorana modes. To realise Kitaev's model with photons, the authors employ the hard-core limit ($U \gg J$) of the BH model and a parametric driving of the inter-cavity field as shown in figure 20. In the hard-core limit ($U \gg |\Delta|$), the effect of the parametric driving (with an amplitude $\Delta = |\Delta|e^{i\phi}$) is to introduce the squeezing term

$$H_{\text{drive}} = |\Delta| \sum_i^{N-1} (e^{i(2\omega_p t + \phi)} a_i a_{i+1} + \text{H.c.}), \quad (24)$$

where a_i s are the hard-core photon operators. Using the Jordan Wigner mapping $c_i = \prod_{j=1}^{i-1} (-\sigma_j^z) \sigma_i^-$ with $\sigma_i^- = a_i$, the total Hamiltonian is written as

$$H = -J \sum_{i=1}^{N-1} (c_i c_{i+1} + \text{H.c.}) + |\Delta| \sum_{i=1}^{N-1} (e^{i\phi} c_i c_{i+1} + \text{H.c.}) - \sum_{i=1}^{N-1} c_i c_i, \quad (25)$$

where c_i s are fermionic operators and $\Delta = \omega_p - \omega_c$ is the pump-resonator detuning.

The above Hamiltonian is identical to Kitaev's model of 1D p-wave superconductor of spinless fermions and hosts localised zero-energy Majorana modes [149]. The latter can most readily be seen in the limit $J = \Delta > 0$ and $\phi = 0$, in which the Hamiltonian can be written as

$$H = iJ \sum_{i=1}^{N-1} d_{2i} d_{2i+1} = -J \sum_{i=1}^{N-1} \sigma_i^x \sigma_{i+1}^x, \quad (26)$$

where the Majorana operators are defined as $d_{2i-1} = c_i + c_i$ and $d_{2i} = -i(c_i - c_i)$. The Majorana operators d_1 and d_{2N} are absent from the Hamiltonian and therefore the energy does not depend on whether or not the non-local fermion $f = (d_1 + d_{2N})/2$ is present. This means that the ground state is two-fold degenerate, characterised by the Majorana qubit operator

$$\sigma_M^z = i d_1 d_{2N} = \prod_{j=1}^N (-\sigma_j^z) \sigma_N^x \sigma_1^x. \quad (27)$$

The stringlike operator $P \equiv \prod_{j=1}^N (-\sigma_j^z)$ corresponds to the parity operator of the total number of (hardcore) photons. It commutes with the Hamiltonian and is therefore conserved, meaning that the Majorana qubit is associated with the end qubits only, thus (topologically) protected from local perturbations that preserves parity.

In the proposed photonic system, local dissipation breaks the parity and therefore also the topological protection of the Majorana qubit. However, the existence of localised Majorana modes and their characteristic non-Abelian braiding do not depend on the parity protection, and can therefore be simulated. The Majorana modes can be detected by attaching two probe cavities at the two ends of the array and measuring their second order cross-correlations. Due to the so-called Majorana mediated Cooper pair splitting [150, 151], the nonlocal Majorana qubit mediates a nonlocal coherent exchange of photons between the probe cavities, and the cross-correlation function reveals strong bunching in the topologically non-trivial regime as shown in figure 21. The braiding operation can also be simulated by using the tunnel-braiding operation [152], where the Majorana edge mode in one end of the array is tunnel-coupled, via an intermediate cavity, to the Majorana edge mode in another array. A sequence of operations such as turning on and off the tunneling amplitude to the intermediate cavity can be performed to simulate the braiding operation.

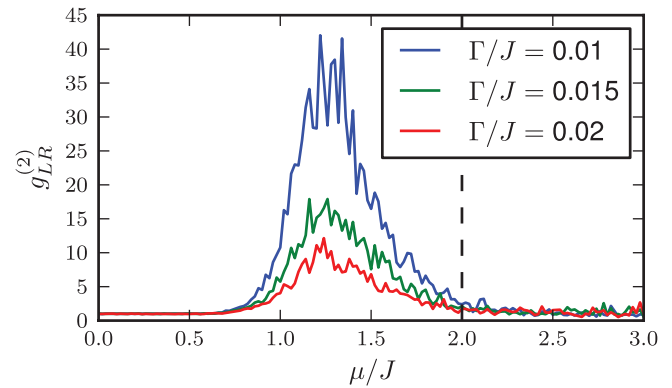


Figure 21. Second-order cross-correlation function between the left and right probe cavities as a function of the detuning μ for 10 cavities (excluding probe cavities), $\Delta/J = 1$, and $J_{L,R}/J = 0.02$. $\Gamma/J = \Gamma_{L,R}/J$ denote cavity loss rates. Majorana-like modes are expected in topologically nontrivial regime (left of the vertical dashed line). Strong bunching is observed inside this region for large J/J and for small dissipation rates. Reprinted with permission from Bardyn and Imamoglu [147]. Copyright 2012 by the American Physical Society.

3.5. Further interesting works

There are many more works that address interesting out-of-equilibrium physics arising in CRAs, which we did not have the space to cover in detail. Here, we provide a brief survey of these works for the interested reader.

Photon statistics in driven-dissipative BH or JCH dimers have been investigated by many authors. One of the main themes is how the photon statistics, as measured by the local intensity intensity correlation function $g^{(2)}$, change with the nonlinearity-hopping ratio. Gerace and coworkers showed that photon correlations can be used to reveal strongly correlated physics in a photonic Josephson junction—a three-site array with two end cavities coherently driven and the middle site containing single-photon nonlinearity [153]. Ferretti *et al* have studied a homogeneously driven case for a BH dimer and found a crossover between coherent and anti-bunched regimes [154]. An independent study on the JCH dimer was carried out by Leib and Hartmann, by mapping the system to an attractive BH model [155]. Driving one of the cavities and measuring $g^{(2)}$ on the other, they observed the same crossover. A more detailed study on photon transport was carried out by Biella *et al* for up to 60 Kerr-nonlinear resonators, in which both the transmission spectrum and second-order correlation functions were evaluated [156]. Going beyond coherent driving, effects of quantised driving fields were investigated by sending two-photon input states into a BH dimer [157]. Effects of incoherent driving was also investigated by Ruiz-Rivas and coworkers, in which a spontaneous build-up of collective coherence was found [158].

The crossover from the weak to strong hopping for a dimer as well as the infinite lattice was investigated by Nissen and coworkers [159]. There, in the dimer case, the antibunching was shown to persist up to a large value of hopping ($J/g \approx 10$), for driving strengths comparable to or larger than the dissipation rate. However, a semiclassical analysis in the limit of large coordination number shows that the antibunching disappears with increasing system size. On the other hand, photon super-bunching was also shown occur in driven dissipative

coupled resonator arrays, if the laser driving is tuned to the lowest-lying two-photon (polaritonic) mode in the BH (and JCH) system as shown by Grujić *et al* [160]. In fact, we have already observed the same behaviour while discussing fermionisation of photons. TEBD simulations of 2–7 coupled JC cavities with homogeneous driving shows that when the hopping strength J is larger than a critical value, the system exhibits photon (super) bunching, the magnitude of which decreases with increasing system size. Next, we would like to discuss an interesting effect called unconventional photon blockade. Normally, a large value of nonlinearity ($U, g \gg \gamma$) is necessary to induce photon antibunching. However, Liew and Savona discovered that antibunching can occur in a weakly nonlinear ($U < \gamma$) dimer upon making a judicious choice of parameters [161]. Soon after, the origin of this effect was identified as a destructive quantum interference between excitation pathways [162] and a similar effect was shown to arise in resonators with a χ^2 nonlinearity [163].

Quantum entanglement in driven-dissipative CRAs has also been investigated. Angelakis *et al* have studied entanglement between polaritons formed at two cavities, where the latter are coupled via an empty resonator mode [164]. Furthermore, a generalisation to three sites that are interconnected via three coherently-driven waveguides modes allows the entanglement to be controlled [165, 166]. In an alternative scheme, Liew and Savona considered three-site BH system with the middle site driven and found steady-state entanglement between the spatially separated modes [167]. An interesting aspect of this work is that, just like in the authors' antibunching work, only a small amount of nonlinearity is required. Furthermore, by repeating the three site setup, a multimode entanglement can be generated [168].

Finally, we would like to mention studies in 2D systems. We have already come across the latter when we reviewed nonequilibrium signatures of the superfluid-insulator transition [133] and the photonic supersolid phase [144, 145]. The phase diagram of the driven-dissipative BH array (without the extra cross-Kerr interaction term) was studied by Le Boit and coworkers [169, 170]. While the Mott-lobe-like structures were found, the phase diagram in the nonequilibrium setting exhibits clear differences to its equilibrium counterpart. This points to rich many-body physics beyond the equilibrium regime, which arises due to the interplay between driving and dissipation. Verifications of these mean-field results are an important future direction, as predicted effects such as bistability may not survive quantum fluctuations. Issues of bistability has been studied in 1D lattices by comparing exact numerical results against mean-field results. Mendoza-Arenas *et al* [171] have used matrix product states to simulate up to 60 sites to observe vanishing bistability, while Wilson *et al* [172] showed that in a finite system, the bistability manifests itself as a switching between macroscopically distinct states. Note that while 1D lattices can be numerically simulated, an efficient method for 2D arrays is still missing. Towards this direction, new numerical methods such as the corner-space renormalisation method [173] and self-consistent projection operator theory [132] are currently being developed.

An interesting possibility in 2D that is absent in 1D is to introduce artificial magnetic fields by inducing phase-dependent hopping terms. This allows one to implement quantum Hall-like models for photons as we have looked at earlier. Driven-dissipative signatures in such systems were studied by various authors. Umucalilar and Carusotto proposed a method to experimentally verify the fractional quantum Hall state hidden in the NESS of a weakly driven array [100]. In a similar setting, Hafezi and coworkers showed how $g^{(2)}$ measurements can be used to infer the underlying fractional quantum Hall states [102]. Efforts to devise methods to experimentally measure topological invariants in integer quantum Hall systems have also been made. Ozawa and Carusotto showed that the Chern number and the Berry curvature can be measured by following the displacement of a localised excitation by a coherent driving field [174], while Berceanu *et al* showed that by adding a weak harmonic potential to the model, the momentum-space Landau levels can be observed [175]. Alternatively, Hafezi [176] and Bardyn *et al* [177] showed that twisted boundary conditions can be implemented to experimentally measure the topological invariants, while Ma *et al* have proposed a way to measure the real space Chern number using spectroscopic signals [178]. Methods to stabilise strongly-correlated states of light using auxiliary two-level atoms have also been suggested [179, 180].

3.6. Experimental implementations

Before we finish this section, perhaps a few words on experimental realisations are in order. There are a number of promising experimental platforms to realise the JCH (or the BH) model: superconducting circuits, photonic crystal devices with quantum dots, microcavities connected by optical waveguides, polaritons in microstructures, and trapped ions. The trapped ion implementation uses phonons, the quantised vibrational motions of trapped ions, instead of photons and have been experimentally demonstrated for the dimer case [181]. 2D patterns of micropillars etched out of a semiconductor microcavity that can host exciton polaritons is a viable experimental platform especially if the polaritonic nonlinearity can be enhanced to the few-photon level. Recently, spin orbit coupling has been demonstrated in this platform [182]. Microcavities plus optical waveguides is an innovative platform suggested by Lepert *et al* [48] that uses cavities formed by open microcavities closed by coated waveguide tips. An emitter placed in each resonator acts as a two-level atom, while evanescent coupling between waveguides provide the photon hopping mechanism. Photonic crystals are dielectric devices with periodically patterned holes, where missing holes called defects can act as cavities. When a semiconductor is used to make a crystal, a quantum dot (artificial atom) grown in each defect resonator can allow the resulting system to be described by the JCH model. Majumdar *et al* have experimentally implemented two cavities coupled to a single quantum dot in this system [183].

The platform that shows most promise is superconducting circuits. The JC dimer has been implemented by Raftery *et al*

[135] (the BH dimer has also been implemented by Eichler *et al* [184]), and lattices up to 200 resonators in a Kagome geometry without atoms (superconducting qubits) have been fabricated [46, 185]. Scanning defect microscopy has been used to experimentally map out the normal-mode structure of microwave photons in such a lattice [186] a technique which may prove useful in studying nonequilibrium phase transitions and photonic quantum simulators. Right after the submission of this review, a report demonstrating a 1D lattice of 72 sites, each coupled to superconducting qubits, have appeared on a preprint server, demonstrating a dissipative phase transition in which the steady state changes drastically as the mean photon number is increased [187].

4. Simulating strongly correlated effects in 1D with photons in waveguides with EIT-based nonlinearities

Simulations of strongly correlated effects with photons are not limited to lattice systems. Continuous 1D systems can also be simulated by using nonlinear waveguide systems instead of coupled resonator arrays. This section reviews proposals in this young field. We first explain the mechanism to produce strongly interacting polaritons in 1D waveguides and show how an effective Hamiltonian can be engineered. Equipped with this knowledge, we go on to review various proposals on simulating strongly correlated many-body system in 1D continuum. These range from the condensed matter models such as the Tonks Girardeau gas of polaritons, quantum sine-Gordon model, Bose Einstein condensation of polaritons, photonic Luttinger liquids and Cooper pairing to interacting relativistic model named the Thirring model. We end the section with a brief survey of experimental progress in realising relevant nonlinear optical setups and a comment on possible future directions.

4.1. Background

Quantum simulations of 1D quantum field theories with strongly interacting photons (or more precisely, polaritons) to be reviewed in this section rely on two main techniques. The first is the technique of stationary light, allowing one to trap pulses of light and describe its time evolution via an effective Hamiltonian. The second is creating strong nonlinearity, achieved by introducing specifically structured atoms to mediate interaction between photons. Both are closely tied to the phenomenon of electromagnetically induced transparency (EIT) [188–190] as we will explain shortly.

4.1.1. Stationary pulses of light. The concept of stationary light has been proposed and demonstrated by Bajcsy *et al* [191]. The main idea is based on dark state polaritons [192] formed in EIT, which we will briefly explain here. Consider an electric field propagating through an atomic medium. Normally, if the electric field is resonant with an atomic transition, it will be strongly attenuated as it propagates through the medium. However, a laser field driving another transition can

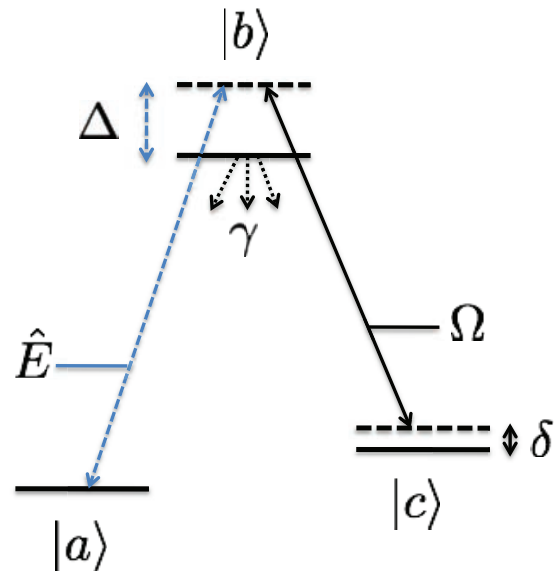


Figure 22. Atomic level scheme to create dark state polaritons. $|a\rangle$ and $|c\rangle$ are stable states, E is a quantum field, and Ω is the Rabi frequency of a classical control field.

induce destructive quantum interference between the excitation pathways and cancel this attenuation, i.e. the extra laser field may induce transparency. In EIT, this is accompanied with a steep dispersion, resulting in a dramatic reduction of the group velocity and enhanced nonlinearity.

Dark state polaritons: Dark state polaritons are collective excitations of light and matter formed when a quantum field propagates under specific conditions that allow EIT. A typical atomic level scheme employed in realising EIT, called a Λ -scheme, is depicted in figure 22. It comprises of a dissipative excited state $|b\rangle$ and two steady states $|a\rangle$ and $|c\rangle$. One transition to the excited state is coupled to a quantum field E while the other is coupled to a classical control (laser) field of Rabi frequency Ω . The Hamiltonian describing the evolution of the atom-field system is

$$H = -n \int dz \left[\Delta \sigma_{bb} + \delta \sigma_{cc} + g \sqrt{2\pi} (\sigma_{ba} E + \text{H.c.}) + (\Omega \sigma_{bc} + \text{H.c.}) \right], \quad (28)$$

where n is the linear density of atoms, g is the single photon-atom coupling strength, and $\sigma_{ij} \equiv \sigma_{ij}(z, t)$ are continuous average spin-flip operators in a small region around the position z . The propagation of the electric field is governed by the equation

$$(\partial_t + v \partial_z) E(z, t) = i \sqrt{2\pi} g n \sigma_{ab}(z, t), \quad (29)$$

where v is the speed of light in the absence of atoms.

Assuming that atoms are mostly in the ground state $|a\rangle$ and adiabatically eliminating the fast-varying atomic coherence σ_{ab} in the Heisenberg Langevin equation, the propagation equation reduces to (for a derivation, see for example [193])

$$(\partial_t + v_g \partial_z) \Psi(z, t) = \frac{i 2\pi g^2 n v_g \delta}{(\Omega^2 - i \delta \Gamma) v} \Psi(z, t). \quad (30)$$

The field operator Ψ describes a collective excitation of the quantum field E and the atomic excitation σ_{ab} which is called the dark state polariton. $\Gamma = \gamma/2 - i\Delta$ where γ is the decay rate from the excited state $|b\rangle$ and $v_g \approx v\Omega^2/(\Omega^2 + 2\pi g^2 n)$ in the limit $\Omega^2 \gg |\delta\Gamma|$, with δ the two-photon detuning as depicted in figure 22. The dark state polariton operator reduces to $\Psi \approx g\sqrt{2\pi n}E(z, t)/\Omega$ if the energy is mostly stored in the form of atomic excitations, which happens when $2\pi g^2 n \gg \Omega^2$. In such a regime the group velocity v_g is much smaller than the speed of light in the empty waveguide, v .

Stationary light: Stationary light is formed when there are two counter-propagating control fields that form a Bragg grating for the quantum fields propagating in the opposite direction. The dark state polaritons are then trapped in the system while maintaining a finite photonic component, following the intensity profile of the control fields. Being stationary, these polaritons have longer time to interact with each other, which effectively enhances the nonlinearity of the system. To derive the equation of motion for these stationary polaritons, we need to first introduce some notations. Counter propagating fields will be denoted as E_{\pm} and Ω_{\pm} , where $E = E_+e^{ik_c z} + E_-e^{-ik_c z}$ and $\Omega = \Omega_+e^{ik_c z} + \Omega_-e^{-ik_c z}$. k_c is the wavenumber of the control field, which we assume to be similar to the wavenumber of the quantum field. In turn, this induces a slowly varying optical coherence $\sigma_{ab, \pm}$ defined through $\sigma_{ab} = \sigma_{ab, +}e^{ik_c z} + \sigma_{ab, -}e^{-ik_c z}$. Because of the wavenumber mismatch, there is an additional term $i\Delta\omega$ in the rhs of the propagation equation (29), where $\Delta\omega = v(k_0 - k_c)$ (assuming the same speed of light v for both the quantum and classical light) [194].

If the atoms are hot enough, we can use the secular approximation, i.e. neglect the fast oscillating contributions proportional to $e^{\pm i2k_c z}$ to obtain propagation equations similar to (30) for counter propagating dark state polaritons $\Psi_{\pm} = g\sqrt{2\pi n}E_{\pm}/\Omega_{\pm}$, but with extra terms that couple the counter propagating fields [191, 193]. When $\Omega_+ = \Omega_- \equiv \Omega_0$, these equations can be grouped into the equations for the sum, $\Psi_S = (\Psi_+ + \Psi_-)/\sqrt{2}$, and the difference, $\Psi_D = (\Psi_+ - \Psi_-)/\sqrt{2}$ modes:

$$\partial_t \Psi_S + 2v_g \partial_z \Psi_D = i \left(\delta - 2\Delta\omega \frac{v_g}{v} \right) \Psi_S \quad (31)$$

$$\partial_t \Psi_D + v \partial_z \Psi_S = -\frac{2\pi g^2 n}{\Gamma} \Psi_D. \quad (32)$$

In the limit of interest, $2\pi g^2 n \gg \Gamma$, the difference mode Ψ_D can be adiabatically eliminated to give

$$i\partial_t \Psi_S = -\frac{1}{2m_{\text{eff}}} \partial_z^2 \Psi_S + V_{\text{eff}} \Psi_S, \quad (33)$$

where $m_{\text{eff}} = -\pi g^2 n / [v v_g (\Delta + i\gamma/2)]$ and $V_{\text{eff}} = 2\Delta\omega v_g / v - \delta$ can be thought of as a (complex) effective mass and an effective potential in analogy to the Schrödinger equation. Note that the group velocity of the sum mode is zero (it becomes non-zero for non-identical control fields Ω_{\pm}), indicating that we have a stationary light.

Assuming $\Delta = -|\Delta| \gg \gamma$, the effective mass becomes real and can be written as $\gamma_{1D} n / 4v_g |\Delta|$, where $\gamma_{1D} = 4\pi g^2 / v$ can be

identified as the spontaneous emission rate of a single atom into the waveguide. $\eta = \gamma_{1D}/\gamma$ then defines a single-atom cooperativity, the efficiency of coupling into the waveguide. With these definitions the optical depth of the waveguide is defined as $OD = \eta n l$, where l is the length of the waveguide. OD quantifies the strength of the interaction between photons and the medium and a large value of it (≈ 1000) is typically required to get into the strongly interacting regime considered in this section.

Preparation and detection of stationary pulses of light:

Quantum simulations using stationary light largely consists of three steps: (1) loading a traveling pulse, (2) converting it to a stationary pulse that undergoes a prescribed evolution, and (3) detecting the resulting stationary light. Here let us illustrate this with a typical example. A quantum pulse of light E_+ is sent in from the left with only the control field Ω_+ initially turned on. In this typical EIT scheme, the quantum pulse travels slowly with the group velocity $v_g \propto \Omega^2$. When the pulse has completely entered the medium $\Omega(t)$ is adiabatically turned to zero, trapping the entire pulse in the system [192]. Following this loading process, stationary light is created by adiabatically increasing both $\Omega_+(t)$ and $\Omega_-(t)$ simultaneously, creating the long-lived sum mode Ψ_S which evolves under an engineered Hamiltonian of choice. After a dynamical evolution or an adiabatic change of the initial state, the pulse is released by turning off Ω_- which converts the stationary pulse to a propagating one. The out-going pulse can then be detected using standard quantum optical measurements; for example, a photon correlation measurement can detect spatial correlations of the stationary pulse that have been converted into temporal correlations.

4.1.2. EIT nonlinearities with four-level atoms. The last essential ingredient in simulating strongly correlated effects with photons is a strong nonlinearity (between photons or more accurately polaritons). Normally, to get photons to interact with each other strongly, one requires them to be resonant with the atoms, which unfortunately entails strong dissipation. As we have already hinted, an effective way to overcome this problem is to use EIT to suppress the linear absorption while enhancing the Kerr-nonlinearity through a quantum interference effect [190]. However, the problem is that the magnitude of the nonlinearity is limited by dissipation in the usual three-level scheme.

A scheme that uses four level atoms to generate a giant resonantly enhanced nonlinearities was first introduced in [195], where the atomic structure depicted in figure 23 was shown to yield a cross-Kerr nonlinearity between the fields E_1 and E_2 . The imaginary part of the third-order susceptibility $\chi^{(3)}$ can be made small by increasing the detuning Δ_2 , while leaving the real part finite and, in fact, orders of magnitude larger than those obtained from the usual 3-level scheme. Self-Kerr nonlinearity can also be obtained by replacing E_2 with E_1 [70]. These types of nonlinearity are exactly what one needs to simulate strongly interacting fields with photons as we will explain in the remainder of this section. We will continue to adopt the Heisenberg Langevin equation approach to study

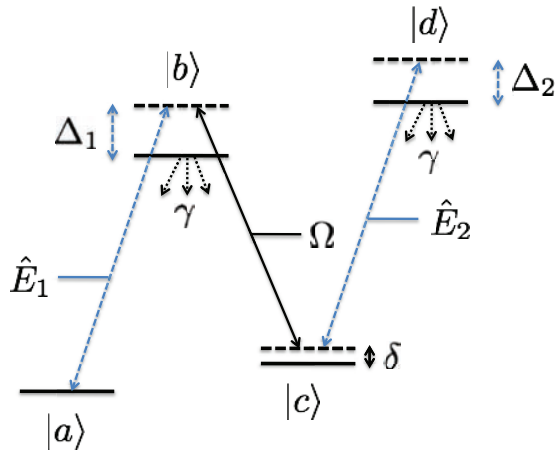


Figure 23. Atomic level scheme to generate a giant resonantly-enhanced Kerr nonlinearity.

the dynamics in the low-loss regime in this review, but a master equation description can also be employed as shown by Kiffner and Hartmann [196].

4.2. Tonks–Girardeau gas of photons

Combining the techniques of stationary light and giant Kerr nonlinearity, Chang *et al* [52] showed that photons can crystallise and mimic the behaviour of strongly interacting 1D bosons called the Tonks–Girardeau (TG) gas [127, 197]. The system consists of an ensemble of four-level atoms interfaced with a tight-confining waveguide such as a tapered optical fibre or a hollow-core optical fibre. There has also been a proposal to observe a TG gas induced by a purely-dissipative interaction [198] in the same setting [199], but we will not discuss it here. Let us start with a gentle introduction to the physics of 1D Bose gas before delving into the proposal of Chang and coworkers.

Studies have shown that in 1 (spatial) dimension, effects of quantum fluctuations are enhanced and interacting particles show behaviour dramatically different from the higher dimensional analogues [200]. A famous example is the TG gas, where strongly interacting bosons are effectively fermionised. Dynamics of the simplest interacting bosons in 1D are governed by the Lieb–Liniger model [201], described by the Hamiltonian

$$-\int dz \Psi(z) \frac{1}{2m} \partial_z^2 \Psi(z) + U \Psi(z) \Psi(z) \Psi(z), \quad (34)$$

which for a fixed linear density n is characterised by a single dimensionless parameter $\gamma_{\text{LL}} = nU/(n^2/2m)$. When $\gamma_{\text{LL}} \gg 1$, the bosons are impenetrable, which means that there is an effective exclusion principle and the system behaves in many ways like a non-interacting Fermi gas. This fermionisation can be observed in the second-order density density correlation function $g^{(2)}(z, z') = \langle I(z)I(z') \rangle / (\langle I(z) \rangle \langle I(z') \rangle)$, for example, as pointed out by Chang and coworkers. The TG gas has been realised with cold atoms in optical lattices [202, 203], but a realisation with photons brings in a new set of techniques such as the standard photon-correlation measurements.

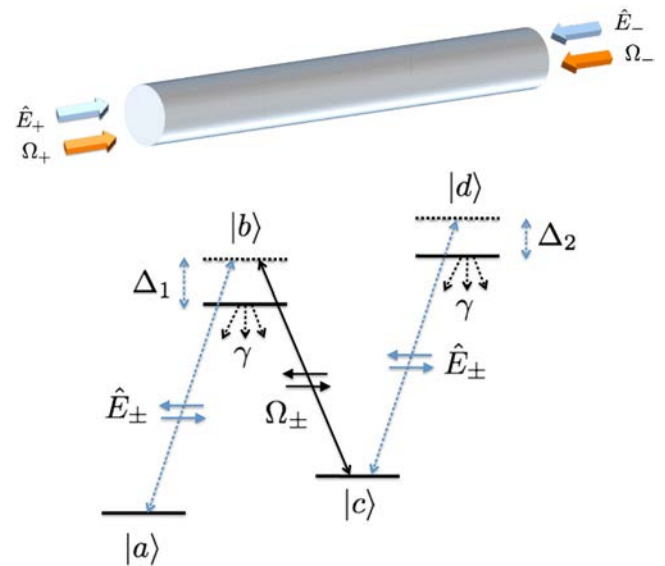


Figure 24. Nonlinear waveguide setup simulating the Lieb–Liniger model with stationary pulses of light. The waveguide contains 4-lv atoms whose coupling scheme with the quantum and control fields is indicated.

A schematic diagram of the proposed setup to realise a TG gas of photons is depicted in figure 24. The two-photon detuning δ is assumed to be zero and each atomic coherence is coupled to two counter-propagating fields as in the stationary light setting. Furthermore, the atomic transition $c \leftrightarrow d$ is coupled to the same quantum fields as the transition $a \leftrightarrow b$ so that the self-Kerr nonlinearity is induced. In the absence of the fourth lv $|d\rangle$, we have already seen that the sum mode obeys the Schrödinger equation (33). With the fourth level, this equation becomes a nonlinear Schrödinger equation (assuming $V_{\text{eff}} = 0$) [52]

$$i\partial_t \Psi(z, t) = -\frac{1}{2m_{\text{eff}}} \partial_z^2 \Psi(z, t) + 2g \Psi(z, t) \Psi^2(z, t), \quad (35)$$

where $m_{\text{eff}} = -\pi g^2 n / [v v_g (\Delta_1 + i\gamma/2)]$ as before and $2g = 2\pi g^2 v_g / [(\Delta_2 + i\gamma/2)v]$. We have assumed for convenience that the two excited states have the same decay rate γ . Because the dark state polariton operators obey the bosonic commutation relations, the above equation describes the evolution under the Lieb–Liniger Hamiltonian (34). In particular, the dimensionless parameter γ_{LL} is written in terms of bare optical parameters as

$$\gamma_{\text{LL}} = \frac{m_{\text{eff}} g}{n_{\text{ph}}} = -\frac{\pi^2 g^4}{(\Delta_1 + i\gamma/2)(\Delta_2 + i\gamma/2)} \frac{n}{n_{\text{ph}}}, \quad (36)$$

where n_{ph} is the linear density of photons at the centre of the pulse. Notice that there is a non-zero imaginary part, which will be neglected on the basis that $|\Delta_{1,2}| \gg \gamma$.

Among the characteristic features of a TG gas is an oscillating density–density correlation function, similar to the Friedel oscillations in electronic systems with an impurity [204]. In the TG limit, the second-order intensity correlation function $g^{(2)}(z, z') = \langle I(z)I(z') \rangle / (\langle I(z) \rangle \langle I(z') \rangle)$ of the ground state takes the form [205]

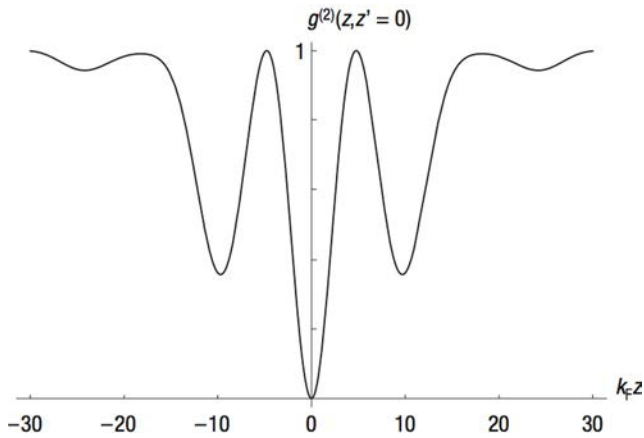


Figure 25. Density density correlation function $g^{(2)}(z, z' = 0)$ of the final TG gas of photons. Initial density profile is $n_{\text{ph}}(z) = n_0(1 - z^2/z_0^2)^{1/2}$, $N_{\text{ph}} = 10$, $z_0 = 5k_F^{-1}$, and $t = 10\omega_f^{-1}$. Reprinted with permission from Chang *et al.*, Macmillan Publishers Ltd: [52]. Copyright 2008.

$$g_{\text{TG}}^{(2)}(z, z') = 1 - \left(\frac{\sin k_F(z - z')}{k_F(z - z')} \right)^2, \quad (37)$$

where $I(z) = \Psi(z)\Psi(z)$ and $k_F = \pi n_{\text{ph}}$ is the Fermi momentum of the photonic TG gas.

The $2k_F$ oscillations can be observed experimentally by following the preparation and detection procedure outlined in section 4.1.1: an initial pulse of coherent state is loaded into the waveguide and turned into a stationary pulse. Then the dimensionless interaction parameter γ_{LL} is increased from zero to a large value by changing, for example, the detuning. The initial coherent state, which is an eigenstate of the free Hamiltonian, remains in an eigenstate of the Hamiltonian (with non-zero interaction strength) and therefore exhibits the Friedel oscillations. The stationary pulse can then be converted to a traveling pulse, whose temporal correlation function reveals the density density correlation function of the simulated quantum state.

An example is shown in figure 25, taken from [52], for an initial density profile $n_{\text{ph}}(z) = n_0(1 - z^2/z_0^2)^{1/2}$ under an exponentially increasing interaction parameter γ_{LL} . The distance is in units of the inverse effective Fermi wave vector k_F and the final time is $t = 10\omega_f^{-1}$, where ω_f is the Fermi energy on the order of $n_{\text{ph}}^2/m_{\text{eff}}$. For an optical depth of ≈ 2000 and the cooperativity $\eta \approx 0.2$, the achievable maximum γ_{LL} is around 10.

4.3. Introducing an effective potential–Bose Hubbard and sine-Gordon models, and the ‘pinning’ transition

Looking back to equation (33), it is not too difficult to see that a spatially dependent two-photon detuning would induce an effective potential for the stationary light. Indeed, this fact has been noticed in a proposal to simulate the Klein tunnelling with stationary light [22]. Upon introducing another transition, one can induce a small spatially-dependent two-photon detuning and as a consequence the resulting nonlinear Schrödinger equation would have an effective potential term. Another

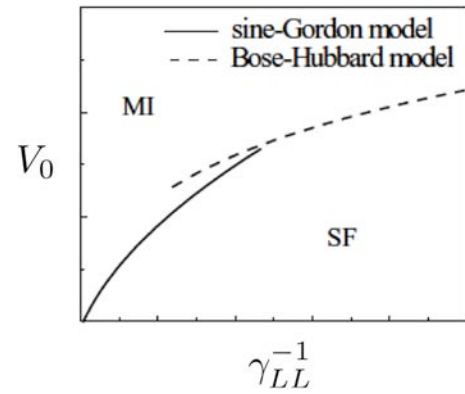


Figure 26. A figure showing the phase diagram of the Lieb Liniger model in the presence of a potential. The interaction strength and the lattice depth is changed by tuning an optical parameter which is not specified here. Reprinted with permission from Huo and Angelakis [206]. Copyright 2012 by the American Physical Society.

method is to induce a small change in the spatial profile of the atomic density [206]. The latter requires cold atomic gas so that the density profile does not change appreciably during the experiment. However, evolution of a stationary light in a cold atomic ensemble is different to that in a hot vapour because of the secular approximation discussed earlier in section 4.1.1 [207, 208] and one has to resort to a different atomic level scheme of a double-lambda type. Here, we discuss the effects of introducing a lattice potential to strongly interacting photons assuming that the lattice has been created via one of the two methods and defer a discussion on stationary light in cold atomic gases to the next section.

We follow Huo and Angelakis [206] and consider the Lieb Liniger model with an additional potential term of the form $V(z) = V_0 \cos^2(\pi n_{\text{ph}} z)$. The periodicity of the lattice potential is set such that the number of sites equals the number of photons in the waveguide. Depending on the lattice depth and the interaction strength, the system shows either the Mott insulating phase or the superfluid phase [209] as depicted schematically in figure 26.

There are two interesting limits in the phase diagram: (i) weakly interacting particles ($\gamma_{\text{LL}} < 1$) in a deep potential ($V_0 \gg E_r$) and (ii) strongly interacting particles ($\gamma_{\text{LL}} > 1$) in a shallow potential ($V_0 \sim E_r$), where $E_r = \pi^2 n_{\text{ph}}^2 / 2m_{\text{eff}}$ is the recoil energy. For case (i), the physics is well described by the well-known Bose Hubbard model [75, 210], where the lowest localised Wannier mode in each lattice site is coupled to the modes in its nearest neighbour sites with depth-dependent on-site interaction strength. As we have seen earlier, the Bose Hubbard hamiltonian reads

$$H_{\text{BH}} = -J \sum_{\langle i,j \rangle} a_i a_j + \frac{U}{2} \sum_i a_i a_i a_i, \quad (38)$$

where a_i is now interpreted as the annihilation operator for the Wannier mode at site i , $\sqrt{\pi} J / E_r = 4(V_0 / E_r)^{3/4} e^{-2\sqrt{V_0 / E_r}}$, and $U / E_r = \sqrt{2/\pi^3} (V_0 / E_r)^{1/4} \gamma_{\text{LL}}$. Note that the effective parameters J and U only depend on V_0 , E_r , and γ_{LL} , all of which can be tuned by changing quantum optical parameters. By tuning the value of U / E_r , through changing the value of

the detuning Δ_2 for example, one can observe the Mott-to-superfluid transition.

There is also an interesting quantum phase transition called a pinning transition in case (ii), when the interaction is strong. In the weak lattice limit, the particle density is weakly modulated and one is able to separate out the density perturbation and phase as canonically conjugate observables. Haldane was the first to consider this case and show that the quantum sine-Gordon model correctly describes the physics in this limit [211]. Following the work of B chler, Blatter, and Zwirger [209], we briefly reproduce the derivation of the sine-Gordon Hamiltonian here.

First consider a hydrodynamic approximation where one describes the bosonic field operator in the low energy limit as $\Psi \approx \sqrt{\rho_0 + \partial_z \theta / \pi} \exp(i\phi)$, where ρ_0 is the mean density of the atoms, $\partial_z \theta / \pi$ is the long-wavelength density fluctuation, and ϕ is the phase field. The latter two obeys the boson commutation relation $[\partial_z \theta(z), \phi(z')] = i\pi \delta(z - z')$. Neglecting the lattice potential for now, the low-energy physics is described by the Hamiltonian

$$H_0 = \frac{1}{2\pi} \int dz [v_J (\partial_z \phi)^2 + v_N (\partial_z \theta)^2]. \quad (39)$$

The first part comes from the kinetic energy where $v_J = \pi \rho_0 / m$ and the second term derives from the interaction energy with the coefficient $v_N = \partial_n / \pi$ determined by the inverse compressibility. To obtain the Hamiltonian due to the lattice potential, one needs to modify the density operator to account for its discrete character:

$$\rho(z) = \left[\rho_0 + \frac{1}{\pi} \partial_z \theta \right] \left[1 + 2 \sum_{l=1}^{\infty} \cos(l\theta + l\pi \rho_0 z) \right]. \quad (40)$$

In the commensurate limit (one particle per lattice cell), the dominant part of the potential arising from the lowest harmonic in the above equation takes the sine-Gordon form

$$H_V = \frac{n_{\text{ph}} V_0}{2} \int dz \cos(2\theta). \quad (41)$$

The Hamiltonian $H_0 + H_V$ is the 1D quantum sine-Gordon equation which is known to exhibit the so-called pinning transition [212]. This phase transition can best be described by the dimensionless parameter $K = \sqrt{v_J / v_N}$ that is related, in the absence of the periodic potential, to the Lieb-Liniger parameter γ_{LL} ; $K(\gamma \leq 10) \approx \pi / \sqrt{\gamma_{\text{LL}} - (1/2\pi)\gamma_{\text{LL}}^{3/2}}$ and $K(\gamma \gg 10) \approx (1 + 2/\gamma_{\text{LL}})^2$. When $K > K_c = 2$, the weak potential is irrelevant and the bosons are in the superfluid phase whereas for $K < K_c$ an arbitrarily weak potential can pin the bosons to lattice sites, achieving the Mott insulating state.

The procedure to observe these phases in the nonlinear waveguide system with a lattice potential is as follows. First a pulse containing a certain number of photons is loaded into the waveguide. Then one turns up the interaction strength and then the lattice potential adiabatically. This step can be realised experimentally by changing the detunings Δ_2 and δ . By the end of this step, the photonic state would have adiabatically

followed the Hamiltonian and consequently would exhibit either the superfluid or the Mott-insulating behaviour which can be observed by releasing the stationary pulse and performing correlation measurement on them as in the observation of a TG gas of photons.

4.4. Bose–Einstein condensation of stationary-light polaritons

The realisation of strongly interacting photons in the previous section relied on having a hot vapour of atoms so that the secular approximation holds. However, it is also possible to create stationary light with cold atoms [213, 214] as demonstrated in [215]. In particular, Zimmer *et al* [214] showed how the linear Schrödinger equation can be obtained with cold atoms using a slightly different atomic level scheme shown in figure 27(a). In this scheme, E_+ and E_- couple to different atomic transitions unlike in the usual Λ scheme where the two couple to the same transition, so the secular approximation no longer needs to be invoked. For equal control field strengths, $\Omega_+ = \Omega_-$, the stationary dark state polariton is defined as

$$\Psi(\mathbf{r}, t) = \frac{\cos \theta}{\sqrt{2}} (E_+(\mathbf{r}, t) + E_-(\mathbf{r}, t)) - \sin \theta S(\mathbf{r}, t), \quad (42)$$

where $\tan^2 \theta = 2\pi g^2 n / \Omega^2$, $\Omega^2 = \Omega_+^2 + \Omega_-^2$, and $S = \sqrt{n} \sigma_{ac}(\mathbf{r}, t)$. The Schrödinger equation obeyed by this field operator reads

$$i \partial_t \Psi(\mathbf{r}, t) = - \left[\frac{1}{2m_{\parallel}} \partial_z^2 + \frac{1}{2m_{\perp}} \Delta_{\perp} \right] \Psi(\mathbf{r}, t), \quad (43)$$

where $m_{\perp} = m v_{\text{rec}} / v_g$ and $m_{\parallel}^{-1} = m_{\perp}^{-1} k_p (\gamma v / 2\pi g^2 n) (2\Delta / \gamma + i)$. Here k_p is the wavenumber of the probe field and $v_{\text{rec}} = k_p / m$ is the recoil velocity of an atom of mass m .

Introduction of additional levels as in figure 27(b) adds the Kerr-type interaction between the dark state polaritons whose elastic collision rate can be much greater than the loss rates and thereby allow thermalisation of polaritons without significant losses [216]. The optical depth required to reach this regime is only modestly high at about $OD > 30$. For realistic parameters, the critical temperature to create a BEC out of dark state polaritons (as compared to the critical temperature for ideal bosonic atoms) is $T_c / T_c^{\text{atoms}} \approx 6 \times 10^5$ which is in the mK regime. The latter is in the same range as the temperature limit of about 1 mK imposed by the finite frequency window of EIT. Therefore, it is possible to observe the BEC of stationary light polaritons at temperatures several orders of magnitude higher than the critical temperature of atomic BECs.

In the stationary light setup, a BEC will be created not by reducing the temperature of the polariton gas, but by increasing the critical temperature of condensation through changing the effective mass. The steps to observe Bose–Einstein condensation of polaritons is then as follows. (i) A pulse of coherent light is trapped as stationary polaritons using the same method described in the previous section. Initially, the critical temperature is below the ambient temperature so there is no condensation. (ii) As the critical temperature is increased, by tuning the strength of the control laser, the polaritons

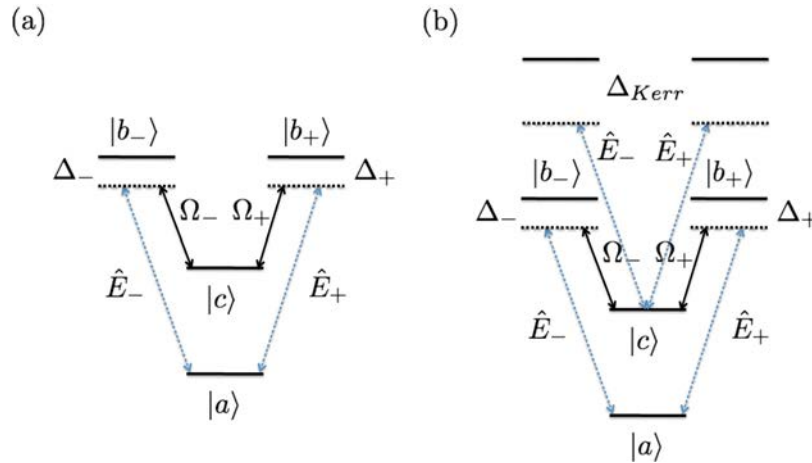


Figure 27. (a) Atomic level scheme for creating dark state polaritons using cold atoms. (b) Modified atomic level scheme to induce the Kerr interaction between dark state polaritons, allowing for them to Bose condense.

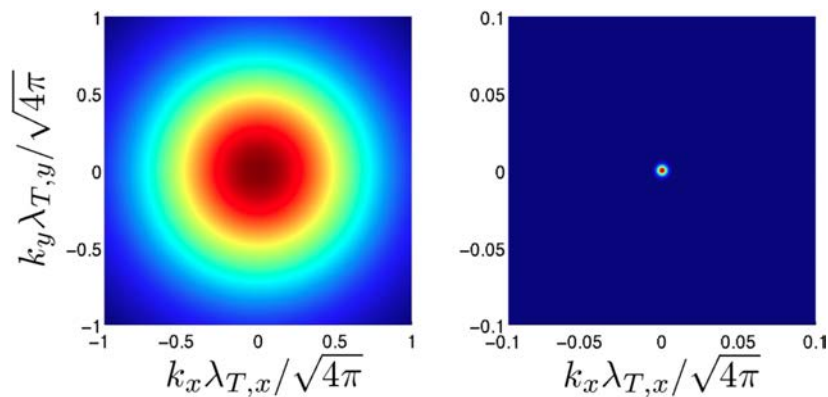


Figure 28. Transverse emission profile above (left) and below (right) the condensation temperature in arbitrary units, assuming an ideal quasi-homogeneous Bose-gas of width $178\lambda_{T,x}$, where $\lambda_{T,x}$ is the transversal de Broglie wavelength at temperature T . Reprinted with permission from Fleischhauer *et al* [216]. Copyright 2008 by the American Physical Society.

thermalise through elastic collisions and reach BEC before significant losses occur. This causes the macroscopic occupation of $\mathbf{k} = 0$ momentum state, which can be (iii) observed by converting the stationary polariton into a traveling one, whose transverse profile shows the onset of BEC. The latter is illustrated in figure 28, where the transverse emission profiles are shown at temperatures above (left) and below (right) the critical temperature. A similar proposal with Rydberg atoms to induce dipolar interaction between dark state polaritons have been made by Nikoghosyan *et al* [217].

4.5. Two-component bosonic models: Luttinger liquids, spin-charge separation and Cooper pairing with photons

So far in this section, we have reviewed works on quantum simulations of strongly interacting bosons when there is only a single species of bosons. Soon after the pioneering work on a TG gas of stationary light, Angelakis *et al* realised that the physics of two interacting bosons can also be simulated in a similar waveguide setup [53, 218]. Here, we describe how this leads to a realisation of the two-component Lieb-Liniger model, which could allow a clear experimental observation of spin-charge separation. Furthermore, by introducing a lattice potential, one

can also simulate a two-component Bose Hubbard model, which exhibits interesting behaviours such as (a 1D analogue of) the famous BEC-BCS crossover [219, 220].

A schematic diagram of the atomic level scheme that yields the two-component Lieb-Liniger model is shown in figure 29. Two different quantum fields E_1 and E_2 with frequencies $\omega_{qu}^{(1)}$ and $\omega_{qu}^{(2)}$ interact with two different species of 4-IV atoms labeled a and b and forms two polariton operators via the usual relation $\Psi_{j,\pm} = g\sqrt{2\pi n^y} E_{j,\pm} / \Omega_{xy}$. The figure depicts the level scheme for type- a atoms; atoms of type b have a similar coupling scheme except that the roles of E_1 and E_2 are reversed and the detunings are accordingly labeled by replacing a with b . We use $j = 1, 2$ to denote the polariton species, $x_1 = a, x_2 = b$ to label the atomic species, and we have assumed that the atom-photon coupling strength is independent of the atomic species and transition. n^a (n^b) denotes the density of atomic species a (b) and $\delta_{ij} = \omega_{qu}^{(i)} - \omega_{qu}^{(j)}$. By setting the detunings such that E_1 (E_2) is only coupled to atoms of type- b (a) through the transition $|3\rangle \leftrightarrow |4\rangle$, one obtains a cross-species interaction term on top of the self-interaction terms. The dynamics of the polaritons are thus governed by the two-component Lieb-Liniger model

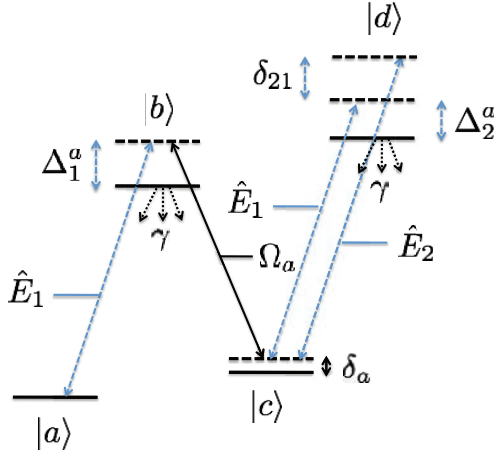


Figure 29. Atomic level scheme to realise the two-component Lieb-Liniger model, for the type- a atoms. Type- b atoms have the role of E_1 and E_2 reversed and the super- and sub-script a replaced by b , as well as $\delta_{21} \rightarrow \delta_{12}$.

$$H_{\text{cell}} = \int dz \sum_j \left[-\frac{1}{2m_j} \Psi_j(z) \partial_z^2 \Psi_j(z) + \frac{U_j}{2} \Psi_j(z) \Psi_j(z) \Psi_j(z) \Psi_j(z) \right] + \frac{V}{2} \rho_1(z) \rho_2(z), \quad (44)$$

where $\rho_j = \Psi_j(z) \Psi_j(z)$. m_j and U_j are defined as m_{eff} and $4g$ introduced earlier, with species-dependent optical parameters, whereas the inter-species interaction parameter V is new. For simplicity, we will assume that all species-dependence are suppressed. Then the inter-species interaction strength is compactly written as

$$V = \frac{16\pi g^2 n v_g}{\Delta_2}. \quad (45)$$

An alternative scheme where the two species correspond to different polarisations has also been proposed in [218]. We will come back to this setup in section 4.6 where a quantum simulation of an interacting relativistic model will be reviewed.

4.5.1. Luttinger liquid and spin-charge separation. We have already seen how Lieb-Liniger bosons can be described, in the low-energy sector, in terms of the long-wave density function $\partial_z \theta$ and the phase field ϕ . It turns out that the same decomposition applied to the two-component Lieb-Liniger model separates the Hamiltonian into two independent components, describing spin and charge components that travel in different speeds. Let us assume that the two species have identical parameters, i.e. $m_j = m$, $U_j = U$, and $\langle \rho_j \rangle = \rho$. Following the notations in [221] (see also [222]), the Hamiltonian (44) becomes $H = H_c + H_s$, where

$$H_c = \frac{1}{2\pi} \int dz v_c K_c (\partial_z \theta_c)^2 + \frac{v_c}{K_c} (\partial_z \phi_c)^2 \quad (46)$$

and

$$H_s = \frac{1}{2\pi} \int dz v_s K_s (\partial_z \theta_s)^2 + \frac{v_s}{K_s} (\partial_z \phi_s)^2 + \frac{V}{(\pi \rho^{-1})^2} \cos(\sqrt{8} \phi_s). \quad (47)$$

Here the subscripts c and s refer to the charge and spin components and $v_{c,s} = v_0 \sqrt{1 \pm VK/\pi v_0}$ and $K_{c,s} = K/\sqrt{1 \pm VK/(\pi v_0)}$, where analytic expressions $v_0 = \sqrt{U\rho/m}$ and $K = \sqrt{\pi^2 \rho/(mU)}$ hold in the weakly interacting regime.

The physics of this system is fully determined by the velocities $v_{c,s}$ and the so-called Luttinger parameters $K_{c,s}$. Note that the speed of the spin and charge degrees of freedom can be different and could even have different signs. In terms of polaritons, the spin and charge densities correspond to the difference and the sum of the densities of two stationary polariton components. Therefore one could create an excitation in the original polariton field and observe as it splits into two components. One would go through the preparation stage discussed before, then let the two components evolve under different speeds, followed by the conversion into traveling slow-light which can be detected via standard optical measurements and post-processed to determine the velocities of the spin and charge parts, for example. In [53], it was shown that the optical depth of ≈ 3000 is sufficient to create the difference $v_c/v_s = 2$ and observe spin-charge separation by measuring the single particle spectral function, which can be determined from the first order correlation function of one of the fields, say E_1 at a certain quasi-momentum.

4.5.2. BCS-BEC like crossover. Introducing an effective lattice potential to the two-component setup, one can also experimentally realise a 1D two-component Bose-Hubbard model [220], which exhibits some interesting properties. For example, upon inducing strong repulsive interaction between the same species, one can go into an effective Fermi-Hubbard regime where a 1D analogue of the famous BCS-BEC crossover can be observed. This requires an attractive inter-species interaction, which is easily achieved in the stationary light setup by changing the sign of a single-photon detuning. In the strongly attractive case, the two species tend to pair up to form a molecule although no more than a pair is allowed at a single site because of the effective Pauli exclusion due to the strong intra-species repulsion. This is reminiscent of the short-range-correlated bosonic molecules forming in the BEC regime. In the weakly attractive case, two species tend to stay away from each other and form a long-range correlated pair analogous to the Cooper pair. Thus, by continuously tuning the inter-species interaction strength, it is possible to observe a 1D analogue of the BEC-BCS cross-over. A schematic illustration of these phases is provided in figure 30.

An optical depth of approximately 1000 was shown to be sufficient for simulating the crossover, where tuning the frequency difference between the quantum fields changes

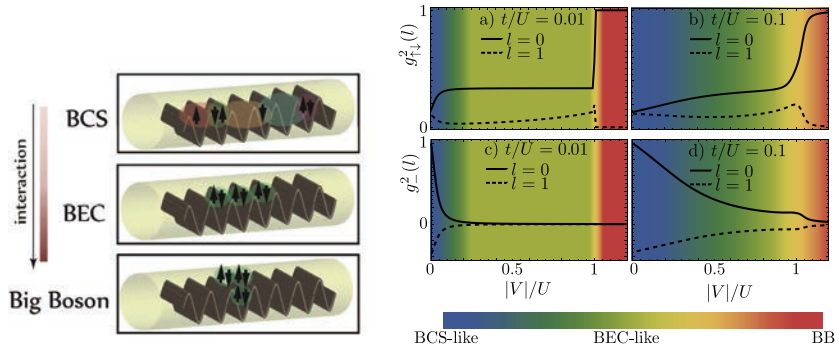


Figure 30. Left: a schematic representation of the three regimes achievable in the system for different inter-species interaction strength. A crossover from a BCS-like to a BEC-like phase occurs for small inter-species strengths compared to the intra-species repulsion, whereas in the opposite limit all the stationary polaritons gather at one site to form the so-called big-Boson state. Right: cross-species density density correlation function, $g_{\uparrow\downarrow}^2$, and the density density correlations between the cross-species population difference, g_{\pm}^2 , as functions of the inter-species interaction strength. The left column is deeper into the effective Fermi Hubbard regime compared to the right column, displaying sharper crossovers and transitions. Reprinted with permission from Huo *et al* [220]. Copyright 2012 by the American Physical Society.

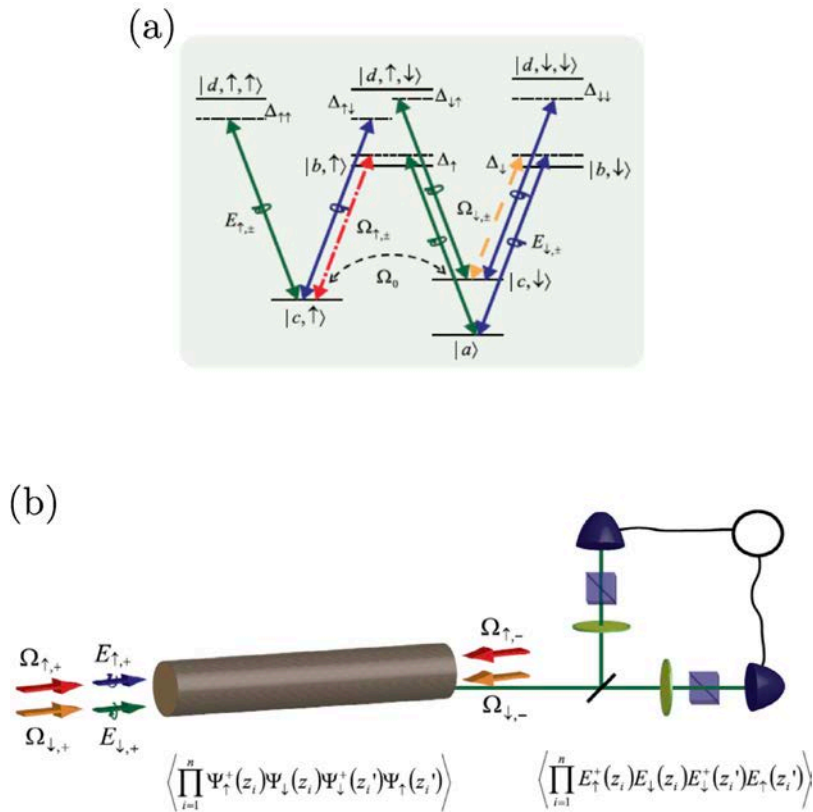


Figure 31. (a) Proposed atomic level scheme to realise the Thirring model using two polarised stationary light pulses. (b) Experimental setup illustrating photon correlation measurements at the output that facilitates the direct measurement of the n -point correlation functions. Reprinted with permission from Angelakis *et al* [54]. Copyright 2013 by the American Physical Society.

the ratio between the inter- and intra-species interaction strengths. Going through the standard preparation and release processes, one could measure the cross-species intensity correlation function to clearly distinguish all three (BCS-like, BEC-like, and the big-Boson) phases. In figure 30 we plot two types of correlation functions: $g_{\uparrow\downarrow}^2(l) = \sum_i \langle n_i \uparrow n_{i+l} \downarrow \rangle$ and $g_{\pm}^2(l) = \sum_i \langle (n_{i\uparrow} - n_{i\downarrow})(n_{i+l\uparrow} - n_{i+l\downarrow}) \rangle$. The same-site cross-species density density correlation function $g_{\uparrow\downarrow}^2(0)$ clearly shows the cross-over behaviour upon changing the inter-species interaction strength, whereas a sharp transition is

observed as the inter-species attraction becomes stronger than the intra-species repulsion. Correlations in the population difference, g_{\pm}^2 , is sensitive to the BCS-BEC cross over, but not the transition to the big-Boson phase.

4.6. Interacting relativistic theories with slow light

Simulations of quantum field theories using nonlinear waveguides can go beyond non-relativistic models. In particular, it was shown that the Thirring model (TM) [223], a relativistic

quantum field theory describing the self-interaction of a Dirac field in 2 spacetime dimensions, can be implemented [54]. The atomic level scheme required is shown in figure 31(a). It consists of two sets of the standard four-level arrangements $\{|a\rangle, |b, s\rangle, |c, s\rangle, |d, s, s'\rangle\}$, with $s, s' = \{\uparrow, \downarrow\}$ denoting the two oppositely-polarised quantum pulses E_\uparrow and E_\downarrow . Two self-interacting stationary polaritons Ψ_s appear in exactly the same manner as discussed earlier and interact through the extra level $|d, s, s\rangle$, $s \neq s'$, with strength dependent on $\Delta_{s,s'}$. Making the usual assumptions, these polaritons can be shown to obey the two-component Lieb-Liniger model [218]. To allow for the linear momentum term required in relativistic models, a small but finite difference between the forward and backward propagating control fields is necessary. Accommodating this change, the (quasi-) stationary lights are now defined as $\Psi_s = \alpha_{s,+}\Psi_{s,+} + \alpha_{s,-}\Psi_{s,-}$ with $\alpha_{s,\pm} = \Omega_{s,\pm}/(\Omega_{s,+}^2 + \Omega_{s,-}^2)$ and $\Psi_{s,\pm} = \sqrt{2\pi n} g E_{s,\pm}/\Omega_{s,\pm}$. The dynamics of these fields are governed by

$$i\partial_t \Psi_s = -\frac{1}{2m_{nr,s}} \partial_z^2 \Psi_s + i\eta_s \partial_z \Psi_s + \Omega_0 \Psi_s + \chi_{ss} \Psi_s^2 + \chi_{s\bar{s}} \Psi_s \Psi_{\bar{s}}, \quad (48)$$

where $m_{nr,s} = -\Omega_s^2/(4v_s^2 \Delta_s \sin^2 2\varphi_s)$, $\eta_s = -2v_s \cos 2\varphi_s$, $\chi_{ss} = 4\Omega_s^2/(\Delta_{ss} n)$, and $\chi_{s\bar{s}} = 2\Omega_s^2 [2 + \cos(\varphi_s - \varphi_{\bar{s}})]/(\Delta_{s\bar{s}} n)$. v_s is the reduced group velocity for the dark state polaritons, φ_s is determined from the relation $\tan^2 \varphi_s = \Omega_{s,-}^2/\Omega_{s,+}^2$, and $\Omega_s^2 = (\Omega_{s,+}^2 + \Omega_{s,-}^2)/2$, and Ω_0 is the coupling rate between $|c, \uparrow\rangle$ and $|c, \downarrow\rangle$ as shown in figure 31(a).

To transform the above equation into the bosonic TM, we need to throw away the quadratic dispersion term and set $\eta_\uparrow = -\eta_\downarrow = \eta$. The latter can be achieved by setting $v_\uparrow = v_\downarrow$ and $\cos 2\varphi_\uparrow = -\cos 2\varphi_\downarrow$, whereas the former requires the non-relativistic kinetic energy to be much smaller than the relativistic kinetic energy, which can be achieved by an appropriate tuning of the single photon detunings Δ_s . Defining a spinor field $\Psi = (\Psi_\uparrow, \Psi_\downarrow)^T$, the Hamiltonian generating the equation can be written as

$$H = \int dz \Psi (-i|\eta|\gamma_1 \partial_z + m_0 \eta^2) \Psi + \sum_s \frac{\chi_{ss}}{2} \Psi_s \Psi_s \Psi_s \Psi_s + \frac{\chi}{2} \Psi_\uparrow \Psi_\downarrow \Psi_\uparrow \Psi_\downarrow, \quad (49)$$

where $\Psi = \Psi \gamma_0$ with the gamma matrices defined as $\gamma_0 = \gamma^0 = \sigma_x$, $\gamma_1 = -\gamma^1 = i\sigma_y$ and $m_0 = -\Omega_0/\eta^2$. Thus, neglecting the small quadratic dispersion term, the dynamics of the stationary polaritons is governed by the bosonic TM. Furthermore, by entering the hardcore regime in which the self-interaction energy dominates over all other terms, one can get into the fermionic regime where, as discussed earlier, the 1D bosons behave in many ways as fermions. Figure 32 illustrates that this regime (small kinetic energy + hardcore) can be reached in a possible experiment, assuming achievable values for the optical parameters: $|\cos 2\varphi_s| = 0.004$, $n = 10^7 \text{ m}^{-1}$, $\Omega_2 \approx 1.5\gamma$, $0 < \chi/|\eta| < \pi$, and the single atom cooperativity $\gamma_{1D}/\gamma = 0.2$.

One of the methods to extract interesting physical information in field theories is to calculate correlation functions. In the

massless fermionic TM, the n -point correlation function defined as $\langle 0 | \prod_{i=1}^n \Psi_\uparrow(z_i) \Psi_\downarrow(z_i) \Psi_\downarrow(z'_i) \Psi_\uparrow(z'_i) | 0 \rangle$ has been explicitly calculated [224], and serves as an excellent check for the quantum simulator. After a satisfactory agreement has been obtained in the massless case, one can increase the value of the mass and explore the correlation functions in the relatively unexplored massive regime. To see how the correlation function can be measured, it is helpful to define the fields $\Psi_{x,\pm} = (\Psi_\uparrow \pm \Psi_\downarrow)/\sqrt{2}$ and $\Psi_{y,\pm} = (\Psi_\uparrow \mp i\Psi_\downarrow)/\sqrt{2}$. When written in terms of these fields, the original correlation function becomes a combination of various density-density correlation functions involving the densities of x and y , which can be straightforwardly measured. The detection scheme is depicted in figure 31(b). The waveplates mix the \uparrow and \downarrow components into x and y fields, one of which is then detected by using a polarisation beam splitter in each arm. In this way, one could probe the scaling behaviour of the correlation functions and moreover infer the renormalisation of mass due to the interaction.

4.7 Experimental progress

There are largely two promising experimental techniques to produce the waveguide-atom interface considered in this section. One is loading atoms in a hollow-core photonic band gap fibres (HCPBFs) and the other is coupling atoms to a tapered-fibre or more recently a 2D photonic crystal. The purpose of this section is to discuss briefly the experimental progress in these fields.

The HCPBF is a waveguide which has a hollow-core surrounded by a photonic crystal structure [225, 226] and can therefore accommodate atoms in its core, where the guided mode resides. Strong confinement of light at the core then facilitates the sought-after strong atom-light interaction. The first experimental effort used pressure difference to pump hydrogen atoms into a HCPBF and thereby demonstrate stimulated Raman scattering [227]. It was soon followed by the generation of optical solitons in a xenon-filled fibre [228]. A step towards strong light-matter interaction has been made by demonstrating EIT using acetylene molecules [229] and rubidium molecules [230]. Optical guiding of thermal [231] and cold atoms [232] through a HCPBF and trapping of ultracold atoms in a HCPBF [233] have also been achieved. Most importantly for the subject of this review, guiding and trapping of laser cooled atoms was achieved using a magnetic guide [234]. In the same experiment, authors demonstrated all-optical switching using the four-level giant cross-Kerr effect introduced in section 4.1.1 with a moderate value of optical depth ≈ 30 . More recently, the use of hollow-optical-beam has allowed more efficient guiding of atoms, leading to an improved optical depth of 180 [235].

The second promising system consists of atoms coupled to the guided mode of a tapered fibre. When an optical fibre is drawn out such that its diameter is smaller than the wavelength of the guided light [236], light mostly resides outside the fibre in the form of an evanescent wave, which enables easy coupling between the guided light and surrounding atoms. Coupling trapped cold atoms to the guided mode of

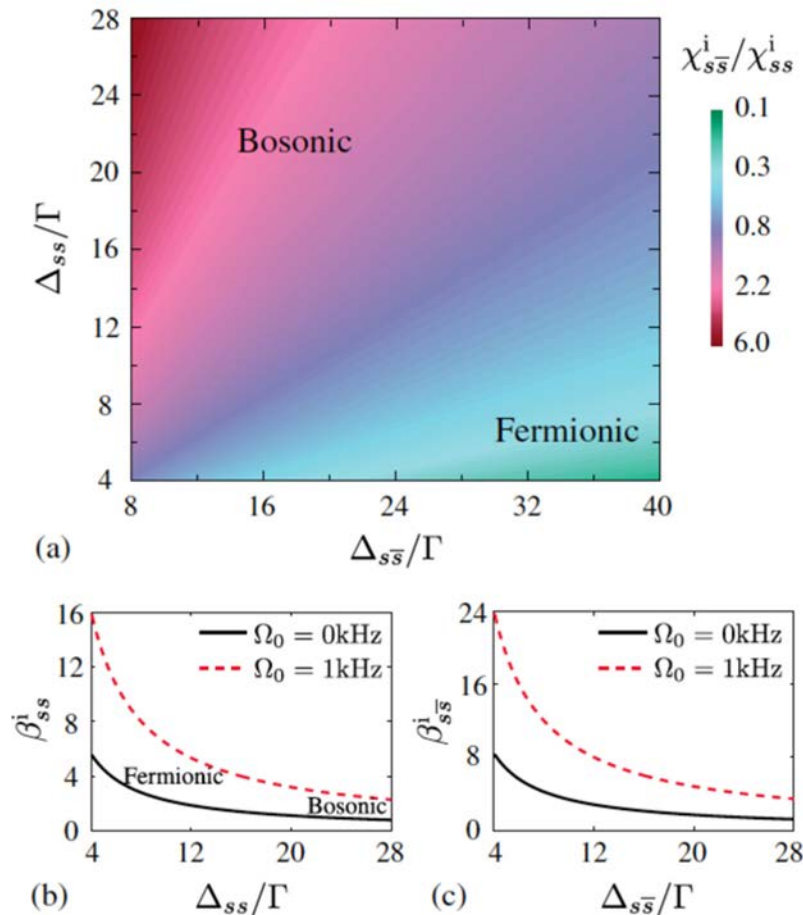


Figure 32. (a) The ratio of inter- to intra-species interaction strength as a function of two experimentally controllable detunings for $m_0 = 0$. (b) and (c): The ratio of intra- and inter-species interaction energy to kinetic energy, respectively. Reprinted with permission from Angelakis *et al* [54]. Copyright 2013 by the American Physical Society.

a tapered fibre has been demonstrated [237, 238] and a hot vapour of atoms has been used to demonstrate EIT with a very low pump power [239]. Trapping and interrogation of cold atoms on the surface of a tapered-fibre by creating an optical lattice above the nanofibre surface has been achieved with an optical depth as high as ≈ 30 [240, 241]. Most recently, state-insensitive trapping of atoms has been achieved with an optical depth of 66.

More recently, people have started looking at 2D nanophotonic structures involving photonic-crystal patterns [242, 243]. These types of systems allow strong light-atom coupling and may lead to an alternative platform to realise the models reviewed in this section. Moreover, other types of models can be readily simulated in this setup, such as the conventional cavity-QED physics [244] and tunable many-body spin models [245]. As such, the platform is also a good candidate for a quantum information processor.

4.8. Outlook: Rydberg polaritons

Before we close the section, we would like to briefly mention another interesting paradigm to realise strong photon-photon interaction that has attracted much interest recently: Rydberg EIT. In Rydberg EIT, the strong long-range Rydberg interaction between atoms are converted to an

effective photon-photon interaction through the appropriate use of EIT— one chooses the third state ($|c\rangle$) of the atom to be a Rydberg state (typically requiring the level scheme to be of the ladder type). Due to an energy shift induced by the interaction between Rydberg states, the presence of a single photon in the system creates a range (called blockade radius) around the excitation where light propagation is forbidden. This means that two Rydberg excitations cannot travel within the blockade radius, or in other words they repel each other. The nonlinear interaction not only allows one to build photonic quantum information processors [246–252], but also provides an opportunity to investigate many-body physics. One can for example create a BEC of stationary-light dark state Rydberg polaritons [217], or observe Wigner Crystallisation of photons in cold Rydberg ensembles [253]. Experimental progress in the field has been equally impressive; there have been demonstrations of EIT in a Rydberg medium [254], a strong Rydberg blockade [255–257], and even a microwave-controlled polariton-polariton interaction [258]. It is also possible to make Rydberg polaritons in a cavity, which has been demonstrated in [259, 260]. It will be interesting to further investigate how the unique advantages of the Rydberg polaritons can be harnessed for the purpose of quantum simulations and studying nonequilibrium many-body physics.

5. Summary and outlook

In this review, we have summarised numerous theoretical proposals and a few experimental demonstrations of strongly-interacting many-body photonic systems. We have started with the early proposals that realised that atom-induced photon-photon interactions used in tandem with coupled resonator structures can give rise to Hubbard-like models often studied in condensed matter physics and cold atoms in optical lattices.

Section 2 reviewed the properties of the many-body ground states of closed coupled-resonator arrays as well as the possible equilibrium phases as calculated via mean-field approaches. We also presented proposals to simulate quantum spin-models and fractional quantum Hall states with photons.

Section 3 focused on works that go beyond equilibrium approaches, exploring experimentally valid situations where the system is naturally out of equilibrium. The differences and similarities between the driven-dissipative photonic Bose Hubbard and Jaynes-Cummings Hubbard systems were first highlighted, followed by reviews on early investigations on interaction-driven fermionisation and crystallisation of photons in different scenarios. We also discussed two quenching scenarios, where transient effects of an initially prepared state are probed to reveal the underlying eigenstates of the system in an open but not driven system. Apart from observing the signatures of Mott-superfluid transition, an interesting self-trapping was shown to occur, which has been verified experimentally in a superconducting circuit setup. We then summarised a couple of proposals to implement more exotic models. The first is an extended Hubbard model with the cross-Kerr interaction between nearest neighbours which, within the mean-field description, was shown to exhibit a supersolid-like phase. The second is a bosonic Kitaev chain with localised Majorana-like modes near the end cavities. Such proposals reveal the versatility of CRA simulators. The section ends with a brief overview of interesting works that we could not cover in detail as well as a short survey on possible experimental platforms.

Section 4 presented a very different paradigm which is more suitable for simulating continuum 1D quantum models, but nevertheless shares the main theme in that the central players are interacting photons. The system consists of an ensemble of 3- or 4-level atoms coupled to a 1D waveguide, with EIT or EIT-like coupling schemes. We showed how stationary states of light are formed, whose dynamics can be engineered to a large degree. This way, one can realise a photonic Tonks-Girardeau gas and furthermore add an effective potential whose depth can be varied to allow tuning between the Bose-Hubbard and quantum sine-Gordon limit, which in turn allows the pinning transition to occur. We then reviewed a proposal to achieve the Bose-Einstein condensation of dark-state stationary-polaritons if the 2D nature of the cross-section of the waveguide becomes important and interaction is sufficiently strong. Next we discussed a generalisation of the 1D system involving two species of atoms or two polarisations for the input pulses, which allows simulations of Luttinger liquids physics, spin-charge separation and BEC-BCS-like crossover. We then showed that one can also implement an interacting

relativistic theory, namely the Thirring model, by engineering the dispersion relation of the propagating pulses of light and exploiting the strong EIT-based interactions. Strong interactions between intra-species photons enforce an effective Pauli exclusion in this 1D system, so that a fermionic model can be implemented in the photonic system. The section was ended with a mini survey on experimental progress in the field and an outlook on a promising platform using Rydberg-EIT.

Hopefully we have convinced the reader that there have been many exciting and still ongoing developments in this young field. Although tremendous progress has been made in the last decade, there is still plenty of room for development. Experimentally, a large-size coupled resonator array with strong atom-resonator coupling in each site has not yet been fabricated, although impressive technological developments in circuit-QED indicate that we are very close to seeing one. Further developments in tools to probe and measure the nonequilibrium many-body states are necessary both experimentally and theoretically. Current theoretical tools are not sufficient to study even a moderate-sized driven-dissipative 2D arrays as we have discussed already, and developing a good numerical or analytical tool is of fundamental importance for further progress. One can ask many questions such as: Will developments in the tensor-networks help? Can we apply techniques from other areas such as the Keldysh formalism to analytically find meaningful quantities? What are the optimal observables and ways to characterise the out-of-equilibrium phases in driven-dissipative photonic systems?

Regarding simulations of field theories using photonic systems, one of the key questions is whether the EIT-based platform can be generalised to higher dimensions or a different platform is needed. A straightforward option is to utilise the two-dimensions within the waveguide (as we have seen in the BEC of dark state polaritons), but one difficulty is in maintaining a large optical depth while doing so. One can think of increasing the atom-photon coupling strength for this purpose or utilising the strong interactions between the Rydberg atoms. The latter looks to be a promising avenue with exciting prospects for further discoveries.

Acknowledgments

We would like to acknowledge the financial support provided by the National Research Foundation and Ministry of Education Singapore (partly through the Tier 3 Grant Random numbers from quantum processes), and travel support by the EU IP-SIQS. DGA would like to thank the hospitality of the KITP during the program Many-body physics with light.

References

- [1] Cirac J I and Zoller P 2012 Goals and opportunities in quantum simulation *Nat. Phys.* **8** 264–6
- [2] Hauke P, Cucchietti F M, Tagliacozzo L, Deutsch I and Lewenstein M 2012 Can one trust quantum simulators? *Rep. Prog. Phys.* **75** 082401
- [3] Blatt R and Roos C F 2012 Quantum simulations with trapped ions *Nat. Phys.* **8** 277–84

- [4] Bloch I, Dalibard J and Zwerger W 2008 Many-body physics with ultracold gases *Rev. Mod. Phys.* **80** 885–964
- [5] Angelakis D G, Santos M F and Bose S 2007 Photon-blockade-induced Mott transitions and XY spin models in coupled cavity arrays *Phys. Rev. A* **76** 031805
- [6] Hartmann M J, Brandao F G S L and Plenio M B 2006 Strongly interacting polaritons in coupled arrays of cavities *Nat. Phys.* **2** 849–55
- [7] Greentree A D, Tahan C, Cole J H and Hollenberg L C L 2006 Quantum phase transitions of light *Nat. Phys.* **2** 856–61
- [8] Rossini D and Fazio R 2007 Mott-insulating and glassy phases of polaritons in 1D arrays of coupled cavities *Phys. Rev. Lett.* **99** 186401
- [9] Na N, Utsunomiya S, Tian L and Yamamoto Y 2008 Strongly correlated polaritons in a 2D array of photonic crystal microcavities *Phys. Rev. A* **77** 031803
- [10] Bose S, Angelakis D and Burgarth D 2007 Transfer of a polaritonic qubit through a coupled cavity array *J. Mod. Opt.* **54** 2307–14
- [11] Hu F M, Zhou L, Shi T and Sun C P 2007 Coupled cavity QED for coherent control of photon transmission: Green-function approach for hybrid systems with two-level doping *Phys. Rev. A* **76** 013819
- [12] Chakrabarti R and Sreekmari G 2011 Propagation of single-excitation quantum states through Jaynes–Cummings Hubbard arrays *J. Phys. B: At. Mol. Opt. Phys.* **44** 115505
- [13] Makin M I, Cole J H, Hill C D, Greentree A D and Hollenberg L C L 2009 Time evolution of the 1D Jaynes–Cummings–Hubbard Hamiltonian *Phys. Rev. A* **80** 043842
- [14] Knap M, Arrigoni E and von der Linden W 2010 Quantum phase transition and excitations of the Tavis–Cummings lattice model *Phys. Rev. B* **82** 045126
- [15] Hartmann M J, Brandao F G S L and Plenio M B 2007 Effective spin systems in coupled microcavities *Phys. Rev. Lett.* **99** 160501
- [16] Angelakis D G and Kay A 2008 Weaving light-matter qubits into a one way quantum computer *New J. Phys.* **10** 023012
- [17] Cho J, Angelakis D G and Bose S 2008 Heralded generation of entanglement with coupled cavities *Phys. Rev. A* **78** 022323
- [18] Cho J, Angelakis D G and Bose S 2008 Fractional quantum Hall state in coupled cavities *Phys. Rev. Lett.* **101** 246809
- [19] Lamata L, Lenj J, Schtz T and Solano E 2007 Dirac equation and quantum relativistic effects in a single trapped ion *Phys. Rev. Lett.* **98** 253005
- [20] Vaishnav J Y and Clark C W 2008 Observing zitterbewegung with ultracold atoms *Phys. Rev. Lett.* **100** 153002
- [21] Juzeliūnas G, Ruseckas J, Lindberg M, Santos L and Hollenberg P 2008 Quasirelativistic behavior of cold atoms in light fields *Phys. Rev. A* **77** 011802
- [22] Otterbach J, Unanyan R G and Fleischhauer M 2009 Confining stationary light: Dirac dynamics and Klein tunneling *Phys. Rev. Lett.* **102** 063602
- [23] Longhi S 2010 Klein tunneling in binary photonic superlattices *Phys. Rev. B* **81** 075102
- [24] Casanova J, García-Ripoll J J, Gerritsma R, Roos C F and Solano E 2010 Klein tunneling and Dirac potentials in trapped ions *Phys. Rev. A* **82** 020101
- [25] Noh C, Rodríguez-Lara B M and Angelakis D G 2012 Quantum simulation of neutrino oscillations with trapped ions *New J. Phys.* **14** 033028
- [26] Angelakis D G, Das P and Noh C 2014 Probing the topological properties of the Jackiw–Rebbi model with light *Sci. Rep.* **4** 6110
- [27] Gerritsma R, Kirchmair G, Zähringer F, Solano E, Blatt R and Roos C F 2010 Quantum simulation of the Dirac equation *Nature* **463** 68–71
- [28] Gerritsma R, Lanyon B P, Kirchmair G, Zähringer F, Hempel C, Casanova J, García-Ripoll J J, Solano E, Blatt R and Roos C F 2011 Quantum simulation of the Klein paradox with trapped ions *Phys. Rev. Lett.* **106** 060503
- [29] Dreisow F, Heinrich M, Keil R, Tinnermann A, Nolte S, Longhi S and Szameit A 2010 Classical simulation of relativistic zitterbewegung in photonic lattices *Phys. Rev. Lett.* **105** 143902
- [30] Dreisow F, Keil R, Tinnermann A, Nolte S, Longhi S and Szameit A 2012 Klein tunneling of light in waveguide superlattices *Europhys. Lett.* **97** 10008
- [31] Hartmann M J 2016 Quantum simulation with interacting photons *J. Opt.* **18** 104005
- [32] Huo M X, Li Y, Song Z and Sun C P 2008 Atomic entanglement versus visibility of photon interference for quantum criticality of a hybrid system *Phys. Rev. A* **77** 022103
- [33] Irish E K 2009 Ground-state entanglement in a coupled-cavity model *Phys. Rev. A* **80** 043825
- [34] Giampaolo S M and Illuminati F 2010 Long-distance entanglement in many-body atomic and optical systems *New J. Phys.* **12** 025019
- [35] Aichhorn M, Hohenadler M, Tahan C and Littlewood P B 2008 Quantum fluctuations, temperature, and detuning effects in solid-light systems *Phys. Rev. Lett.* **100** 216401
- [36] Zhao J, Sandvik A W and Ueda K 2008 Insulator to superfluid transition in coupled photonic cavities in two dimensions arXiv:0806.3603
- [37] Mering A, Fleischhauer M, Ivanov P A and Singer K 2009 Analytic approximations to the phase diagram of the Jaynes–Cummings–Hubbard model *Phys. Rev. A* **80** 053821
- [38] Schmidt S and Blatter G 2010 Excitations of strongly correlated lattice polaritons *Phys. Rev. Lett.* **104** 216402
- [39] Knap M, Arrigoni E and von der Linden W 2010 Spectral properties of coupled cavity arrays in one dimension *Phys. Rev. B* **81** 104303
- [40] Makin M I, Cole J H, Tahan C, Hollenberg L C L and Greentree A D 2008 Quantum phase transitions in photonic cavities with two-level systems *Phys. Rev. A* **77** 053819
- [41] Chen Z-X, Zhou Z-W, Zhou X, Zhou X-F and Guo G-C 2010 Quantum simulation of Heisenberg spin chains with next-nearest-neighbor interactions in coupled cavities *Phys. Rev. A* **81** 022303
- [42] Hartmann M J, Brandao F G S L and Plenio M B 2008 A polaritonic two-component Bose–Hubbard model *New J. Phys.* **10** 033011
- [43] Paternostro M, Agarwal G S and Kim M S 2009 Solitonic behaviour in coupled multi atom-cavity systems *New J. Phys.* **11** 013059
- [44] Schmidt S and Blatter G 2009 Strong coupling theory for the Jaynes–Cummings–Hubbard Model *Phys. Rev. Lett.* **103** 086403
- [45] Kyoseva E S, Angelakis D G and Kwek L C 2010 A single-interaction step implementation of a quantum search in coupled micro-cavities *Europhys. Lett.* **89** 20005
- [46] Houck A A, Türeci H E and Koch J 2012 On-chip quantum simulation with superconducting circuits *Nat. Phys.* **8** 292–9
- [47] Majumdar A, Rundquist A, Bajcsy M, Dasika V D, Bank S R and Vučković J 2012 Design and analysis of photonic crystal coupled cavity arrays for quantum simulation *Phys. Rev. B* **86** 195312
- [48] Lepert G, Trupke M, Hartmann M J, Plenio M B and Hinds E A 2011 Arrays of waveguide-coupled optical cavities that interact strongly with atoms *New J. Phys.* **13** 113002
- [49] Hämmer T, Reuther G M, Hänggi P and Zueco D 2012 Nonequilibrium phases in hybrid arrays with flux qubits and nitrogen-vacancy centers *Phys. Rev. A* **85** 052320
- [50] Yang W L, Yin Z-q, Chen Z X, Kou S-P, Feng M and Oh C H 2012 Quantum simulation of an artificial Abelian gauge field using nitrogen-vacancy-center ensembles coupled to superconducting resonators *Phys. Rev. A* **86** 012307

- [51] You J-B, Yang W L, Xu Z-Y, Chan A H and Oh C H 2014 Phase transition of light in circuit-QED lattices coupled to nitrogen-vacancy centers in diamond *Phys. Rev. B* **90** 195112
- [52] Chang D E, Gritsev V, Morigi G, Vuletić V, Lukin M D and Demler E A 2008 Crystallization of strongly interacting photons in a nonlinear optical fibre *Nat. Phys.* **4** 884 9
- [53] Angelakis D G, Huo M, Kyoseva E and Kwek L C 2011 Luttinger liquid of photons and spin-charge separation in hollow-core fibers *Phys. Rev. Lett.* **106** 153601
- [54] Angelakis D G, Huo M-X, Chang D, Kwek L C and Korepin V 2013 Mimicking interacting relativistic theories with stationary pulses of light *Phys. Rev. Lett.* **110** 100502
- [55] Carusotto I and Ciuti C 2013 Quantum fluids of light *Rev. Mod. Phys.* **85** 299 366
- [56] Carusotto I, Volz T and Imamoğlu A 2010 Feshbach blockade: single-photon nonlinear optics using resonantly enhanced cavity polariton scattering from biexciton states *Europhys. Lett.* **90** 37001
- [57] Kasprzak J *et al* 2006 Bose-Einstein condensation of exciton polaritons *Nature* **443** 409 14
- [58] Baboux F *et al* 2016 Bosonic condensation and disorder-induced localization in a flat band *Phys. Rev. Lett.* **116** 066402
- [59] Lai Y and Haus H A 1989 Quantum theory of solitons in optical fibers. I. Time-dependent Hartree approximation *Phys. Rev. A* **40** 844 53
- [60] Lai Y and Haus H A 1989 Quantum theory of solitons in optical fibers. II. Exact solution *Phys. Rev. A* **40** 854 66
- [61] Larr P- and Carusotto I 2015 Propagation of a quantum fluid of light in a cavityless nonlinear optical medium: general theory and response to quantum quenches *Phys. Rev. A* **92** 043802
- [62] Yariv A, Xu Y, Lee R K and Scherer A 1999 Coupled-resonator optical waveguide: a proposal and analysis *Opt. Lett.* **24** 711 3
- [63] Bayindir M, Temelkuran B and Ozbay E 2000 Tight-binding description of the coupled defect modes in 3D photonic crystals *Phys. Rev. Lett.* **84** 2140 3
- [64] Paloczi G, Huang Y, Yariv A and Mookherjee S 2003 Polymeric Mach-Zehnder interferometer using serially coupled microring resonators *Opt. Express* **11** 2666 71
- [65] Shih M H, Kim W J, Kuang W, Cao J R, Yukawa H, Choi S J, O'Brien J D, Dapkus P D and Marshall W K 2004 2D photonic crystal Mach-Zehnder interferometers *Appl. Phys. Lett.* **84** 460 2
- [66] Altug H and Vučković J 2004 2D coupled photonic crystal resonator arrays *Appl. Phys. Lett.* **84** 161 3
- [67] Badolato A, Hennessy K, Atatüre M, Dreiser J, Hu E, Petroff P M and Imamoğlu A 2005 Deterministic coupling of single quantum dots to single nanocavity modes *Science* **308** 1158 61
- [68] Wallraff A, Schuster D I, Blais A, Frunzio L, Huang R S, Majer J, Kumar S, Girvin S M and Schoelkopf R J 2004 Strong coupling of a single photon to a superconducting qubit using circuit quantum electrodynamics *Nature* **431** 162 7
- [69] Angelakis D G, Santos M F, Yannopoulos V and Ekert A 2007 A proposal for the implementation of quantum gates with photonic-crystal waveguides *Phys. Lett. A* **362** 377 80
- [70] Imamoğlu A, Schmidt H, Woods G and Deutsch M 1997 Strongly interacting photons in a nonlinear cavity *Phys. Rev. Lett.* **79** 1467 70
- [71] Birnbaum K M, Boca A, Miller R, Boozer A D, Northup T E and Kimble H J 2005 Photon blockade in an optical cavity with one trapped atom *Nature* **436** 87 90
- [72] Duan L-M, Demler E and Lukin M D 2003 Controlling spin exchange interactions of ultracold atoms in optical lattices *Phys. Rev. Lett.* **91** 090402
- [73] Hartmann M J, Brandt F G S L and Plenio M B 2008 Quantum many-body phenomena in coupled cavity arrays *Laser Photonics Rev.* **2** 527 56
- [74] Hartmann M J and Plenio M B 2007 Strong photon nonlinearities and photonic Mott insulators *Phys. Rev. Lett.* **99** 103601
- [75] Jaksch D, Bruder C, Cirac J I, Gardiner C W and Zoller P 1998 Cold bosonic atoms in optical lattices *Phys. Rev. Lett.* **81** 3108 11
- [76] Pippin P, Evertz H G and Hohenadler M 2009 Excitation spectra of strongly correlated lattice bosons and polaritons *Phys. Rev. A* **80** 033612
- [77] Hohenadler M, Aichhorn M, Schmidt S and Pollet L 2011 Dynamical critical exponent of the Jaynes-Cummings Hubbard model *Phys. Rev. A* **84** 041608
- [78] Hohenadler M, Aichhorn M, Pollet L and Schmidt S 2012 Polariton Mott insulator with trapped ions or circuit QED *Phys. Rev. A* **85** 013810
- [79] Nielsen M A 2006 Cluster-state quantum computation *Rep. Math. Phys.* **57** 147 61
- [80] Li B P, Gu Y, Gong H Q and Guo C G 2009 Generation of Ising interaction and cluster states in a 1D coupled resonator waveguide *Eur. Phys. J. D* **55** 205 9
- [81] Kay A and Angelakis D G 2008 Reproducing spin lattice models in strongly coupled atom-cavity systems *Europhys. Lett.* **84** 20001
- [82] Burgarth D 2007 Quantum state transfer with spin chains *PhD thesis* University College London (arXiv:0704.1309)
- [83] Sarkar S 2012 Quantum field theoretical study of an effective spin model in coupled optical cavity arrays *Physica B* **407** 44 8
- [84] Zhu G, Schmidt S and Koch J 2013 Dispersive regime of the Jaynes-Cummings and Rabi lattice *New J. Phys.* **15** 115002
- [85] Bruder C, Fazio R and Schön G 1993 Superconductor-Mott-insulator transition in Bose systems with finite-range interactions *Phys. Rev. B* **47** 342 7
- [86] Loss D and DiVincenzo D P 1998 Quantum computation with quantum dots *Phys. Rev. A* **57** 120 6
- [87] García-Ripoll J J, Martín-Delgado M A and Cirac J I 2004 Implementation of spin Hamiltonians in optical lattices *Phys. Rev. Lett.* **93** 250405
- [88] Cho J, Angelakis D G and Bose S 2008 Simulation of high-spin Heisenberg models in coupled cavities *Phys. Rev. A* **78** 062338
- [89] Tsui D C, Stormer H L and Gossard A C 1982 2D magnetotransport in the extreme quantum limit *Phys. Rev. Lett.* **48** 1559 62
- [90] Lewenstein M, Sanpera A, Ahufinger V, Damski B, Sen(De) A and Sen U 2007 Ultracold atomic gases in optical lattices: mimicking condensed matter physics and beyond *Adv. Phys.* **56** 243 379
- [91] Wilkin N K and Gunn J M F 2000 Condensation of composite bosons in a rotating BEC *Phys. Rev. Lett.* **84** 6
- [92] Juzeliūnas G and Hohenberg P 2004 Slow light in degenerate Fermi gases *Phys. Rev. Lett.* **93** 033602
- [93] Jaksch D and Zoller P 2003 Creation of effective magnetic fields in optical lattices: the Hofstadter butterfly for cold neutral atoms *New J. Phys.* **5** 56
- [94] Sørensen A S, Demler E and Lukin M D 2005 Fractional quantum Hall states of atoms in optical lattices *Phys. Rev. Lett.* **94** 086803
- [95] Koch J, Houck A A, Le Hur K and Girvin S M 2010 Time-reversal-symmetry breaking in circuit-QED-based photon lattices *Phys. Rev. A* **82** 043811
- [96] Nunnenkamp A, Koch J and Girvin S M 2011 Synthetic gauge fields and homodyne transmission in Jaynes-Cummings lattices *New J. Phys.* **13** 095008

- [97] Umucalılar R O and Carusotto I 2011 Artificial gauge field for photons in coupled cavity arrays *Phys. Rev. A* **84** 043804
- [98] Hafezi M, Demler E A, Lukin M D and Taylor J M 2011 Robust optical delay lines with topological protection *Nat. Phys.* **7** 907 12
- [99] Hafezi M, Mittal S, Fan J, Migdall A and Taylor J M 2013 Imaging topological edge states in silicon photonics *Nat. Photon.* **7** 1001 5
- [100] Umucalılar R O and Carusotto I 2012 Fractional quantum Hall states of photons in an array of dissipative coupled cavities *Phys. Rev. Lett.* **108** 206809
- [101] Hayward A L C, Martin A M and Greentree A D 2012 Fractional quantum Hall physics in Jaynes–Cummings Hubbard lattices *Phys. Rev. Lett.* **108** 223602
- [102] Hafezi M, Lukin M D and Taylor J M 2013 Non-equilibrium fractional quantum Hall state of light *New J. Phys.* **15** 063001
- [103] Roushan P *et al* 2016 Chiral groundstate currents of interacting photons in a synthetic magnetic field (arXiv:1606.00077)
- [104] Schine N, Ryou A, Gromov A, Sommer A and Simon J 2016 Synthetic Landau levels for photons *Nature* **534** 671–5
- [105] Haldane F D M and Rezayi E H 1985 Periodic Laughlin–Jastrow wave functions for the fractional quantized Hall effect *Phys. Rev. B* **31** 2529 31
- [106] Hafezi M, Sørensen A S, Demler E and Lukin M D 2007 Fractional quantum Hall effect in optical lattices *Phys. Rev. A* **76** 023613
- [107] Noh C and Angelakis D G 2014 Simulating topological effects with photons in coupled QED cavity arrays *Int. J. Mod. Phys. B* **28** 1441003
- [108] Kapit E, Ginsparg P and Mueller E 2012 Non-Abelian braiding of lattice bosons *Phys. Rev. Lett.* **108** 066802
- [109] Julicher B, Graßinger T, Barberi-Nunziati N and Lewenstein M 2012 Fractional quantum Hall states of a few bosonic atoms in geometric gauge fields *New J. Phys.* **14** 055003
- [110] Hafezi M, Adhikari P and Taylor J M 2015 Chemical potential for light by parametric coupling *Phys. Rev. B* **92** 174305
- [111] Baumann K, Guerlin C, Brennecke F and Esslinger T 2010 Dicke quantum phase transition with a superfluid gas in an optical cavity *Nature* **464** 1301 6
- [112] Klaers J, Schmitt J, Vewinger F and Weitz M 2010 Bose–Einstein condensation of photons in an optical microcavity *Nature* **468** 545 8
- [113] Chiochetta A, Gambassi A and Carusotto I 2015 Laser operation and Bose–Einstein condensation: analogies and differences arXiv:1503.02816
- [114] Tomadin A and Fazio R 2010 Many-body phenomena in QED-cavity arrays (invited) *J. Opt. Soc. Am. B* **27** A130 6
- [115] Schmidt S and Koch J 2013 Circuit QED lattices: towards quantum simulation with superconducting circuits *Ann. Phys.* **525** 395 412
- [116] Sieberer L M, Huber S D, Altman E and Diehl S 2013 Dynamical critical phenomena in driven-dissipative systems *Phys. Rev. Lett.* **110** 195301
- [117] Müller M, Diehl S, Pupillo G and Zoller P 2012 *Engineered Open Systems, Quantum Simulations with Atoms and Ions* vol 61 (New York: Academic) pp 1–80
- [118] Diehl S, Tomadin A, Micheli A, Fazio R and Zoller P 2010 Dynamical phase transitions and instabilities in open atomic many-body systems *Phys. Rev. Lett.* **105** 015702
- [119] Prosen T and Pižorn I 2008 Quantum phase transition in a far-from-equilibrium steady state of an xy spin chain *Phys. Rev. Lett.* **101** 105701
- [120] Horstmann B, Cirac J I and Giedke G 2013 Noise-driven dynamics and phase transitions in Fermionic systems *Phys. Rev. A* **87** 012108
- [121] Leib M, Deppe F, Marx A, Gross R and Hartmann M J 2012 Networks of nonlinear superconducting transmission line resonators *New J. Phys.* **14** 075024
- [122] Grujić T, Clark S R, Jaksch D and Angelakis D G 2012 Non-equilibrium many-body effects in driven nonlinear resonator arrays *New J. Phys.* **14** 103025
- [123] Carmichael H J 2002 *Statistical Methods in Quantum Optics* 1 vol 1 (Berlin: Springer)
- [124] Carusotto I, Gerace D, Tureci H E, de Liberato S, Ciuti C and Imamoglu A 2009 Fermionized photons in an array of driven dissipative nonlinear cavities *Phys. Rev. Lett.* **103** 033601
- [125] Hartmann M J 2010 Polariton crystallization in driven arrays of lossy nonlinear resonators *Phys. Rev. Lett.* **104** 113601
- [126] Biondi M, van Nieuwenburg E P L, Blatter G, Huber S D and Schmidt S 2015 Incompressible polaritons in a flat band *Phys. Rev. Lett.* **115** 143601
- [127] Girardeau M 1960 Relationship between systems of impenetrable Bosons and Fermions in one dimension *J. Math. Phys.* **1** 516 23
- [128] Knap M, Arrighi E, von der Linden W and Cole J H 2011 Emission characteristics of laser-driven dissipative coupled-cavity systems *Phys. Rev. A* **83** 023821
- [129] Verstraete F, Murg V and Cirac J I 2008 Matrix product states, projected entangled pair states, and variational renormalization group methods for quantum spin systems *Adv. Phys.* **57** 143 224
- [130] Schollwöck U 2011 The density-matrix renormalization group in the age of matrix product states *Ann. Phys.* **326** 96 192
- [131] del Valle E and Hartmann M J 2013 Correlator expansion approach to stationary states of weakly coupled cavity arrays *J. Phys. B: At. Mol. Opt. Phys.* **46** 224023
- [132] Degenfeld-Schonburg P and Hartmann M J 2014 Self-consistent projection operator theory for quantum many-body systems *Phys. Rev. B* **89** 245108
- [133] Tomadin A, Giovannetti V, Fazio R, Gerace D, Carusotto I, Tureci H E and Imamoglu A 2010 Signatures of the superfluid-insulator phase transition in laser-driven dissipative nonlinear cavity arrays *Phys. Rev. A* **81** 061801
- [134] Schmidt S, Gerace D, Houck A A, Blatter G and Tureci H E 2010 Nonequilibrium delocalization–localization transition of photons in circuit quantum electrodynamics *Phys. Rev. B* **82** 100507
- [135] Raftery J, Sadri D, Schmidt S, Tureci H E and Houck A A 2014 Observation of a dissipation-induced classical to quantum transition *Phys. Rev. X* **4** 031043
- [136] Jensen S M 1982 The nonlinear coherent coupler *IEEE J. Quantum Electron.* **18** 1580 3
- [137] Eilbeck J C, Lomdahl P S and Scott A C 1985 The discrete self-trapping equation *Physica D* **16** 318 38
- [138] Smerzi A, Fantoni S, Giovanazzi S and Shenoy S R 1997 Quantum coherent atomic tunneling between two trapped Bose–Einstein condensates *Phys. Rev. Lett.* **79** 4950 3
- [139] Albiez M, Gati R, Fölling J, Hunsmann S, Cristiani M and Oberthaler M K 2005 Direct observation of tunneling and nonlinear self-trapping in a single Bosonic Josephson junction *Phys. Rev. Lett.* **95** 010402
- [140] Levy S, Lahoud E, Shomroni I and Steinhauer J 2007 The a.c. and d.c. Josephson effects in a Bose–Einstein condensate *Nature* **449** 579 83
- [141] Sarchi D, Carusotto I, Wouters M and Savona V 2008 Coherent dynamics and parametric instabilities of microcavity polaritons in double-well systems *Phys. Rev. B* **77** 125324
- [142] Schetakakis N, Grujić T, Clark S, Jaksch D and Angelakis D 2013 Frozen photons in Jaynes–Cummings arrays *J. Phys. B: At. Mol. Opt. Phys.* **46** 224025

- [143] Shapourian H and Sadri D 2016 Fock-space localization of polaritons in the Jaynes Cummings dimer model *Phys. Rev. A* **93** 013845
- [144] Jin J, Rossini D, Fazio R, Leib M and Hartmann M J 2013 Photon solid phases in driven arrays of nonlinearly coupled cavities *Phys. Rev. Lett.* **110** 163605
- [145] Jin J, Rossini D, Leib M, Hartmann M J and Fazio R 2014 Steady-state phase diagram of a driven QED-cavity array with cross-Kerr nonlinearities *Phys. Rev. A* **90** 023827
- [146] Bujnowski B, Corso J K, Hayward A L C, Cole J H and Martin A M 2014 Supersolid phases of light in extended Jaynes Cummings Hubbard systems *Phys. Rev. A* **90** 043801
- [147] Bardyn C-E and Imamoglu A 2012 Majorana-like modes of light in a 1D array of nonlinear cavities *Phys. Rev. Lett.* **109** 253606
- [148] Joshi C, Nissen F and Keeling J 2013 Quantum correlations in the 1D driven dissipative xy model *Phys. Rev. A* **88** 063835
- [149] Kitaev A Yu 2001 Unpaired Majorana fermions in quantum wires *Phys.-Usp.* **44** 131
- [150] Nilsson J, Akhmerov A R and Beenakker C W J 2008 Splitting of a Cooper pair by a pair of Majorana bound states *Phys. Rev. Lett.* **101** 120403
- [151] Law K T, Lee P A and Ng T K 2009 Majorana Fermion induced resonant Andreev reflection *Phys. Rev. Lett.* **103** 237001
- [152] Flensberg K 2011 Non-Abelian operations on Majorana fermions via single-charge control *Phys. Rev. Lett.* **106** 090503
- [153] Gerace D, Terci H E, Imamoglu A, Giovannetti V and Fazio R 2009 The quantum-optical Josephson interferometer *Nat. Phys.* **5** 281 4
- [154] Ferretti S, Andreani L C, Terci H E and Gerace D 2010 Photon correlations in a two-site nonlinear cavity system under coherent drive and dissipation *Phys. Rev. A* **82** 013841
- [155] Leib M and Hartmann M J 2010 Bose Hubbard dynamics of polaritons in a chain of circuit quantum electrodynamics cavities *New J. Phys.* **12** 093031
- [156] Biella A, Mazza L, Carusotto I, Rossini D and Fazio R 2015 Photon transport in a dissipative chain of nonlinear cavities *Phys. Rev. A* **91** 053815
- [157] Lee C, Noh C, Schetakakis N and Angelakis D G 2015 Few-photon transport in many-body photonic systems: a scattering approach *Phys. Rev. A* **92** 063817
- [158] Ruiz-Rivas J, del Valle E, Gies C, Gartner P and Hartmann M J 2014 Spontaneous collective coherence in driven dissipative cavity arrays *Phys. Rev. A* **90** 033808
- [159] Nissen F, Schmidt S, Biondi M, Blatter G, Terci H E and Keeling J 2012 Nonequilibrium dynamics of coupled qubit-cavity arrays *Phys. Rev. Lett.* **108** 233603
- [160] Grujic T, Clark S R, Jaksch D and Angelakis D G 2013 Repulsively induced photon superbunching in driven resonator arrays *Phys. Rev. A* **87** 053846
- [161] Liew T C H and Savona V 2010 Single photons from coupled quantum modes *Phys. Rev. Lett.* **104** 183601
- [162] Bamba M, Imamoglu A, Carusotto I and Ciuti C 2011 Origin of strong photon antibunching in weakly nonlinear photonic molecules *Phys. Rev. A* **83** 021802
- [163] Gerace D and Savona V 2014 Unconventional photon blockade in doubly resonant microcavities with second-order nonlinearity *Phys. Rev. A* **89** 031803
- [164] Angelakis D G, Bose S and Mancini S 2009 Steady-state entanglement between hybrid light-matter qubits *Europhys. Lett.* **85** 20007
- [165] Angelakis D G, Dai L and Kwek L C 2010 Coherent control of long-distance steady-state entanglement in lossy resonator arrays *Europhys. Lett.* **91** 10003
- [166] Dai L, Angelakis D G, Kwek L C and Mancini S 2011 Correlations and thermalization in driven cavity arrays *AIP Conf. Proc.* **1384** 168 76
- [167] Liew T C H and Savona V 2012 Quantum entanglement in nanocavity arrays *Phys. Rev. A* **85** 050301
- [168] Liew T C H and Savona V 2013 Multimode entanglement in coupled cavity arrays *New J. Phys.* **15** 025015
- [169] Le Boit A, Orso G and Ciuti C 2013 Steady-state phases and tunneling-induced instabilities in the driven dissipative Bose Hubbard model *Phys. Rev. Lett.* **110** 233601
- [170] Le Boit A, Orso G and Ciuti C 2014 Bose Hubbard model: relation between driven-dissipative steady states and equilibrium quantum phases *Phys. Rev. A* **90** 063821
- [171] Mendoza-Arenas J J, Clark S R, Felicetti S, Romero G, Solano E, Angelakis D G and Jaksch D 2016 Beyond mean-field bistability in driven-dissipative lattices: bunching antibunching transition and quantum simulation *Phys. Rev. A* **93** 023821
- [172] Wilson R M, Mahmud K W, Hu A, Gorshkov A V, Hafezi M and Foss-Feig M 2016 Collective phases of strongly interacting cavity photons *Phys. Rev. A* **94** 033801
- [173] Finazzi S, Le Boit A, Storme F, Baksic A and Ciuti C 2015 Corner-space renormalization method for driven-dissipative 2D correlated systems *Phys. Rev. Lett.* **115** 080604
- [174] Ozawa T and Carusotto I 2014 Anomalous and quantum Hall effects in lossy photonic lattices *Phys. Rev. Lett.* **112** 133902
- [175] Berceanu A C, Price H M, Ozawa T and Carusotto I 2016 Momentum-space Landau levels in driven-dissipative cavity arrays *Phys. Rev. A* **93** 013827
- [176] Hafezi M 2014 Measuring topological invariants in photonic systems *Phys. Rev. Lett.* **112** 210405
- [177] Bardyn C-E, Huber S D and Zilberberg O 2014 Measuring topological invariants in small photonic lattices *New J. Phys.* **16** 123013
- [178] Ma R, Owens C, LaChapelle A, Schuster D I and Simon J 2016 Hamiltonian tomography of photonic lattices arXiv:1607.05180
- [179] Kapit E, Hafezi M and Simon S H 2014 Induced self-stabilization in fractional quantum Hall states of light *Phys. Rev. X* **4** 031039
- [180] Lebreuilly J, Carusotto I and Wouters M 2016 Towards strongly correlated photons in arrays of dissipative nonlinear cavities under a frequency-dependent incoherent pumping *Comptes Rendus Physique* **17** 836–60
- [181] Toyoda K, Matsuno Y, Noguchi A, Haze S and Urabe S 2013 Experimental realization of a quantum phase transition of polaritonic excitations *Phys. Rev. Lett.* **111** 160501
- [182] Sala V G *et al* 2015 Spin orbit coupling for photons and polaritons in microstructures *Phys. Rev. X* **5** 011034
- [183] Majumdar A, Rundquist A, Bajcsy M and Vučković J 2012 Cavity quantum electrodynamics with a single quantum dot coupled to a photonic molecule *Phys. Rev. B* **86** 045315
- [184] Eichler C, Salathe Y, Mlynek J, Schmidt S and Wallraff A 2014 Quantum-limited amplification and entanglement in coupled nonlinear resonators *Phys. Rev. Lett.* **113** 110502
- [185] Underwood D L, Shanks W E, Koch J and Houck A A 2012 Low-disorder microwave cavity lattices for quantum simulation with photons *Phys. Rev. A* **86** 023837
- [186] Underwood D L, Shanks W E, Li A C Y, Ateshian L, Koch J and Houck A A 2016 Imaging photon lattice states by scanning defect microscopy *Phys. Rev. X* **6** 021044
- [187] Fitzpatrick M, Sundaresan N M, Li A C Y, Koch J and Houck A A 2016 Observation of a dissipative phase transition in a 1D circuit QED lattice (arXiv:1607.06895)

- [188] Harris S E, Field J E and Imamoglu A 1990 Nonlinear optical processes using electromagnetically induced transparency *Phys. Rev. Lett.* **64** 1107 10
- [189] Harris S E 1997 Electromagnetically induced transparency *Phys. Today* **50** 36 42
- [190] Fleischhauer M, Imamoglu A and Marangos J P 2005 Electromagnetically induced transparency: optics in coherent media *Rev. Mod. Phys.* **77** 633 73
- [191] Bajcsy M, Zibrov A S and Lukin M D 2003 Stationary pulses of light in an atomic medium *Nature* **426** 638 41
- [192] Fleischhauer M and Lukin M D 2000 Dark-state polaritons in electromagnetically induced transparency *Phys. Rev. Lett.* **84** 5094 7
- [193] Zimmer F E, Andr A, Lukin M D and Fleischhauer M 2006 Coherent control of stationary light pulses *Opt. Commun.* **264** 441 53
- [194] Andr A, Bajcsy M, Zibrov A S and Lukin M D 2005 Nonlinear optics with stationary pulses of light *Phys. Rev. Lett.* **94** 063902
- [195] Schmidt H and Imamoglu A 1996 Giant Kerr nonlinearities obtained by electromagnetically induced transparency *Opt. Lett.* **21** 1936 8
- [196] Kiffner M and Hartmann M J 2010 Master equation approach for interacting slow- and stationary-light polaritons *Phys. Rev. A* **82** 033813
- [197] Tonks L 1936 The complete equation of state of one, two and 3D gases of hard elastic spheres *Phys. Rev.* **50** 955 63
- [198] Syassen N, Bauer D M, Lettner M, Volz T, Dietze D, Garcia-Ripoll J J, Cirac J I, Rempe G and Durr S 2008 Strong dissipation inhibits losses and induces correlations in cold molecular gases *Science* **320** 1329 31
- [199] Kiffner M and Hartmann M J 2010 Dissipation-induced Tonks Girardeau gas of polaritons *Phys. Rev. A* **81** 021806
- [200] Giamarchi T 2003 *Quantum Physics in One Dimension* (Oxford: Oxford University Press)
- [201] Lieb E H and Liniger W 1963 Exact analysis of an interacting bose gas. I. The general solution and the ground state *Phys. Rev.* **130** 1605 16
- [202] Kinoshita T, Wenger T and Weiss D S 2004 Observation of a 1D Tonks Girardeau gas *Science* **305** 1125 8
- [203] Paredes B, Widera A, Murg V, Mandel O, Fölling S, Cirac I, Shlyapnikov G V, Hansch T W and Bloch I 2004 Tonks Girardeau gas of ultracold atoms in an optical lattice *Nature* **429** 277 81
- [204] Friedel J 1958 Metallic alloys *Il Nuovo Cimento* **7** 287 311
- [205] Lenard A 1966 1D impenetrable bosons in thermal equilibrium *J. Math. Phys.* **7** 1268 72
- [206] Huo M-X and Angelakis D G 2012 Sine-Gordon and Bose Hubbard dynamics with photons in a hollow-core fiber *Phys. Rev. A* **85** 023821
- [207] Hansen K R and Moller K 2007 Trapping of light pulses in ensembles of stationary atoms *Phys. Rev. A* **75** 053802
- [208] Nikoghosyan G and Fleischhauer M 2009 Stationary light in cold-atomic gases *Phys. Rev. A* **80** 013818
- [209] Bchler H P, Blatter G and Zwerger W 2003 Commensurate incommensurate transition of cold atoms in an optical lattice *Phys. Rev. Lett.* **90** 130401
- [210] Fisher M P A, Weichman P B, Grinstein G and Fisher D S 1989 Boson localization and the superfluid-insulator transition *Phys. Rev. B* **40** 546 70
- [211] Haldane F D M 1981 Effective harmonic-fluid approach to low-energy properties of 1D quantum fluids *Phys. Rev. Lett.* **47** 1840 3
- [212] Haller E, Hart R, Mark M J, Danzl J G, Reichsollner L, Gustavsson M, Dalmonde M, Pupillo G and Nagerl H-C 2010 Pinning quantum phase transition for a Luttinger liquid of strongly interacting bosons *Nature* **466** 597 600
- [213] Moiseev S A and Ham B S 2006 Quantum manipulation of two-color stationary light: quantum wavelength conversion *Phys. Rev. A* **73** 033812
- [214] Zimmer F E, Otterbach J, Unanyan R G, Shore B W and Fleischhauer M 2008 Dark-state polaritons for multicomponent and stationary light fields *Phys. Rev. A* **77** 063823
- [215] Lin Y-W, Liao W-T, Peters T, Chou H-C, Wang J-S, Cho H-W, Kuan P-C and Yu I A 2009 Stationary light pulses in cold atomic media and without Bragg gratings *Phys. Rev. Lett.* **102** 213601
- [216] Fleischhauer M, Otterbach J and Unanyan R G 2008 Bose Einstein condensation of stationary-light polaritons *Phys. Rev. Lett.* **101** 163601
- [217] Nikoghosyan G, Zimmer F E and Plenio M B 2012 Dipolar Bose Einstein condensate of dark-state polaritons *Phys. Rev. A* **86** 023854
- [218] Huo M-X, Angelakis D G and Kwek L C 2012 Spinons and holons with polarized photons in a nonlinear waveguide *New J. Phys.* **14** 075027
- [219] Paredes B and Cirac J I 2003 From Cooper pairs to Luttinger liquids with Bosonic atoms in optical lattices *Phys. Rev. Lett.* **90** 150402
- [220] Huo M-X, Noh C, Rodriguez-Lara B M and Angelakis D G 2012 Quantum simulation of Cooper pairing with photons *Phys. Rev. A* **86** 043840
- [221] Kleine A, Kollath C, McCulloch I P, Giamarchi T and Schollwöck U 2008 Spin-charge separation in two-component Bose gases *Phys. Rev. A* **77** 013607
- [222] Orignac E and Giamarchi T 1998 Vortices in coupled planes with columnar disorder and Bosonic ladders *Phys. Rev. B* **57** 11713 29
- [223] Thirring W E 1958 A soluble relativistic field theory *Ann. Phys.* **3** 91 112
- [224] Coleman S 1975 Quantum sine-Gordon equation as the massive Thirring model *Phys. Rev. D* **11** 2088 97
- [225] Cregan R F, Mangan B J, Knight J C, Birks T A, Russell P St J, Roberts P J and Allan D C 1999 Single-mode photonic band gap guidance of light in air *Science* **285** 1537 9
- [226] Smith C M, Venkataraman N, Gallagher M T, Muller D, West J A, Borrelli N F, Allan D C and Koch K W 2003 Low-loss hollow-core silica/air photonic bandgap fibre *Nature* **424** 657 9
- [227] Benabid F, Knight J C, Antonopoulos G and Russell P St J 2002 Stimulated Raman scattering in hydrogen-filled hollow-core photonic crystal fiber *Science* **298** 399 402
- [228] Ouzounov D G, Ahmad F R, Moller D, Venkataraman N, Gallagher M T, Thomas M G, Silcox J, Koch K W and Gaeta A L 2003 Generation of megawatt optical solitons in hollow-core photonic band-gap fibers *Science* **301** 1702 4
- [229] Ghosh S, Sharping J E, Ouzounov D G and Gaeta A L 2005 Resonant optical interactions with molecules confined in photonic band-gap fibers *Phys. Rev. Lett.* **94** 093902
- [230] Light P S, Benabid F, Couny F, Maric M and Luiten A N 2007 Electromagnetically induced transparency in RB-filled coated hollow-core photonic crystal fiber *Opt. Lett.* **32** 1323 5
- [231] Takekoshi T and Knize R J 2007 Optical guiding of atoms through a hollow-core photonic band-gap fiber *Phys. Rev. Lett.* **98** 210404
- [232] Vorrath S, Moller S A, Windpassinger P, Bongs K and Sengstock K 2010 Efficient guiding of cold atoms through a photonic band gap fiber *New J. Phys.* **12** 123015
- [233] Christensen C A, Will S, Saba M, Jo G-B, Shin Y-I, Ketterle W and Pritchard D 2008 Trapping of ultracold atoms in a hollow-core photonic crystal fiber *Phys. Rev. A* **78** 033429

- [234] Bajcsy M, Hofferberth S, Balic V, Peyronel T, Hafezi M, Zibrov A S, Vuletic V and Lukin M D 2009 Efficient all-optical switching using slow light within a hollow fiber *Phys. Rev. Lett.* **102** 203902
- [235] Bajcsy M, Hofferberth S, Peyronel T, Balic V, Liang Q, Zibrov A S, Vuletic V and Lukin M D 2011 Laser-cooled atoms inside a hollow-core photonic-crystal fiber *Phys. Rev. A* **83** 063830
- [236] Tong L, Gattass R R, Ashcom J B, He S, Lou J, Shen M, Maxwell I and Mazur E 2003 Subwavelength-diameter silica wires for low-loss optical wave guiding *Nature* **426** 816 9
- [237] Nayak K P, Melentiev P N, Morinaga M, Le Kien F, Balykin V I and Hakuta K 2007 Optical nanofiber as an efficient tool for manipulating and probing atomic fluorescence *Opt. Express* **15** 5431 8
- [238] Sagu G, Vetsch E, Alt W, Meschede D and Rauschenbeutel A 2007 Cold-atom physics using ultrathin optical fibers: light-induced dipole forces and surface interactions *Phys. Rev. Lett.* **99** 163602
- [239] Spillane S M, Pati G S, Salit K, Hall M, Kumar P, Beausoleil R G and Shahriar M S 2008 Observation of nonlinear optical interactions of ultralow levels of light in a tapered optical nanofiber embedded in a hot rubidium vapor *Phys. Rev. Lett.* **100** 233602
- [240] Vetsch E, Reitz D, Sagu G, Schmidt R, Dawkins S T and Rauschenbeutel A 2010 Optical interface created by laser-cooled atoms trapped in the evanescent field surrounding an optical nanofiber *Phys. Rev. Lett.* **104** 203603
- [241] Dawkins S T, Mitsch R, Reitz D, Vetsch E and Rauschenbeutel A 2011 Dispersive optical interface based on nanofiber-trapped atoms *Phys. Rev. Lett.* **107** 243601
- [242] Hung C-L, Meenehan S M, Chang D E, Painter O and Kimble H J 2013 Trapped atoms in 1D photonic crystals *New J. Phys.* **15** 083026
- [243] Goban A *et al* 2014 Atom-light interactions in photonic crystals *Nat. Commun.* **5** 3808
- [244] Chang D E, Jiang L, Gorshkov A V and Kimble H J 2012 Cavity QED with atomic mirrors *New J. Phys.* **14** 063003
- [245] Douglas J S, Habibian H, Hung C-L, Gorshkov A V, Kimble H J and Chang D E 2015 Quantum many-body models with cold atoms coupled to photonic crystals *Nat. Photon.* **9** 326 31
- [246] Friedler I, Petrosyan D, Fleischhauer M and Kurizki G 2005 Long-range interactions and entanglement of slow single-photon pulses *Phys. Rev. A* **72** 043803
- [247] Petrosyan D and Fleischhauer M 2008 Quantum information processing with single photons and atomic ensembles in microwave coplanar waveguide resonators *Phys. Rev. Lett.* **100** 170501
- [248] Mller M, Lesanovsky I, Weimer H, Bchler H P and Zoller P 2009 Mesoscopic Rydberg gate based on electromagnetically induced transparency *Phys. Rev. Lett.* **102** 170502
- [249] Shahmoon E, Kurizki G, Fleischhauer M and Petrosyan D 2011 Strongly interacting photons in hollow-core waveguides *Phys. Rev. A* **83** 033806
- [250] He B, MacRae A, Han Y, Lvovsky A I and Simon C 2011 Transverse multimode effects on the performance of photon-photon gates *Phys. Rev. A* **83** 022312
- [251] Gorshkov A V, Otterbach J, Fleischhauer M, Pohl T and Lukin M D 2011 Photon-photon interactions via Rydberg blockade *Phys. Rev. Lett.* **107** 133602
- [252] He B, Sharypov A V, Sheng J, Simon C and Xiao M 2014 Two-photon dynamics in coherent Rydberg atomic ensemble *Phys. Rev. Lett.* **112** 133606
- [253] Otterbach J, Moos M, Muth D and Fleischhauer M 2013 Wigner crystallization of single photons in cold Rydberg ensembles *Phys. Rev. Lett.* **111** 113001
- [254] Pritchard J D, Maxwell D, Gauguier A, Weatherill K J, Jones M P A and Adams C S 2010 Cooperative atom-light interaction in a blocked Rydberg ensemble *Phys. Rev. Lett.* **105** 193603
- [255] Peyronel T, Firstenberg O, Liang Q-Y, Hofferberth S, Gorshkov A V, Pohl T, Lukin M D and Vuletic V 2012 Quantum nonlinear optics with single photons enabled by strongly interacting atoms *Nature* **488** 57 60
- [256] Dudin Y O and Kuzmich A 2012 Strongly interacting Rydberg excitations of a cold atomic gas *Science* **336** 887 9
- [257] Hofmann C S, Gnter G, Schempp H, Robert-de Saint-Vincent M, Grttrner M, Evers J, Whitlock S and Weidemller M 2013 Sub-Poissonian statistics of Rydberg-interacting dark-state polaritons *Phys. Rev. Lett.* **110** 203601
- [258] Maxwell D, Szwed D J, Paredes-Barato D, Busche H, Pritchard J D, Gauguier A, Weatherill K J, Jones M P A and Adams C S 2013 Storage and control of optical photons using Rydberg polaritons *Phys. Rev. Lett.* **110** 103001
- [259] Parigi V, Bimbard E, Stanojevic J, Hilliard A J, Nogrette F, Tualle-Brouiri R, Ourjoumtsev A and Grangier P 2012 Observation and measurement of interaction-induced dispersive optical nonlinearities in an ensemble of cold Rydberg atoms *Phys. Rev. Lett.* **109** 233602
- [260] Ningyuan J, Georgakopoulos A, Ryou A, Schine N, Sommer A and Simon J 2016 Observation and characterization of cavity Rydberg polaritons *Phys. Rev. A* **93** 041802



Changsuk Noh is a KIAS assistant professor at the Korea Institute for Advanced Study. He received his PhD in 2009 at the University of Auckland, then worked as a postdoctoral researcher at Auckland and Singapore before he arrived to KIAS. His research interests include many-body physics and quantum simulations in quantum optical systems.



Dimitris Angelakis was born and raised in Crete, Greece where he also did his undergraduate studies. After completing his PhD at Imperial College London, he was elected junior research fellow at University of Cambridge (St Catharine's College). He held this position at the Department of Applied Mathematics and Theoretical Physics and at the Centre for Quantum Computation. In 2008, he took over a faculty appointment at the Technical University of Crete, where he is now based at the School of Electrical and Computer Engineering. He is also a Principal Investigator at the Centre for Quantum Technologies, National University of Singapore. His research interests include quantum optics, quantum many-body physics and implementations of quantum computation and quantum simulation.